UNIVERSIDADE FEDERAL DE SANTA CATARINA
PROGRAMA DE PÓS - GRADUAÇÃO EM ENGENHARIA DE AUTOMAÇÃO E SISTEMAS

Leonardo Martins Rodrigues

A TEMPERATURE-DEPENDENT BATTERY MODEL FOR WIRELESS SENSOR NETWORK NODES

Florianópolis
2017

Leonardo Martins Rodrigues

A TEMPERATURE-DEPENDENT BATTERY MODEL FOR WIRELESS SENSOR NETWORK NODES

Thesis submitted to the Automation and Systems Engineering Postgraduate Program in partial fulfilment of the requirements for the degree of Doctor of Philosophy in Automation and Systems Engineering.
Supervisor: Carlos B. Montez
Co-supervisor: Paulo Portugal

Florianópolis
2017

Ficha de identificação da obra elaborada pelo autor,
através do Programa de Geração Automática da Biblioteca Universitária da UFSC.

Rodrigues, Leonardo Martins
A temperature-dependent battery model for wireless sensor network nodes / Leonardo Martins Rodrigues ; orientador, Carlos Barros Montez, coorientador, Paulo Portugal, 2017.
187 p.

Tese (doutorado) - Universidade Federal de Santa Catarina, Centro Tecnológico, Programa de Pós Graduação em Engenharia de Automação e Sistemas, Florianópolis, 2017.

Inclui referências.

1. Engenharia de Automação e Sistemas. 2. WSN. 3. Battery Modelling. 4. Thermal Effect. I. Montez, Carlos Barros. II. Portugal, Paulo. III. Universidade Federal de Santa Catarina. Programa de Pós-Graduação em Engenharia de Automação e Sistemas. IV. Título.

A TEMPERATURE-DEPENDENT BATTERY MODEL FOR WIRELESS SENSOR NETWORK NODES

Leonardo Martins Rodrigues

This Thesis is hereby approved and recommended for acceptance in partial fulfilment of the requirements for the degree of "Doctor of Philosophy in Automation and Systems Engineering".

September 22th, 2017.

Prof. Carlos B. Montez, Dr. Eng.
Supervisor

Prof. Daniel Coutinho, PhD.
Coordinator of the Automation and Systems Engineering Postgraduate Program

Examining Committee:

Prof. Luiz Affonso Guedes, PhD. – UFRN
(Por videoconferência)

Prof. Eduardo Augusto Bezerra, PhD. – UFSC

Prof. Daniel Coutinho, PhD. – UFSC

"I'm a great believer in luck, and I find the harder I work, the more luck I have". – Thomas Jefferson

ACKNOWLEDGEMENTS

First of all, I thank my parents, Norma and Milton, for all the support since the beginning of this course. Without them, the way would certainly be more difficult. Also, a special thanks to my girlfriend, Luciana, who understood my purpose and always hoped for my success, even if it meant the distance between us. It was she who always listened to my reactions and knew how to keep my motivation to the conclusion of this project.

Second, I thank my advisor, Carlos Montez, for accepting me as his student. His advice during the course was precious for the development of this work. I would like to praise my co-advisor, Paulo Portugal, for his ability to share the effort employed in this project. Without his help, we would not have the experimental testing platform mentioned in this document. Professor Francisco Vasques also deserves great thanks for his ideas and definitions during this project. Both Paulo and Francisco received me very enthusiastically in Portugal and certainly made a difference in that period outside my native land.

Third, I would like to thank my friends Luís, Tadeu, Fernando, Rejane, Karila, Sidney, Daniel, Alexandre, Leonardo, José, Stephanie, Benedito, Renata, Danilo, Erico, Mara, Carlos and Gerson. Everyone participated actively in this process, sharing moments and ideas.

Finally, I thank CAPES, which was responsible for financing my scholarship and also guaranteeing a period of seven months in Portugal.

RESUMO

As Redes de Sensores sem Fios (RSSFs) são amplamente utilizadas em várias áreas (residencial, comercial e industrial), pois facilitam o processo de implantação dos nodos sensores que integram a rede, independentemente das condições ambientais. No entanto, há uma grande preocupação com o consumo de energia nas RSSFs, já que seus nodos são alimentados por baterias. Estes dispositivos armazenam uma capacidade de carga limitada e dependem de reações eletroquímicas para gerar energia. Assim, vários fatores podem influenciar as baterias, como corrente de descarga e temperatura, principalmente, em RSSFs ao ar livre. Em geral, as baterias têm comportamento não-linear ao longo do tempo, o que pode ser acentuado dependendo da combinação desses fatores. Isso dificulta prever informações importantes para a organização e manutenção da RSSF, como o estado de carga, o tempo de vida e o nível de tensão das baterias. Tais parâmetros são amplamente utilizados em algoritmos/protocolos cientes de energia. O objetivo desta tese é desenvolver um modelo de bateria capaz de lidar com o efeito térmico, que pode ocasionar uma forte influência em RSSFs implantadas em ambientes com grandes variações de temperatura. Além disso, os seguintes requisitos são essenciais para o modelo de bateria proposto: (i) precisão para estimar o comportamento das baterias, principalmente, seu tempo de vida e nível de tensão em diferentes temperaturas; e (ii) baixa complexidade computacional para permitir a sua integração com nodos de baixo consumo energético comercialmente disponíveis no mercado. As avaliações são realizadas através de análises experimentais, analíticas e de simulação. Os resultados mostram que o modelo de bateria proposto pode lidar com o efeito térmico de forma adequada, podendo estimar tanto o tempo de vida quanto o nível de tensão da bateria em diferentes temperaturas. Assim, a principal contribuição desta tese é o desenvolvimento de um modelo de bateria dependente da temperatura, que pode ser implementado tanto em simuladores quanto em nodos de RSSFs para estimar o comportamento de suas baterias.

Palavras-chave: RSSF, Modelo de Bateria, Efeito Térmico.

RESUMO EXPANDIDO

Introdução

O interesse na pesquisa sobre as RSSFs cresceu a partir dos anos 2000 devido ao desenvolvimento tecnológico e redução nos custos de fabricação dos componentes eletrônicos necessários para sua implementação, tais como, sensores, microcontroladores (ou *Micro-Controller Unit*s (MCUs)) e transceptores (rádios sem fio) (AKYILDIZ et al., 2002). Essa evolução tecnológica permitiu o desenvolvimento de RSSFs compostas por muitos nodos autônomos, dispersos espacialmente, a fim de capturar dados físicos do ambiente de forma colaborativa (STANKOVIC, 2008). Assim, este tipo de rede de sensores constitui um novo paradigma para a aquisição de dados, melhorando a confiabilidade e a eficiência na construção de sistemas de informação e comunicação devido à sua baixa complexidade de implantação e flexibilidade para se adaptar a qualquer tipo de ambiente, ao contrário do que ocorre ao usar redes cabeadas (IEC, 2014).

Atualmente, as RSSFs podem ser encontradas em muitas áreas diferentes, por exemplo, residencial, comercial e industrial. Além disso, o conceito conhecido como Internet das Coisas (do inglês, *Internet of Things* (IoT)) expandiu o uso deste tipo de rede para várias aplicações. Neste conceito, qualquer objeto (ou parte dele) pode se tornar um sistema computacional para se comunicar com outros objetos (ou partes do mesmo objeto) através do uso da Internet. Por exemplo, aviões, carros, edifícios, máquinas, qualquer "coisa" pode se tornar um dispositivo que interage com o ambiente. Isso traz benefícios significativos para setores relacionados ao transporte, segurança, energia, saúde, agricultura e outros, visto que usar os fundamentos de RSSFs para IoT implica em uma maneira efetiva de adquirir informações, possibilitando a implementação de sistemas inteligentes de monitoramento em tempo real para relatar o estado operacional e garantir a confiabilidade da aplicação (IEC, 2014).

Por outro lado, existem limitações inerentes ao uso de RSSFs que desafiam os pesquisadores nessa área. Algumas limitações estão relacio-

nadas aos recursos de hardware dos nodos sensores, como baixa capacidade de processamento e largura de banda, além de uma pequena quantidade de memória, o que aumenta a necessidade de agregar os dados coletados dos nodos sensores e influencia o desenvolvimento de novos protocolos de comunicação e de controle de acesso ao meio. Em paralelo, a questão do consumo energético dos nodos constitui uma das principais limitações das RSSFs, visto que baterias são usadas como fonte de alimentação para os seus componentes eletrônicos. Assim, dependendo das condições de operação dos nodos sensores, tais limitações podem se tornar uma grande desvantagem do ponto de vista da eficiência, gerenciamento e manutenção das RSSFs (ANASTASI et al., 2009).

Além disso, as RSSFs podem ser implantadas em qualquer tipo de ambiente, seja interno, externo ou submerso, devido à flexibilidade oferecida pelos sensores, transceptores e baterias. Neste contexto, é bastante comum expor os nodos sensores a condições extremas de operação. Particularmente, a temperatura desempenha um papel fundamental nos nodos sensores, uma vez que pode afetar o estado operacional padrão de seus componentes (BANNISTER; GIORGETTI; GUPTA, 2008). Até mesmo a comunicação entre os nodos sensores pode ser comprometida dependendo da temperatura ambiente (BOANO et al., 2010). Apesar disso, esta tese se concentra na influência causada pela temperatura no componente responsável por manter a operação dos nodos da rede, ou seja, a bateria.

A bateria em um nodo sensor é um dos componentes mais afetados pelo efeito térmico, uma vez que reações eletroquímicas internas, necessárias para a geração de energia, são facilmente influenciadas pela variação da temperatura externa. Isso aumenta o comportamento não-linear das baterias (FEENEY et al., 2012; FEENEY; ROHNER; LINDGREN, 2014). Um fato conhecido na literatura indica que as baterias fornecem uma capacidade de carga efetiva mais alta quando usadas sob altas temperaturas e, por outro lado, uma capacidade de carga efetiva menor quando utilizadas em ambientes com baixas temperaturas (JAGUEMONT et al., 2016). Esse problema é percebido, principalmente, quando os nodos sensores operam em ambientes com grandes variações térmicas ao longo do dia e em esquema de ciclo de trabalho (do inglês, *duty cycle*), isto é,

alternando entre seus modos de operação de forma cíclica ao longo do tempo, por exemplo, transmitindo/recebendo dados, escutando o meio, executando tarefas ou "desligado". Tais variações na capacidade de carga fornecida pelas baterias dificultam a previsibilidade em relação ao seu comportamento ao longo do tempo, em particular, a estimativa sobre seu estado de carga e tempo de vida. Essas informações podem ser úteis na implementação de abordagens cientes de energia para RSSFs.

Objetivo

Esta tese tem como objetivo desenvolver um modelo de bateria capaz de lidar com o efeito térmico em nodos de RSSFs, apresentando alta precisão para modelar o comportamento das baterias em diferentes temperaturas, particularmente, em relação à informação sobre seu estado de carga, nível de tensão e tempo de vida. Um requisito importante é que o modelo de bateria desenvolvido deve ter uma baixa complexidade computacional para permitir sua integração com nodos sensores tipicamente utilizados em implantações físicas de RSSFs.

Metodologia

A metodologia utilizada para a realização desta tese se baseia em três tipos de análises: (i) experimentais, (ii) analíticas e (iii) via simulação. Sobre o item (i), uma plataforma de testes para descarga de baterias foi projetada e desenvolvida especificamente para a realização desta tese. Tal plataforma de testes permitiu a coleta de dados experimentais sobre o comportamento das baterias em diferentes situações, por exemplo, corrente de descarga (incluindo diferentes esquemas de ciclo de trabalho) e temperatura. Sobre o item (ii), o *software* Matlab foi utilizado para a implementação e avaliação analítica de um modelo de bateria cinético dependente de temperatura, do inglês, *Temperature-Dependent Kinetic Battery Model (T-KiBaM)*. Através dos dados experimentais obtidos no item (i), pôde-se validar o modelo de bateria proposto nesta tese para diferentes situações de utilização da bateria. Sobre o item (iii), um simulador de

RSSFs amplamente utilizado pela comunidade científica foi empregado para receber a implementação do modelo de bateria mencionado. Essa implementação permitiu a análise do comportamento das baterias em nodos sensores de uma RSSF de forma mais precisa, ao contrário do que se observava utilizando o modelo de energia padrão do simulador.

Resultados e Discussão

Os resultados apresentados nesta tese de doutorado podem ser divididos em três seções: (i) validação do modelo de bateria; (ii) verificação sobre a viabilidade de sua implementação em microcontroladores de baixa capacidade computacional; e (iii) verificação sobre a viabilidade de sua implementação em um simulador de RSSF tipicamente utilizado pela comunidade científica. Sobre o item (i), o Capítulo 4 desta tese mostra o desenvolvimento do modelo T-KiBaM, bem como a sua validação para situações utilizando correntes de descarga constantes (uma avaliação sobre o comportamento do modelo de bateria proposto em regime de ciclo de trabalho também é realizada no Capítulo 5 desta tese de doutorado). Os resultados apresentados mostram que o modelo de bateria proposto é capaz de lidar com diferentes temperaturas e, ao mesmo tempo, aumentar a precisão sobre as estimativas realizadas em comparação com outros dois modelos de bateria. Sobre o item (ii), o Capítulo 5 desta tese apresenta um estudo sobre as características do modelo de bateria proposto com relação ao seu tempo de execução, ocupação de memória e consumo de energia. Os resultados apresentados indicam a viabilidade de implementação do modelo T-KiBaM em microcontroladores com baixa capacidade computacional. O mesmo capítulo ainda apresenta um exemplo de aplicação do modelo de bateria executando em um nodo de RSSF. Sobre o item (iii), o Capítulo 6 desta tese apresenta um estudo sobre a implementação do modelo T-KiBaM no simulador Castalia. Tal simulador não contém recursos que permitam configurar o ambiente no qual a RSSF está inserida, o que é uma lacuna a ser preenchida. Através da implementação

apresentada, tornou-se possível definir um perfil térmico para modelar o comportamento da bateria em ambientes com temperaturas variáveis. Os resultados obtidos, quando comparados com dados experimentais, indicam a corretude da implementação do modelo T-KiBaM no simulador Castalia. Um exemplo de aplicação também foi apresentado neste capítulo para avaliar o comportamento de uma rede ao utilizar o modelo de bateria proposto, o que gerou resultados diferentes daqueles observados ao utilizar o modelo de energia padrão do simulador.

Considerações Finais

As RSSFs são muito importantes no mundo moderno, pois permitem a interconexão de dispositivos computacionais sem a necessidade de um cabo para intermediar a comunicação. Apesar disso, essas redes apresentam uma grande restrição energética, visto que os nodos sensores são alimentados por baterias. Tais dispositivos eletroquímicos apresentam tempo de operação limitado e precisam ser utilizados de forma eficiente para evitar o consumo desnecessário de energia. Além disso, as baterias sofrem influências da temperatura ambiente, o que altera a sua capacidade de fornecer energia aos nodos sensores. Tal condição dificulta a previsibilidade sobre o seu comportamento ao longo do tempo. Esta tese de doutorado tratou sobre esse problema, gerando quatro publicações científicas (até a data de escrita deste documento). Os resultados obtidos nesta pesquisa, sobretudo as implementações apresentadas no Capítulo 6, permitem o desenvolvimento de trabalhos futuros incluindo abordagens cientes de energia para RSSFs em ambientes com temperaturas variáveis.

Palavras-chave: RSSF, Modelo de Bateria, Efeito Térmico.

ABSTRACT

Wireless Sensor Networks (WSNs) are widely used in several areas (residential, commercial and industrial), as they facilitate the process of deployment of the sensor nodes that integrate the network, regardless of the environmental conditions. However, there is great concern regarding the energy consumption of WSNs, since their sensor nodes are powered by batteries. These chemical devices store a limited charge capacity and depend on electrochemical reactions to generate energy. Within this context, several factors can influence the behaviour of batteries, such as discharge current and temperature, mainly in outdoor WSNs. In general, batteries have non-linear behaviour over time, which can be accentuated depending on the combination of these factors. This makes it difficult to predict important information for the organization and maintenance of the WSN, such as the battery state of charge, lifetime and voltage level, all of them widely used in energy-aware algorithms/protocols. The objective of this thesis is to develop a battery model capable of dealing with the thermal effect, which may represent a strong influence in WSNs deployed in environments with large temperature variations. In addition, the following requirements are essential for the proposed battery model: (i) precision to estimate the behaviour of the batteries, mainly their lifetime and voltage level, at different temperatures; and (ii) low computational complexity to allow its integration with COTS low-power nodes. Evaluations are performed through experimental, analytical and simulated analyses. The results show that the proposed battery model can handle the thermal effect adequately, being able to estimate the lifetime and the voltage level of the battery at different temperatures. Thus, the main contribution of this thesis is the development of a temperature-dependent battery model that can be implemented both in simulators and in commercially available sensor nodes to estimate the behaviour of their batteries.

Keywords: WSN, Battery Modelling, Thermal Effect.

LIST OF FIGURES

LIST OF TABLES

CONTENTS

LIST OF ABBREVIATIONS AND ACRONYMS

BAN	Body Area Network
BDM	Battery Dynamic Model
BTP	Battery Test Platform
CF	Correction Factor
COTS	Commercial Off-The-Shelf
DC	Duty Cycle
DP	Discharge Profile
ELT	Estimated Battery Lifetime
EMF	Electromotive Force
ENL	Estimated Network Lifetime
ERR	Relative Error
ET	Execution Time
EV	Electric Vehicle
FPU	Floating Point Unit
HEV	Hybrid Electric Vehicle
IC	Integrated Circuit
IoT	Internet of Things
KiBaM	Kinetic Battery Model
MAC	Medium Access Control
MCU	*Micro-Controller Unit*
Ni-MH	Nickel-Metal Hydride

OCV	Open-Circuit Voltage
SoC	State of Charge
T-KiBaM	Temperature-Dependent Kinetic Battery Model
TNL	Total Network Lifetime
TVM	Temperature-Dependent Voltage Model
WSN	Wireless Sensor Network

LIST OF SYMBOLS

a	Battery capacity (Peukert' Law)
A	Pre-exponential factor (Arrhenius)
A_b	Exponential zone amplitude (TVM)
A_e	Surface area of the electrode
α	Battery capacity (Diffusion Model)
b	Peukert constant
B	Exponential zone time constant inverse (TVM)
β	Non-linearity in battery behaviour
c	Fraction of charge (KiBaM)
C^*	Concentration in $t = 0$ (Diffusion Model)
C_{cut}	Minimum concentration of electro-active species
$C(x,t)$	Active material concentration (Diffusion Model)
D	Diffusion constant (Diffusion Model)
DP_{set}	Discharge Profile set
δ	Difference between heights h_1 and h_2 (KiBaM)
Δt	Time interval
E	Internal voltage of the battery (KiBaM)
E_{min}	Battery minimal internal voltage (KiBaM)
$E_{0,d}$	Battery maximum internal voltage (KiBaM)
E_0	Battery constant reference voltage (TVM)
E_a	Activation Energy (Arrhenius)

E_n	Energy consumption
$Exp(t)$	Exponential zone voltage (TVM)
e^-	Electron
F	Faraday constant
H_{ab}	Absorbed hydrogen
h_1	Available Charge tank level (KiBaM)
h_2	Bound Charge tank level (KiBaM)
I	Discharge current
i^*	Filtered current (TVM)
$i(t)$	Instantaneous discharge current
it	Actual battery charge, $\int idt$ (TVM)
$J(x,t)$	Flux of active material
k	Rate constant (KiBaM)
K_b	Polarization resistance (TVM)
L	Battery lifetime
M	Hydrogen-absorbing alloy
ν	Electrons in the electrochemical reaction
P	Electric power
q_0	Amount of charge in the battery (KiBaM)
q_1	Charge in the Available Charge tank (KiBaM)
q_2	Charge in the Bound Charge tank (KiBaM)
q_{max}	Maximum charge capacity of the battery (KiBaM)

Q	Battery capacity (TVM)
R	Universal gas constant (Arrhenius)
R_b	Battery internal resistance
T	Temperature (Arrhenius)
t	Time
TP_{set}	Temperature Profile set
τ_b	Smoothing constant (TVM)
u	Unavailable charge (KiBaM)
$u(t)$	Charge/Discharge mode (TVM)
V	Battery Voltage (KiBaM)
V_b	Battery Voltage (TVM)
V_{cut}	Cut-off Voltage
V_{OC}	Open-Circuit Voltage
x	Distance of the electrode (Diffusion Model)

1 INTRODUCTION

Wireless Sensor Networks (WSNs) were created for military purposes with the objective of monitoring conflict zones. Within this context, one of the first successful WSN implementation was the SOSUS (Sound Surveillance System) project, developed by the US Navy in the 1950s, which aimed to detect and monitor the presence of submarines near the coasts through the use of submerged acoustic sensor nodes (SILICON LABS INC, 2013).

The interest in research on WSNs has grown due to the technological development and reduction in the manufacturing costs of the electronic components necessary for their implementation, e.g., sensors, micro-controllers and transceivers (wireless radios) (AKYILDIZ et al., 2002). From this, it became feasible to develop WSNs composed of many spatially scattered autonomous nodes in order to capture physical data from the environment in a collaborative way (STANKOVIC, 2008). Thus, this type of sensor network constitutes a new paradigm for data acquisition in order to improve reliability and efficiency in the construction of information and communication systems due to its low deployment complexity and flexibility to adapt to any type of environment, contrary to what occurs when using wired devices (IEC, 2014).

WSNs can now be found in many different areas (e.g., residential, commercial and industrial). In addition, the concept known as Internet of Things (IoT) has boosted the use of this type of network for various applications. In this concept, any object (or part of it) can become a computer system to communicate with other objects (or parts of the same object) through the use of the Internet. For example, aeroplanes, cars, buildings, people, machines, anything can become a device that interacts with the environment. This brings significant benefits to sectors related to transportation, security, energy, health, agriculture and others, since using the fundamentals of WSNs for IoT implies an effective way of acquiring information, enabling the implementation of intelligent monitoring real-time systems to report the operating state and ensure the reliability of applications. (IEC, 2014).

On the other hand, there are limitations inherent in the use of WSNs that impose great challenges for researchers in this area. The main limitations are related to the hardware resources of the sensor nodes, e.g., low processing capacity and bandwidth, as well as a small amount of memory, which increases the need to aggregate the data collected from the nodes and influences the development of new communication and Medium Access Control (MAC) protocols. In addition, there is the energy limitation, since batteries are used as the power supply to the electronic components. Thus, depending on the operating conditions of the sensor nodes, such limitations can become a major drawback from the point of view of efficiency, management, and maintenance of WSNs (ANASTASI et al., 2009).

1.1 RESEARCH CONTEXT

WSNs can be deployed in many kind of environments, whether indoors or outdoors, due to the flexibility offered by sensors, transceivers, and batteries. Within this context, it is quite common to expose the sensor nodes to extreme operating conditions. Particularly, the temperature plays a key role in the performance of sensor nodes, since it may affect the standard operating state of their components (BANNISTER; GIORGETTI; GUPTA, 2008). Even the communication between sensor nodes can be compromised depending on the ambient temperature (BOANO et al., 2010). Nevertheless, this work focus on the influence caused by the temperature in the component responsible for maintaining the operation of the WSN node, i.e., the battery.

The battery in a WSN node is one of the components most affected by the thermal effect, since internal electrochemical reactions, which are required for energy generation, are easily influenced by external temperature variations. This increases the non-linear behaviour of the batteries (FEENEY et al., 2012; FEENEY; ROHNER; LINDGREN, 2014). A well-known issue in the literature indicates that the batteries have a higher effective charge capacity when used under high temperatures and, on the other hand, lower effective charge capacity

when used in low-temperature environments (JAGUEMONT et al., 2016). These variations in capacity hinder predictability with respect to the behaviour of the batteries over time, particularly, the State of Charge (SoC) and lifetime estimation, which can be useful in the implementation of energy-aware approaches.

Generally, WSN designers use simulators before deploying the physical network to implement energy-aware approaches. However, many of these simulators use simplified battery models that assume a linear behaviour for the battery, i.e., they do not consider the main effects that interfere with battery operation, such as thermal, rate capacity and recovery effects (STETSKO; STEHLÍK; MATYAS, 2011; MUSZNICKI; ZWIERZYKOWSKI, 2012). In fact, modelling battery behaviour is a complex task since these effects can influence the reactions inside an electrochemical cell (JONGERDEN; HAVERKORT, 2008; DANIIL; DRURY; MELLOR, 2015). Besides, WSN simulators are not able to provide accurate information on the battery SoC and/or voltage level of the sensor nodes. The lack of accurate battery models for WSN simulators decreases the quality of the estimates with respect to the behaviour of the battery in different scenarios/environments.

Particularly, the combination of information on charge capacity and the voltage level is a traditional and convenient method to estimate the SoC, since the electronic circuits used in the sensor nodes have minimum requirements to operate. In other words, although the node indicates the existence of charge on the battery, the voltage level may be close to the lower-bound operation value of the electronic components, which may produce errors of estimation over the remaining operation time of the node, affecting the network management. In this way, it becomes relevant to use more accurate battery models that consider the main effects that affect the batteries and provide relevant information about their state, in order to improve the predictability of the simulations with respect to the behaviour of the batteries on WSN nodes operating in different environments.

In addition, many implementations of battery models used in WSN simulators can not be embedded into real nodes due to hardware

constraints, such as memory usage, processing power, bandwidth allocation and power consumption. Thus, some information that can be obtained through simulation is not available in the operating systems of Commercial Off-The-Shelf (COTS) WSN nodes. In other words, it becomes important that the same features offered in simulators are also available in real-world WSN deployments.

In the context of this work, the following items can be cited as essential functionalities for the development of energy-aware approaches: (i) knowledge about SoC; and (ii) battery lifetime estimation. In this work, such functionalities do not require specific software or hardware resources. Thus, the use of the same models in both WSN simulators and real-world sensor nodes can facilitate the software implementation process and accelerate physical network deployment.

In the light of the aforementioned issues, it can be seen that there are many challenges with regard to battery modelling in WSNs. Within this context, the main hypothesis of this thesis is to verify if *"it is possible to develop a battery model with low computational requirements capable of accurately estimating the battery behaviour of sensor nodes in WSN scenarios with temperature variations"*.

From the main hypothesis, other specific problems must be addressed throughout this document, such as:

1. Since WSNs present severe hardware constraints, is it possible that such a battery model to be simple enough to be embedded in sensor nodes with low computing capacity?

2. Since WSN designers often perform simulations before physically deploying the sensor nodes, is it possible that such a battery model to be implemented in simulators typically used by the scientific community?

1.2 RESEARCH OBJECTIVES

The questions presented above serve as a reference to guide the efforts applied in the development of this thesis. In this way, this work

has the purpose of developing a battery model capable of dealing with the thermal effect in WSN nodes, presenting high accuracy to model the behaviour of batteries operating under a wide range of temperatures, particularly, with respect to the information on SoC, voltage level and lifetime. An important requirement is that such a battery model must have a low computational complexity to allow its integration with nodes typically used in physical WSN deployments. The specific objectives of this thesis are presented below, followed by a brief discussion on some delimitations in the scope of this research work.

1.2.1 Specific Objectives

Aiming at success in propositions of the general objective, the present work intends to fulfil the following specific objectives[1]:

1. Developing a flexible test-bed platform to evaluate the behaviour of batteries under various operating conditions, including different temperatures and discharge profiles;

2. Proposing a battery model capable of dealing with the thermal effect, which can influence in a significant way the reaction rate inside electrochemical cells;

3. Validating the proposed battery model through experiments using temperatures and discharge profiles compatible with typical scenarios in WSN applications;

4. Assessing the performance of the proposed battery model in low-power hardware compatible with sensor nodes typically used in WSN deployments;

5. Implementing the proposed battery model in a WSN simulator widely used by the scientific community.

[1] Specific objectives are not listed in order of importance.

1.2.2 Scope

The following discussions reflect the definitions made to allow the execution of this research work.

The first item concerns the battery technology used in the experiments carried out in this research project. The use of several types of batteries, mainly based on Nickel and Lithium, has been reported in the literature in the context of WSNs (FEENEY et al., 2012; FEENEY; ROHNER; LINDGREN, 2014; RUKPAKAVONG; GUAN; PHILLIPS, 2014). In this case, Nickel-Metal Hydride (Ni-MH) technology was chosen for this work due to its (i) lower cost per cell, (ii) standard format (AAA), and (iii) low-cost chargers, which are widely available in the market. This means that this thesis does not test the Li-ion technology in the performed experiments. Despite this, the literature indicates that the results obtained with Ni-MH batteries can be extended to Li-ion batteries since the battery models proposed in this work allow the adjustment of the parameters for different battery technologies.

The second item is related to the mode of operation of such Ni-MH batteries. Only the battery discharging process is considered in this case. That is, this work assumes that the sensor node has no power generating devices to power its battery, which should be recharged when its charge is no longer sufficient to maintain the node's activities. Thus, the presented battery model has not been validated for the case of recharging the battery. Despite this, the literature indicates that such a process can be performed since the presented battery models support such condition. This evaluation should be carried out in future work for the proposed temperature-dependent battery model.

The third aspect that limits the scope of this thesis refers to the various effects that influence the batteries, whether internal or external. Only the effects related to temperature, rate capacity and recovery are considered in this work. Such effects cause short-term changes during battery discharge, changing their behaviour almost instantaneously. Other long-term effects influence the batteries slowly (which can take months or years), such as self-discharge, ageing and

recharge cycle counting (RUKPAKAVONG; GUAN; PHILLIPS, 2014). However, these characteristics will be addressed in future works.

1.3 RESEARCH CONTRIBUTIONS

This thesis presents a series of steps related to the proposed theme, which encompasses: (i) the development of a battery model; (ii) its validation and implementation in hardware with low computational capacity, typically used in sensor nodes; and (iii) its validation and implementation in a specific WSN simulator. The effort to plan, develop and carry out all these three steps in the context of WSNs is one of the great advances of this research project.

The extension of the proposed approach can not yet be precisely determined. Such a scheme can be used in different design stages, according to the needs of WSN designers. For example, in the network design, to estimate the lifetime of the battery according to the tasks performed by the sensor nodes; or in the implementation of the network, by embedding the battery model in the nodes, enabling verification of the battery SoC and voltage level, which can be used in energy-aware approaches. Specifically, given the objectives and the scope of this work, this thesis presents the following contributions[2]:

1. Development of a temperature-dependent battery model with low computational cost for use within WSN context;
2. Demonstration of the feasibility of implementing such analytical battery model in hardware with low computational capacity;
3. Improvement of the evaluation methods regarding the energy level in the batteries at nodes within WSN simulators;
4. Presentation of experimental results with Ni-MH batteries, which are tested in environments with different temperatures;
5. Development of a reliable, low-cost and flexible (configurable) test-bed platform for conducting future research.

[2] The research contributions are listed in order of importance.

1.4 THESIS OUTLINE

This document is divided into seven chapters, including the Introduction, presented here. This division favours the description about the concepts involved in this thesis, as well as the presentation of the results obtained from the published articles. Thus, the next chapters of this document are organized as follows.

Chapter 2 introduces some concepts about batteries, important for the understanding of the subjects treated in this thesis. These concepts address terminology issues, the used technologies and a study on the types of existing battery models.

Chapter 3 presents the state-of-the-art concerning to the main theme of this research project, i.e., battery models that include temperature dependence. Some works related to the other development stages of this research are also presented in this chapter.

Chapter 4 introduces the battery model known as T-KiBaM, the main proposition of this research project. In addition, the validation of the T-KiBaM model, performed through experiments with Ni-MH batteries at different temperatures, is presented in the context of WSNs.

Chapter 5 demonstrates that it is feasible to implement the proposed battery model in micro-controllers with low computational capacity, typically used in sensor nodes. This chapter also includes an application example, which tests the hardware implementation.

Chapter 6 presents the implementation of the T-KiBaM model in a WSN simulator. This chapter also includes the results of experiments with Ni-MH batteries in variable temperature environments.

Chapter 7 presents the final remarks regarding this project, including the list of published papers and suggestions for future works.

2 BATTERIES: CONCEPTS AND MODELS

Batteries are essential within the WSN context. These electrochemical devices keep the operation of the sensor nodes, allowing the monitoring and processing of data, as well as the communication through the network. However, batteries are complex devices since many effects influence their behaviour, e.g., rate capacity, recovery and thermal effects (FEENEY; ROHNER; LINDGREN, 2014).

The purpose of this chapter is to present the fundamental concepts about batteries (LINDEN; REDDY, 2001; MIT ELECTRIC VEHICLE TEAM, 2008; PANASONIC, 2015) in order to facilitate the understanding of the contents throughout this document. The sections of this chapter are divided as follows. Section 2.1 deals with the definition of several aspects about batteries, including basic characterization, operational modes, and terminology issues. Section 2.2 discusses battery technologies used in portable devices, particularly, within WSN context. Section 2.3 presents a classification of battery models, which are used to predict the behaviour of batteries in different operating conditions. Section 2.4 provides the final remarks of the chapter.

2.1 BATTERY BASICS

Batteries are devices capable of generating electricity. However, there are many complex concepts behind this simple definition. The basic theory regarding batteries is presented in this section, which includes the definition of a cell and other information about its design.

Although the term “battery” is often used, the basic electrochemical component is called a “cell”. A cell is formed of a series of components, such as terminals, electrodes, electrolyte, separator and enclosure (casing). Together, such components function as a source of energy, allowing the conversion of chemical energy into electrical energy through an oxidation-reduction reaction. Thus, a battery may be composed of one or more cells connected in series and/or parallel, depending on the application requirements on its output voltage and

charge capacity. In this document, the term "battery" is used in general, and the term "cell" is used only when it is necessary to make explicit the characteristics and internal components of the cell itself.

The main components of a cell are as follows:

1. **Anode**: the negative electrode, which provides electrons to the external circuit. This electrode undergoes oxidation during the electrochemical reaction.

2. **Cathode**: the positive electrode, which receives electrons from the external circuit. This electrode undergoes reduction during the electrochemical reaction.

3. **Electrolyte**: a medium that separates the electrodes and enables the transfer of charge (in the form of ions) inside the cell, between the anode and the cathode. The electrolyte may be a liquid or solid medium, depending on the design requirements of the cell.

In practice, a separator material is often added to prevent contact between the anode and the cathode and, therefore, prevent a short-circuit of the cell. However, such a separator must be permeable to maintain ionic conductivity in the cell. Other materials can also be added to the electrodes to decrease the internal resistance of the cell. Figure 1 depicts the components of an electrochemical cell.

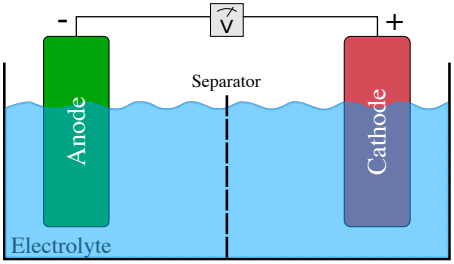

Figure 1 – Components of an electrochemical cell.

The combination of different materials for the cell components allows the development of batteries with different formats and characteristics (e.g., output voltage and charge capacity). However, such

materials must be chemically compatible to reduce, mainly, stability problems and costs, among other possible shortcomings.

A cell can assume several shapes: cylindrical, flat (or button) and prismatic. In these cases, it becomes necessary to adapt the shape of the internal components to ensure the safety of the cell, avoiding problems of leakage of gases or of the electrolyte itself (when in liquid state). Therefore, manufacturers often include ventilation systems in the design of cells to prevent such problems.

2.1.1 Cell and Battery Classification

Electrochemical cells are classified as primary or secondary, depending on their ability to reuse electrical energy. The difference between these terms is presented below.

A *primary cell* can convert chemical energy into electrical energy. However, it is not capable of performing the reverse process, i.e., converting electrical energy into chemical energy. In other words, primary cells can not be recharged; they can be used only once and shall be discarded after that. These type of cells are typically used in applications with moderate discharge rate requirements and are available in different formats (e.g., button or cylindrical). These cells are inexpensive and can be conveniently used in a wide range of portable devices, e.g., toys, cameras, radios, etc. This type of battery is also widely used in industrial and military applications, such as radars, night vision goggles, and laser sights. The main advantages of primary cells are good shelf life, high energy density, little or no maintenance and ease of use.

Conversely, a *secondary cell* is capable of converting electrical energy into chemical energy, i.e., receiving current in the opposite direction of the discharge process to re-establish the electronic equilibrium of its internal components, which gives it the ability to recharge. Thus, these type of cells can be reused countless times if handled appropriately. Note that the charge retention of these cells is usually worse than in primary cells. However, this is easily solved by recharging.

Secondary cells support high discharge rates and are generally

found in the same formats as the primary cells. Other interesting features are high energy density (usually lower than primary batteries), flat discharge curves and good performance even in low-temperature environments. They are often used in applications where the recharge process is performed after the use of the devices, such as smart-phones, laptops, and more recently, electric vehicles, where the required power level exceeds the capacity of primary cells. Thus, the long-term cost decreases when operating these types of devices.

The focus of this work is on secondary batteries. Therefore, from now on, the use of the term "battery" implies that we are dealing with electrochemical cells with recharge power.

2.1.2 Operating Modes of an Electrochemical Cell

An electrochemical cell supports two operating modes: discharge and recharge. Figure 2 depicts these two processes.

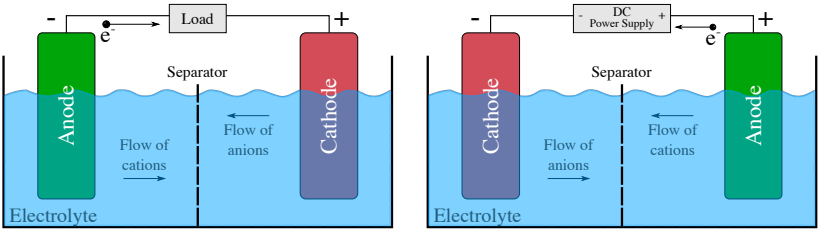

(a) Discharge. (b) Recharge (for secondary cells).

Figure 2 – Operating modes of an electrochemical cell.

Figure 2 (a) depicts the discharge process of an electrochemical cell. In this case, when an external load is connected to the cell, the electrons (e^-) move from the anode (which undergoes oxidation), through the external load, to the cathode (which is reduced), where they are absorbed due to the electronic attraction. The electric circuit is completed in the electrolyte through the flow of anions (negative ions) and cathodes (positive ions) between the electrodes. The following formulation is an example of an electrochemical reaction using the metal Zinc (Zn) as the anode and Chlorine (Cl_2) as the cathode:

- **Negative Electrode**: anodic reaction (oxidation, loss of e^-)

$$\mathrm{Zn} \longrightarrow \mathrm{Zn}^{2+} + 2\,e$$

- **Positive Electrode**: cathodic reaction (reduction, gain of e^-)

$$\mathrm{Cl}_2 + 2\,e \longrightarrow 2\,\mathrm{Cl}^-$$

- **Overall Reaction (discharge)**:

$$\mathrm{Zn} + \mathrm{Cl}_2 \longrightarrow \mathrm{Zn}^{2+} + 2\,\mathrm{Cl}^-(\mathrm{ZnCl}_2)$$

Figure 2 (b) depicts the process of recharging an electrochemical cell. In this case, the current direction is reversed so that the oxidation occurs at the positive electrode and the reduction occurs at the negative electrode. By definition, the oxidation occurs at the anode and the reduction at the cathode, so the positive electrode becomes the anode, and the negative electrode becomes the cathode. The reaction to recharge the $\mathrm{Zn}/\mathrm{Cl}_2$ cell is as follows:

- **Electrode Negative**: cathodic reaction (reduction, gain of e^-)

$$\mathrm{Zn}^{2+} + 2\,e \longrightarrow \mathrm{Zn}$$

- **Positive Electrode**: anodic reaction (oxidation, loss of e^-)

$$2\,\mathrm{Cl}^- \longrightarrow \mathrm{Cl}_2 + 2\,e$$

- **Overall Reaction (recharge)**:

$$\mathrm{Zn}^{2+} + 2\,\mathrm{Cl}^- \longrightarrow \mathrm{Zn} + \mathrm{Cl}_2$$

2.1.3 Terminology

This section introduces the basic terminology on battery theory, which includes expressions that are used throughout this document. The list below addresses terms related to voltage, charge capacity, and energy of a regular battery.

- **Nominal Voltage**: value associated with the battery to classify its standard operating voltage, in Volts (V). Note that a battery can operate within a voltage range and, generally, the nominal voltage is the midpoint of this range. For example, the nominal voltage of a Ni-MH battery is 1.2 V. However, the same battery can operate between 1.0 V and 1.4 V.

- **Open-Circuit Voltage**: the difference of electrical potential between the two terminals of the battery when disconnected from any load, also known as V_{OC} or Electromotive Force (EMF).

- **Cut-off Voltage**: the minimum operating voltage of a battery, also known as V_{cut}. At this point, the discharge is considered complete. Note that the cut-off voltage of a battery may be different from the cut-off voltage requirements of the connected electrical circuit.

- **Nominal Capacity**: the standard value for the amount of electricity which can be obtained from the battery with a full charge state, in Ampere-hour (Ah) or Coulomb (C). Generally, the nominal capacity is obtained by discharging the battery under a specific discharge current, temperature and cut-off voltage.

- **State of Charge (SoC)**: expression representing the actual battery charge capacity as a percentage of its maximum capacity, i.e., 100% = full and 0% = empty. Typically, the SoC is calculated by integrating the discharge current (i) over time, i.e., $\int i\, dt$.

- **Battery Lifetime**: the total time obtained by using the battery from its full charge (SoC = 100%, full) to its full discharge value (SoC = 0%, empty), i.e., the cut-off voltage.

- **C-Rate**: the unit used to normalize both the charging or discharging currents. This unit is relative to the nominal battery capacity, which can vary greatly according to the specification of each battery. For example, during battery discharge, a 1C rate means that the applied current discharges the battery in 1 hour. That is, the current required to discharge a battery with a nominal capacity of 1 Ah, in 1 hour, is equal to 1 A. Analogously, a 2C rate for the same battery means a discharge current equal to 2 A and the C/2 rate means a discharge current equal to 0.5 A.

- **High Rate Discharge**: expression used when a high current value is used to discharge the battery, compared to its nominal charge capacity. For example, considering a 1 Ah battery, a current of 0.8 A (0.8C) may already be considered a high discharge current.

- **Cycle**: a complete discharge of the battery, i.e., 100% of its nominal capacity. However, such a value can be achieved in more than one battery use. This means that the battery can be discharged from 100% to 50%, recharged completely, and then again discharged from 100% to 50%. In this case, one cycle is added to the battery history. Ni-MH batteries usually support up to 500 cycles while Li-ion batteries can reach up to 1000 cycles.

- **Specific Energy**: also known as *gravimetric energy density*, it represents the nominal battery energy per unit mass, usually in Wh/kg. In other words, specific energy indicates how much energy a cell contains compared to its mass. This energy is related to the electrochemical characteristics of the cell and its casing.

- **Energy Density**: also known as *volumetric energy density*, it represents the nominal battery energy per unit volume, usually in Wh/L. In other words, energy density indicates how much energy a cell contains compared to its volume. This energy is related to the electrochemical characteristics of the cell and its casing.

In addition to the nomenclature related to the capacity and voltage of the batteries, there are intrinsic effects that can affect any electrochemical cell. Such effects may be more noticeable in certain technologies since they depend on the characteristics of the electrochemical reactions between the internal components of the cells. The main intrinsic effects of the batteries are presented below.

- **Rate Capacity**: refers to the applied discharge current intensity. Larger discharge currents imply faster battery discharges, reducing its lifetime. This is due to the battery voltage level, which decays slowly during the discharge process, reducing the effective charging capacity provided by the battery for higher discharge currents (JONGERDEN; HAVERKORT, 2008).

- **Recovery Effect**: refers to the ability of a battery to partially recover its charge during an idle interval, between discharge periods. That is, it is possible to stabilize the electrochemical reactions inside the cell through a specific idle period, which depends on the battery technology. This allows a better use of available energy.

- **Self-Discharge**: a medium-term phenomenon that occurs mainly in secondary cells. Self-discharge is characterized by loss of battery capacity even if no load is applied to the external circuit.

- **Ageing**: a long-term effect that occurs by the natural use of the battery. The charge and discharge cycles cause the internal components of the cell to wear out. These damages are irreversible and cause the battery charge capacity loss over time.

- **Memory**: a long-term effect caused by the accumulation of crystals on the internal components of Ni-Cd batteries, mainly. The active Cadmium material is applied on the negative electrode plate with the incorrect use of the cell, which causes a crystalline formation and, consequently, reduces the performance of the cell.

2.2 TECHNOLOGIES

An “ideal” electrochemical cell would have the following characteristics: low cost, high energy density, support to provide all power levels, and the possibility to operate at any environmental condition. However, the current technology stage does not allow the development of an ideal electrochemical cell, since chemical reactions naturally cause irreversible physical changes in the components of the cell. Besides, the use of new technologies for the components of electrochemical cells requires precautions to avoid safety-related problems. Thus, there is still no such “ideal” battery that operates optimally in any condition.

Despite this, different applications require different operating characteristics, such as charge capacity, output voltage and resistance to withstand environmental adversities. This need influences the development of new technologies and battery formats, which in many cases are unique to meet specific operating conditions. Thus, many types of batteries have been investigated and supported over the last few years.

In the case of portable devices, including sensor nodes in WSNs, the demand for smaller and higher energy density batteries is increasing. Within this context, both the selection of the most effective battery and its appropriate use in the electronic device are critical factors to achieve better performances in each application. With the objective of covering such issues, Section 2.2.1 discusses the main criteria for selecting a battery, and Section 2.2.2 presents the main characteristics of the battery technology chosen for the development of this work.

2.2.1 Battery Selection Criteria

The process of choosing a battery for a given application involves many factors, which should be carefully evaluated to achieve the best results regarding battery usage. Choosing the battery technology during the development process of the portable device is also important, as this allows to extract the maximum capacity of the battery in the face of the requirements of each equipment. Thus, the following characteristics should be considered in the process of choosing a battery:

- **Battery Type**: primary or secondary;
- **Nominal Voltage**: minimum/maximum allowed voltage values;
- **Discharge Profile**: constant, variable or pulsed currents;
- **Duty cycle**: continuous or intermittent;
- **Temperature Requirements**: normal operating range;
- **Service Life**: Expected time of operation;
- **Format**: size, weight, dimensions, terminal type;
- **Charge-Discharge Cycle**: time needed to recharge;
- **Maintenance**: availability for acquisition/replacement/disposal;
- **Cost**: value per electrochemical cell, charger cost;
- **Environment conditions**: vibration, acceleration, pressure, etc.

The first item on the list, "battery type", is possibly the most decisive. The use of primary or secondary batteries is based on the trade-off between having a lower life-cycle cost (for secondary batteries, as they can be recharged and reused) or the convenience of using disposable batteries (for primary batteries). In this work, secondary (rechargeable) batteries are used for the following reasons. Although the charge capacity of secondary batteries is generally lower than conventional primary batteries, their performance under high discharge currents is better. In addition, secondary batteries perform best when used in low temperatures and have flatter discharge curves, which make them preferred for utilization in devices with critical operating voltage requirements (LINDEN; REDDY, 2001). Table 1 presents the key technologies of secondary batteries for portable devices.

Lead-Acid and Ni-Cd technologies are considered outdated in the context of portable devices, since they have little specific energy and suffer from the "memory" effect, respectively. The Li-ion battery, which was introduced commercially during the 1990s, presents greater energy density when compared to the other technologies. In addition,

Table 1 – Characteristics of secondary batteries for portable devices[†].

Characteristic	Battery Type			
	Lead-Acid	Ni-Cd	Ni-MH	Li-ion
Nominal Voltage (V)	2.0	1.2	1.2	3.7
Cut-off Voltage (V)	1.75	1.00	1.00	2.5–3.0
Specific Energy (Wh/kg)	30–50	45–80	60–120	100–150
Shelf Life, 20 °C (months)	6-9	3–6	3–6	9–12
Calendar Life (years)	3–8	4–6	4–6	5+
Cycle Life (cycles)	200–300	300–500	300–500	500–1000
Operating Temperature (°C)	–20 to 50	–20 to 65	–20 to 65	–20 to 60
Cost per Cell	Low	Moderate	Moderate	High

[†]<http://batteryuniversity.com/learn/article/secondary_batteries>. Accessed on May 23, 2017.

the cycle life of Li-ion batteries is much higher, reaching up to 1000 charge/discharge cycles. However, the cost per cell of this technology is significantly higher, hindering its adoption in large-scale WSNs. Another downside of Li-ion technology lies in the fact that it requires specific and usually more expensive chargers. Although not having the best characteristics, Ni-MH batteries present a good trade-off between its cost per cell and its charge capacity. Besides, the charger for this technology is inexpensive and widely available in the market. This work uses this technology for experimental assessments. Section 2.2.2 introduces in depth the Ni-MH technology.

2.2.2 Ni-MH Batteries

Recent portable devices require increasingly light, compact and high-density batteries. Ni-MH batteries are capable of providing a good balance between charge capacity and lifetime. In addition, this technology exhibits a high degree of reliability and safety, even when used in extreme temperatures (from –20 to 65 °C). This facilitates the adoption of Ni-MH batteries in a variety of applications, e.g., wireless communication devices, particularly, those used within the IoT/WSN context.

Ni-MH batteries consist of the following items: (i) positive plate containing Nickel hydroxide as the main active material; (ii) negative plate composed mainly of alloys for hydrogen absorption; (iii) separator

made of fine fibres; (iv) alkaline electrolyte, predominantly an aqueous solution of potassium hydroxide; (v) metal casing; and (iv) a sealing plate provided with a ventilation system for safety. Figure 3 depicts the structure of a regular Ni-MH battery.

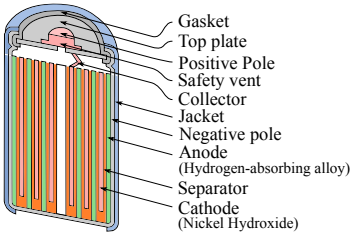

Figure 3 – Structure of Ni-MH batteries.

Briefly, the operating principle of Ni-MH batteries is described as follows. The overall reaction principle concerns the hydrogen movement from the positive to the negative electrode during the charging process, without the electrolyte taking part in the reaction. The opposite reaction occurs during the discharge process. The charge and discharge reactions are shown below (in this case, M is the hydrogen-absorbing alloy and H_{ab} is the absorbed hydrogen).

- **Positive electrode**:

$$Ni(OH)_2 + OH^- \underset{\text{Discharge}}{\overset{\text{Charge}}{\rightleftharpoons}} NiOOH + H_2O + e^-$$

- **Negative electrode**:

$$M + H_2O + e^- \underset{\text{Discharge}}{\overset{\text{Charge}}{\rightleftharpoons}} MH_{ab} + OH^-$$

- **Overall reaction**:

$$Ni(OH)_2 + M \underset{\text{Discharge}}{\overset{\text{Charge}}{\rightleftharpoons}} NiOOH + MH_{ab}$$

A Ni-MH battery presents five important characteristics: (i) the *charge* procedure is influenced by current, time and temperature, which modifies the battery voltage behaviour; this procedure can be speed-up

by higher currents or lower temperatures. Temperatures between 0 °C and 40 °C are suitable for charging, with a current of 1C or less; (ii) the *discharge* procedure is influenced by the same factors. In this case, the voltage curve is flat at 1.2 V (assuming only one electrochemical cell). However, the discharge voltage and discharge efficiency decrease as the current rises or the temperature drops; (iii) the *storage* for long periods of time often causes capacity losses due to the self-discharge effect, which is influenced by the temperature at which the battery is stored. Thus, self-discharge increases with higher temperatures or long storage periods; (iv) the battery *life cycle* depends on several factors, e.g., temperature, discharge current, storage conditions, etc. Generally, Ni-MH batteries can reach up to 500 recharge cycles, if used appropriately over time; (v) the *safety* of an electrochemical cell must be protected against overload, short circuit and reverse recharge. In the case of any of these events, the self-sealing vent is opened to prevent the battery damage.

From the concepts presented earlier in this section, in this thesis, the battery selection criteria should take into account the following restrictions: (i) low-power WSN nodes require the use of low-capacity batteries due to their weight and size constraints; (ii) batteries should withstand a wide range of operating temperatures, e.g., from –5 °C to 40 °C. (iii) batteries must support the operating modes with constant and intermittent currents since these profiles are the most common in WSNs that operate in a duty cycle scheme; (iv) the cost of the batteries should be low since the experiments require the purchase of several units to guarantee better results; (v) the format of the battery should be compatible with those used in low-power WSN nodes.

According to the above restrictions, the battery chosen for the experimental assessments in this work is manufactured by Panasonic (HHR-4MRT/2BB, Ni-MH, 2xAAA, 1.2 V, 750 mAh, rechargeable). This model meets the imposed requirements satisfactorily and can be easily found in the consumer market. Note that, the fact that the battery has a lower charge capacity does not mean a disadvantage, since this condition reduces the time of the experiments, making possible the execution of a larger number of tests.

2.3 BATTERY MODELS

Batteries are essential within the WSN context since these electrochemical devices guarantee the operation of the circuits in sensor nodes. However, many factors influence the battery operation. Thus, estimating their behaviour over time is a complex task. In this sense, battery models are abstractions that help estimate the behaviour of batteries in a variety of situations. With this, it becomes possible to understand which task has the greatest influence on the operation of the batteries in each application, which allows extending their lifetime with only a few adjustments in the use of available resources.

Many battery models have been proposed in recent years. However, only a few of them can be used within the WSN context. The objective of this section is to present the main types of battery models and justify their use in WSNs, which require the use of optimised solutions regarding battery modelling. Thus, this section presents the following types of battery models: (i) empirical; (ii) electrochemical; (iii) electrical; (iv) analytical; (v) stochastic; and (vi) hybrids. A comparison of these battery models is presented at the end of this section.

2.3.1 Empirical Battery Models

Empirical battery models are fairly simple, however, inaccurate in general. In this context, the best-known model is the Peukert's Law, which considers only part of the non-linear effects of the batteries. Details on this battery model are given below.

In the mid-1890s, the German scientist Wilhelm Peukert conducted a series of experimental tests on Lead-Acid batteries using constant discharge currents. The results indicated that a simple equation was sufficient to relate the capacity and the discharge rate to any Lead-Acid battery (DOERFFEL; SHARKH, 2006):

$$L = \frac{a}{I^b}, \tag{2.1}$$

where L is the lifetime of the battery, I is the discharge current, a and b are constants that depend on the type of the used battery. Ideally,

a is equal to the battery capacity and $b = 1$. In practice, however, a usually has a value close to battery capacity and $b > 1$. This means that the battery capacity decreases with increasing discharge rates.

On the other hand, Peukert's Law does not model the recovery effect of batteries. This means that the results regarding battery lifetime with this approach are only valid for constant discharge currents, being unsuitable for variable or intermittent discharge currents (JONGERDEN; HAVERKORT, 2008). Thus, it is infeasible to use the Peukert's Law within the WSN context, since nodes generally operate on a duty cycle basis, i.e., applying intermittent discharge currents over time (LAJARA; PEREZ-SOLANO; PELEGRÍ-SEBASTIA, 2015).

2.3.2 Electrochemical Battery Models

Electrochemical battery models are based on the chemical processes that occur inside the electrochemical cells. This type of approach models the characteristics of the batteries in a very detailed way, which makes this type of model the most accurate.

An example of an electrochemical model is the software Dualfoil (NEWMAN, 1998), a FORTRAN program that models Lithium batteries through six coupled non-linear differential equations. The output of the program allows the evaluation of a series of information, such as voltage and current as a function of time, as well as salt concentration, reaction rate, etc. Thus, this software is able to compute all the changes in the properties of the batteries over time, which allows obtaining their lifetime according to the discharge profile configured by the user (JONGERDEN; HAVERKORT, 2008). Dualfoil is used as a basis for comparing battery models in some scientific studies (RAKHMATOV; VRUDHULA; WALLACH, 2002; RONG; PEDRAM, 2006; PARK; LAHIRI; RAGHUNATHAN, 2005).

Although the electrochemical models consider the physiochemical characteristics of the batteries with great detail, the number of parameters necessary for the use of this type of model is very large, approximately 50 in the case of Dualfoil. Such parameters require

technical knowledge about the chemical composition of the batteries, e.g., electrode thickness, initial electrolyte salt concentration, and total heat capacity. In addition, the solution of non-linear differential equations requires high computational power. This makes it infeasible to implement this type of model in WSN nodes, which are known to use micro-controllers with low computational capacity (ROHNER; FEENEY; GUNNINGBERG, 2013).

2.3.3 Electrical Battery Models

This approach is based on electrical circuits to model the behaviour of batteries. This means that electrical components are used in the construction of the battery model, for example, voltage sources, resistors, capacitors, etc. Generally, capacitors represent the capacity of the battery, resistors represent the internal resistance of the battery, and the complete circuit serves to drain the battery charge. Besides, lookup tables containing a relationship between the battery voltage level and its SoC are commonly used as a reference to feeding the electric model. Figure 4 illustrates an example of an electric battery model.

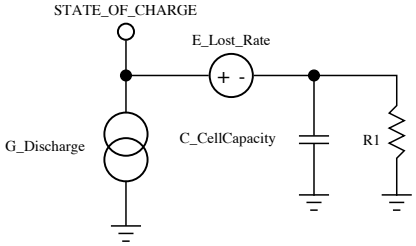

Figure 4 – Electrical battery model (JONGERDEN, 2010).

The advantage of using this approach is that the technical designs of electric models are intuitive for electro-technical professionals. In addition, these models are simpler than the electrochemical models and, therefore, computationally less expensive.

On the other hand, the electrical models still require a configuration effort, since lookup tables require the execution of several ex-

perimental tests for an overview on the behaviour of the used battery. In addition, electric models may be more inaccurate for calculating battery lifetime, reaching errors of up to 12% (JONGERDEN, 2010).

2.3.4 Analytical Battery Models

Analytical battery models are mathematical formulations that describe the properties of batteries using only a few equations (JONGERDEN; HAVERKORT, 2008). These models allow estimating the lifetime of batteries according to the applied discharge profile. In addition, these models become computationally flexible, since they involve the evaluation of analytic expressions (SCHNEIDER; SAUSEN; SAUSEN, 2001). Thus, it becomes possible to use both constant or variable[1] discharge currents, or to change the type of battery.

The main advantage of the analytical battery models is that they consider the main electrochemical effects inherent to the batteries, such as the Rate Capacity and Recovery effects. Three examples of analytical models available in the literature are presented below.

2.3.4.1 Diffusion Model

One of the most cited analytical models in the literature is the Diffusion Model, which describes the process of diffusion of the active material in the battery at a high level of abstraction (RAKHMATOV; VRUDHULA, 2001). In this case, the purpose is to extend the Peukert's Law. Some details about this model are presented below.

The Diffusion Model considers the diffusion process in one dimension in the region of length w of the electrochemical cell, as depicted in Figure 5. Note that $C(x,t)$ is the concentration of the active material in time t with the distance $x \in [0,w]$ of the electrode. The battery lifetime is defined when the concentration of the electro-active species on the surface of the electrode, $C(0,t)$, drops below the level of C_{cut}. Thus, the diffusion process in one dimension can be described by the Fick's Law (RAKHMATOV; VRUDHULA, 2001):

[1] Actually, piecewise constant discharge currents.

$$\begin{cases} -J(x,t) & = D\frac{\partial C(x,t)}{\partial x}, \\ \frac{\partial C(x,t)}{\partial t} & = D\frac{\partial^2 C(x,t)}{\partial x^2}, \end{cases}$$

where $J(x,t)$ is the flux of the active material in time t and position x, and D is the diffusion constant. According to the Faraday's Law, the flow at the left boundary of the diffusion region ($x = 0$) is proportional to the current $i(t)$, and the flow at the right boundary region ($x = w$) is zero. Thus, the following limit condition can be established:

$$\begin{cases} D\frac{\partial C(x,t)}{\partial x}\,|_{x=0} & = \frac{i(t)}{\nu \cdot F \cdot A_e}, \\ D\frac{\partial C(x,t)}{\partial x}\,|_{x=w} & = 0, \end{cases}$$

where A_e is the surface area of the electrode, F is the Faraday constant (96485.31 C·mol^{-1}), and ν is the number of electrons involved in the electrochemical reaction on the surface of the electrode.

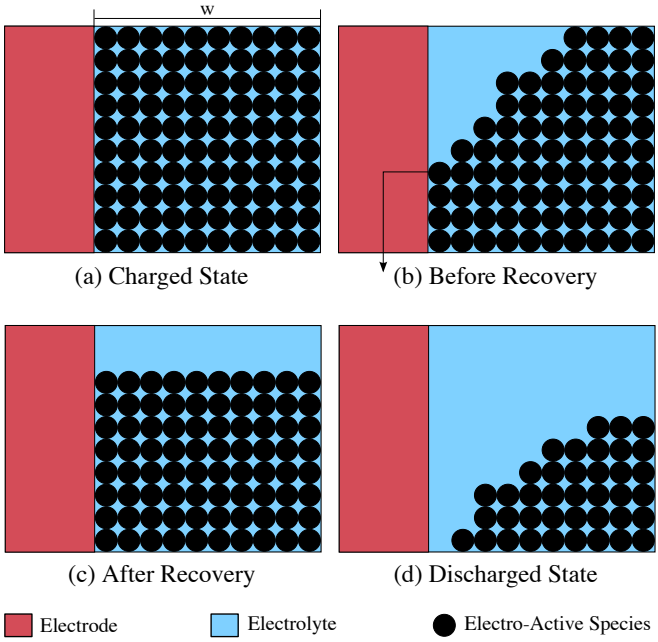

Figure 5 – Diffusion process (JONGERDEN; HAVERKORT, 2008).

By using Laplace Transforms, it becomes possible to obtain an analytical solution from these partial differential equations and boundary conditions. Thus, the load, the lifetime (L) and the battery parameters can be related through the following equation:

$$\alpha = \int_0^L \frac{i(t)}{\sqrt{L-\tau}} \cdot d\tau + 2\sum_{m=1}^{\infty} \int_0^L \frac{i(t)}{\sqrt{L-\tau}} \cdot e^{-\frac{\beta^2 \cdot m^2}{L-\tau} \cdot d\tau}, \tag{2.2}$$

where $\alpha = \nu \cdot F \cdot A \cdot \sqrt{\pi \cdot D} \cdot C^* \cdot \rho(L)$, $\beta = \frac{w}{\sqrt{D}}$, C^* is the concentration in $t = 0$, and $\rho(L) = 1 - \frac{C(0,L)}{C^*}$. Equation (2.2) can be simplified by considering the case in which the discharge current (I) is constant:

$$\alpha = 2 \cdot I \cdot \sqrt{L} + 2\sum_{m=1}^{\infty} \left(\sqrt{L} \cdot e^{-\frac{\beta^2 \cdot m^2}{L}} - \beta \cdot m \cdot \sqrt{\pi} \cdot \Phi\left(\frac{\beta \cdot m}{\sqrt{L}}\right)\right),$$

where $\Phi(x) = 1 - \frac{2}{\sqrt{\pi}} \cdot \int_0^x e^{-y^2} \cdot dy$. A good approximation for α can be obtained by using the first ten terms of the infinite sum. Together with an approximation to Φ, the result can be observed in Equation (2.3).

$$\alpha = 2 \cdot I \cdot \sqrt{L} \left[1 + 2\sum_{m=1}^{10} \left(e^{-\frac{\beta^2 \cdot m^2}{L}} - \frac{\pi \cdot e^{-\frac{\beta^2 \cdot m^2}{L}}}{\pi - 1 + \sqrt{1 + \pi \cdot \frac{L}{\beta^2 \cdot m^2}}} \right) \right], \tag{2.3}$$

where α is the battery capacity and β represents the non-linearity in battery behaviour. Both parameters can be obtained from experimental data. Thus, the lifetime of the battery (L) can be estimated for a given constant discharge current (I).

In the results for constant continuous loads, this model achieves an average error of 3%, with a maximum error of 6% (when compared to simulation results in Dualfoil software). Alternatively, Peukert's Law achieves an average error of 14%, with a maximum error of 43%. For variable and intermittent loads, the Diffusion Model reaches an average error value less than 1%, with a maximum error value of 2.7% (RAKHMATOV; VRUDHULA, 2001).

2.3.4.2 Kinetic Battery Model (KiBaM)

KiBaM is an analytical battery model that considers the behaviour of high-capacity Lead-Acid batteries (MANWELL; MCGOWAN, 1993; MANWELL; MCGOWAN, 1994; MANWELL et al., 1994). This model uses an intuitive approach, based on a two tank analogy, to describe the charge and discharge processes. Figure 6 illustrates the abstraction used by the KiBaM model, including its related variables.

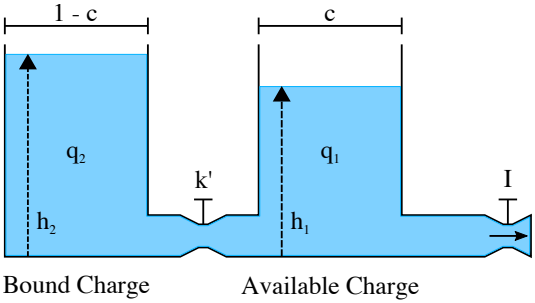

Figure 6 – KiBaM (MANWELL; MCGOWAN, 1993).

In this model, the *Available Charge* tank is the power supply for any device that consumes a current over time, $I(t)$. Note that the average value of I should be considered for each time period t. The *Bound Charge* tank holds a bounded charge that can flow towards the Available Charge tank, regulated by a valve with a fixed conductance k'. Such constant corresponds to the rate of a chemical diffusion/reaction process. The transfer of charge occurs as long as there is a height difference between the charges of both tanks, i.e., $\delta = h_2 - h_1 \neq 0$. The constant c indicates the total charge ratio stored in the Available Charge tank. The battery remains operational as long as there is charge in the Available Charge tank, regardless of whether there is charge in the Bound Charge tank or not. The following system of differential equations describes the KiBaM model:

$$\begin{cases} \frac{dq_1}{dt} = -I + k' \cdot (h_2 - h_1) \\ \frac{dq_2}{dt} = -k' \cdot (h_2 - h_1), \end{cases} \tag{2.4}$$

where q_1 and q_2 represent the charge in both the Available and Bound Charge tanks, respectively. The height values are calculated as $h_1 = \frac{q_1}{c}$ and $h_2 = \frac{q_2}{(1-c)}$. A new rate constant is defined as follows:

$$k = \frac{k'}{c \cdot (1-c)}. \tag{2.5}$$

Substituting h_1, h_2 e k' in the System of Differential Equations (2.4), it becomes possible to obtain the following:

$$\begin{cases} \frac{dq_1}{dt} = -I - k \cdot (1-c) \cdot q_1 + k \cdot c \cdot q_2 \\ \frac{dq_2}{dt} = +k \cdot (1-c) \cdot q_1 - k \cdot c \cdot q_2. \end{cases} \tag{2.6}$$

Laplace transforms can be used to solve this system of differential equations (MANWELL; MCGOWAN, 1993). Thus:

$$\begin{cases} q_1 = q_{1,0} \cdot e^{-k \cdot t} + \frac{(q_0 \cdot k \cdot c - I) \cdot (1 - e^{-k \cdot t})}{k} - \frac{I \cdot c \cdot (k \cdot t - 1 + e^{-k \cdot t})}{k} \\ q_2 = q_{2,0} \cdot e^{-k \cdot t} + q_0 \cdot (1-c) \cdot (1 - e^{-k \cdot t}) - \frac{I \cdot (1-c) \cdot (k \cdot t - 1 + e^{-k \cdot t})}{k}, \end{cases} \tag{2.7}$$

where $q_{1,0}$ and $q_{2,0}$ are the amount of charge in the Available and Bound Charge tanks, respectively, when $t = 0$. In this case, $q_0 = q_{1,0} + q_{2,0}$, where q_0 is the amount of charge in the battery at $t = 0$.

In the KiBaM model, the unavailable charge (u) is given by Equation (2.8), where δ is the difference between heights (JONGERDEN, 2010). Equation (2.9) describes how to compute this difference (JONGERDEN; HAVERKORT, 2009).

$$u = (1-c) \cdot \delta \tag{2.8}$$

$$\delta = (h_2 - h_1) = \frac{q_2}{(1-c)} - \frac{q_1}{c}. \tag{2.9}$$

The reasoning behind the use of δ is to capture the non-linear capacity variation of the battery (GANDOLFO et al., 2015). Thereby, KiBaM can model both the rate capacity and recovery effects of batteries. The non-linear battery behaviour is highly visible, particularly,

when these two effects act together. This is the case of batteries powering-up WSN nodes that operate in duty cycle scheme, i.e., shorter periods during which the radio is in normal operation (high discharge currents), and longer periods during which it is in a low power or sleep mode (low discharge currents).

A great advantage of KiBaM lies in the fact that it requires few constants to model the behaviour of different electrochemical cells, unlike other battery models. The constants required for the use of the KiBaM model are: q_{max} (the maximum charge capacity of the battery), c (a fraction of the charge capacity stored in the Available Charge tank) and k (the rate constant). These constants may be obtained in two ways: (i) by actual battery discharge testing, as presented in (MANWELL; MCGOWAN, 1993); or (ii) from the battery data-sheet, since such a document usually contains at least three results with different discharge currents. Thus, the KiBaM model can be used in analytical assessments to determine the battery SoC, by using $SoC = \frac{q_1(t)}{q_{1,0}} \cdot 100$.

Furthermore, the KiBaM model is also able to track the battery voltage (V) over time (MANWELL; MCGOWAN, 1993). In this case, it is necessary to consider the internal resistance of the battery, R_b:

$$V = E - I \cdot R_b, \tag{2.10}$$

where E is the internal voltage of the battery. For the battery discharge case, the following equation must be used:

$$E = E_{min} + (E_{0,d} - E_{min}) \frac{q_1}{q_{max}}, \tag{2.11}$$

where E_{min} is the minimum allowed internal discharge voltage ("empty"), $E_{0,d}$ is the maximum internal discharge voltage ("full"), and q_{max} is the maximum capacity of the Available Charge tank. The internal resistance, R_b, can be experimentally determined using constant discharge currents. Its value is represented by the slope dV/dI, when the battery is fully charged, i.e., plotting $V \times I$ and finding the slope gives R_b (MANWELL; MCGOWAN, 1993).

2.3.4.3 Battery Dynamic Model (BDM)

Tremblay and Dessaint (TREMBLAY; DESSAINT; DEKKICHE, 2007; TREMBLAY; DESSAINT, 2009) developed a Battery Dynamic Model for different battery technologies, e.g., Lead-Acid, Ni-MH, Ni-Cd and Li-ion. Although this model is able to handle both charge and discharge curves for each battery type, only the Ni-MH battery discharge model is presented in this thesis.

The BDM can accurately represent the voltage dynamics with varying current values. Besides, it considers the Open-Circuit Voltage (OCV) as a function of the battery SoC. Therefore, the battery voltage may be obtained as follows:

$$V_b = E_0 - K_b \cdot \frac{Q}{Q - it} \cdot it - R_b \cdot i + A_b \cdot e^{(-B \cdot it)} - K_b \cdot \frac{Q}{Q - it} \cdot i^*, \quad (2.12)$$

where V_b is the battery voltage (V), E_0 is the battery constant reference voltage (V), K_b is the polarization resistance (Ω), Q is the battery capacity (Ah), $it = \int idt$ is the actual battery charge (Ah), A_b is the exponential zone amplitude (V), B is the exponential zone time constant inverse $(\text{Ah})^{-1}$, R_b is the internal resistance (Ω), i is the discharge current (A) and i^* is the filtered current (A).

Equation (2.12) is valid only for Li-ion batteries, as it presents an exponential term that is not observed in other battery types, such as Lead-Acid, Ni-MH and Ni-Cd. These batteries exhibit a hysteresis phenomenon between the charge and discharge processes, which occurs only at the beginning of the discharge curve, regardless of their SoC. This phenomenon can be represented by a non-linear dynamic system:

$$\dot{Exp}(t) = B \cdot |i(t)| \cdot (-Exp(t) + A_b \cdot u(t)), \quad (2.13)$$

where $Exp(t)$ is the exponential zone voltage (V), $i(t)$ is the discharge current (A) and $u(t)$ is the charge/discharge mode. The exponential voltage relies on its initial value $Exp(t_0)$ and the charge ($u(t) = 1$) or discharge ($u(t) = 0$) mode.

Briefly, the final form for the discharge equation of the voltage model for Ni-MH and Ni-Cd batteries is as follows:

$$V_b = E_0 - R_b \cdot i - K_b \cdot \frac{Q}{Q - it} \cdot (it + i^*) + Exp(t). \tag{2.14}$$

Note that this voltage model presents an inconsistency at the end of the analytical evaluation (cf. Figure 4 of (TREMBLAY; DESSAINT, 2009)), where the following problems arise: (P1) the analytical lifetimes are smaller than the experimental lifetimes at the battery voltage cut-off point; and (P2) the model may return voltage values below zero for time instants close to the end of the analytical evaluation.

2.3.5 Stochastic Battery Models

Stochastic battery models describe the main effects that influence the batteries in an abstract way, similar to the analytical battery models, however, with the difference that the battery behaviour is modelled as a stochastic process. Two examples of this type of battery model are shown below.

2.3.5.1 Chiasserini and Rao Model

The Chiasserini and Rao battery model is based on discrete-time Markov chains (CHIASSERINI; RAO, 1999). In this case, the battery is described by a Markov chain with $N+1$ states, numbered from 0 (N_s represent the start of discharge), as depicted in Figure 7.

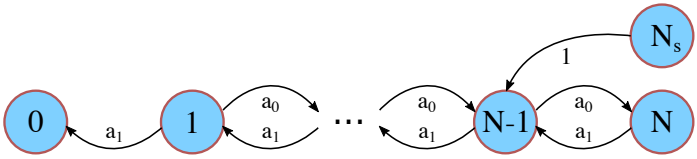

Figure 7 – Binary Markov Chain (CHIASSERINI; RAO, 1999).

The state number corresponds to the number of charge units available on the battery. One charge unit corresponds to the energy required to transmit a single packet since the main application of this

battery model is for mobile device communication. In addition, N is the number of directly available charge units based on continuous use.

In this model, at each time step, either one charge unit can be consumed with a probability of $a_1 = q$ or the recovery of one charge unit can be performed with a probability of $a_0 = 1 - q$. The battery is considered discharged when the 0 state is reached or if a maximum amount of charge T has been consumed from the battery. Note that the number of T charge units is equal to the theoretical capacity of the battery.

In the same paper, Chiasserini and Rao extended their battery model. The difference was that the extended model allows the discharge of more than one unit of charge at each time step, with a maximum of M units of charge ($M \leq N$). In addition, there was a non-zero probability of remaining in the same state. In other words, the processes of discharge or recovery might not occur at a particular time step.

Other papers of these authors have improved such a battery model (CHIASSERINI; RAO, 1999; CHIASSERINI; RAO, 2000; CHIASSERINI; RAO; MEMBER, 2001). For example, the authors have (i) made charge recovery state dependent, (ii) decreased the probability of recovering a unit of charge when the battery is low, and (iii) used their approach to model the behaviour of Li-ion batteries.

The results of the stochastic model showed a maximum deviation of 4% when compared to electrochemical models, with an average deviation of 1% (JONGERDEN; HAVERKORT, 2008). On the other hand, since this is a stochastic model, it becomes difficult to adjust the Markov chains to model constant discharge currents due to the fact the order in which the transitions occur can not be controlled.

2.3.5.2 Stochastic Modified KiBaM

Another stochastic battery model was proposed by Rao et al. (RAO et al., 2005). Such an approach was based on the KiBaM model to represent the behaviour of the battery through a discrete time transient Markov process, as depicted in Figure 8.

The model was adjusted to handle Ni-MH batteries, rather than

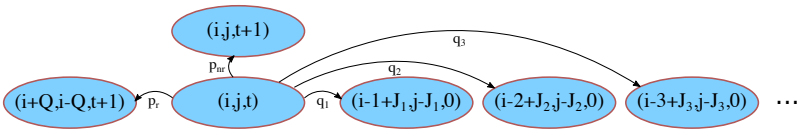

Figure 8 – KiBaM Markov Chain (CHIASSERINI; RAO, 1999).

Lead-Acid batteries as in the original KiBaM. This stochastic model also allows no recovery effect to be added during idle periods.

In this case, the states of the Markov chain are labelled according to three parameters: i and j are the discretised charge quantities stored in the Available and Bound Charge tanks, respectively, and t is the number of time steps since in which a current has been drained from the battery. Transitions occur as follows:

$$(i,j,t) \rightarrow \begin{cases} (i+Q, j-Q, t+1) \\ (i,j,t+1) \\ (i-I+J, j-J, 0), \end{cases} \tag{2.15}$$

The first two conditions correspond to the case where the current is zero. In these cases, there is the probability p_r of the battery to recover Q units of charge or the probability p_{nr} of no recovery occurs. Both p_r and p_{nr} depend on the length of the idle time slot (t). The third condition represents the time steps where a current has been drained from the battery. With probability q_I, I charge units are drained from the Available Charge tank and, at the same time, J charge units are transferred from the Bound Charge tank to the Available Charge tank.

The results of simulations with the stochastic model showed that this approach was quite accurate to estimate both the lifetime and the drained charge of the battery. The maximum error obtained was 2.65%. However, in order to model a Ni-MH battery, it becomes necessary to discretise the contents of the Available and Bound Charge tanks at $45 \cdot 10^7$ and $27 \cdot 10^7$ charge units, respectively. This generates a Markov chain so large that it can not be entirely treated. Thus, no analytical solution can be generated by the model. In other words, several bat-

tery discharge processes must be simulated to obtain a practical result regarding the battery lifetime (JONGERDEN; HAVERKORT, 2008).

2.3.6 Hybrid Battery Models

Hybrid battery models integrate one or more types of battery models into a single approach. The model developed by Kim and Qiao (KIM; QIAO, 2011) can be cited as an example. In this case, the behaviour of the battery is modelled using both the analytical and electric approaches. Figure 9 depicts the mentioned battery model.

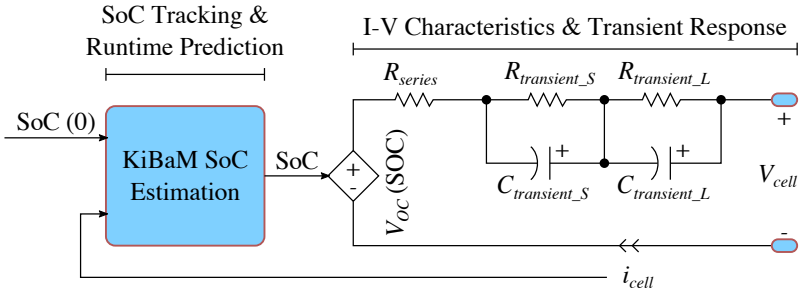

Figure 9 – Hybrid Battery Model (KIM; QIAO, 2011).

This battery model uses an electric model to predict the dynamic circuit characteristics of the battery and the KiBaM analytical model to capture the non-linear effects that influence the estimation of both the SoC and lifetime of the battery. In this case, RC circuits define the transient responses to load changes. The circuit parameters define the voltage of the cell (V_{cell}) and the transient response, which is given by the time constants $\tau_S = R_{transient\_S} \cdot C_{transient\_S}$ and $\tau_L = R_{transient\_L} \cdot C_{transient\_L}$, representing the short- and long-term responses, respectively. Thus, the cell voltage can be calculated as:

$$V_{cell}(t) = V_{OC}(SOC) - i_{cell}(t) \cdot R_S - V_{transient}(t). \tag{2.16}$$

Such a battery model presents interesting results in relation to the SoC tracking and the estimation of the battery lifetime. However, the use of this hybrid battery model requires knowledge of up to 28

parameters, which slows down the simulation process. In addition, the effect of temperature is not considered in this approach. For these reasons, the use of this battery model is not indicated in the context of WSNs (ROHNER; FEENEY; GUNNINGBERG, 2013).

2.3.7 Battery Models Overview

Rao et al. (RAO; VRUDHULA; RAKHMATOV, 2003) and Jongerden and Haverkort (JONGERDEN; HAVERKORT, 2008) have provided an overview of battery models used in the context of mobile devices. Some information has been added to better describe the aspects addressed in this thesis, as presented in Table 2 (at the end of this chapter).

2.4 CHAPTER REMARKS

As discussed in this chapter, batteries are complex electrochemical devices. The composition of electrochemical cells directly influences the characteristics of the battery, such as output voltage, charge capacity, etc. This should be taken into account when designing battery-powered devices. The focus of this work is on secondary batteries which, despite providing a smaller amount of effective charge (compared to primary batteries in general), have a much longer cycle life, making its cost-effectiveness more advantageous in long-term use.

In addition, several factors can influence the operation of the batteries, such as discharge rate, temperature and even the "age" of the electrochemical cell. In this context, the battery type (technology, format, capacity, etc.) should be selected according to the requirements of each application to minimise such influences during the use of the batteries. Ni-MH batteries were chosen for the experimental assessments in this work. Although Ni-MH technology does not have the best characteristics in terms of energy density, cycle counting, and shelf life, both batteries and chargers for this technology can be easily found in the consumer market at a lower cost, when compared to Li-ion bat-

teries. This is welcome in the context of this work since several units of these electrochemical cells are used in the experimental assessments.

Finally, this chapter presented the main types of battery models. Note that only a few of them can be used within WSN context, since sensor nodes have scarce resources (e.g., low processing power, low memory, limited energy). For example, electrochemical models are extremely accurate, however, highly demanding from the point of view of computational complexity. In this sense, this work seeks to use a balanced approach, i.e., a computationally simple and precise battery model. This is necessary so that the battery models should be used both (i) embedded in real sensor nodes and (ii) implemented in WSN simulators in order to support different energy-aware approaches.

According to the literature (JONGERDEN; HAVERKORT, 2008; JONGERDEN; HAVERKORT, 2009; ROHNER; FEENEY; GUNNINGBERG, 2013), the analytical battery models meet these requirements. Thus, these battery models receive special attention in this thesis, particularly the KiBaM model. In Table 2, note that the model KiBaM presents high accuracy to estimate the behaviour of the batteries and has a medium computational complexity, however, its original version was used only in Lead-Acid batteries and the thermal effect was not considered in its development. Thus, it was verified the opportunity for a scientific contribution through the implementation of the thermal effect in this battery model, as well as its evaluation to model the behaviour of Ni-MH batteries. Another promising contribution concerns the evaluation of this battery model in micro-controllers with low computational capacity for specific use in WSN nodes.

Note that KiBaM is already a fairly accurate battery model with respect to the estimated lifetime of the battery. However, its voltage model was developed only for Lead-Acid batteries and is unsuitable for newer battery technologies (e.g., Ni-MH and Li-ion). In this context, the present thesis has an additional challenge of adding to the KiBaM a voltage model suitable for other battery technologies.

Table 2 – Battery models overview.

Type	Model	Battery	R.C.E.†	R.E.‡	T.E.§	Pars.¶	C.C.♣	Accuracy
Empirical	Peukert	All	+	-	-	2	Low	medium (14% error)
Electrochemical	Dualfoil	Li-ion	+	+	+	>50	High	very high
Electrical	Hageman	Ni-Cd, Alkaline, Lead-Acid	+	+	+	15-30	Medium	medium (10% error)
Analytical	Diffusion	Li-ion	+	+	-	2	Medium	high (5% error)
	KiBaM	Lead-Acid	+	+	-	2	Medium	high (3% error)
Stochastic	Chiasserini	Li-ion	-	+	-	2	Low	high (1% error)
	KiBaM (Markov)	Ni-MH	+	+	-	2	Low	high (2% error)
Hybrid	Kim and Qiao	Li-ion, Lead-Acid	+	+	-	28	High	high

†**R.C.E.** = Rate Capacity Effect; ‡**R.E.** = Recovery Effect; §**T.E.** = Thermal Effect; ¶**Pars.** = Parameters; ♣**C.C.** = Computational Complexity.

3 RELATED WORK

This chapter presents the main research on battery models, including their applications in areas other than WSNs, such as electric-vehicle batteries. The criteria used in surveying the theoretical reference are also described in this chapter.

3.1 SEARCH CRITERIA

In June 2017, we performed an extensive search for terms related to this thesis by using Google Scholar, as this platform encompasses several scientific databases, such as IEEE Xplore and Scopus.

The search included the following terms: (i) “battery model”; (ii) “temperature”; (iii) “wsn”; and (iv) “simulator”. Particularly, the first search addressed the combination between terms (i) and (ii), which returned approximately 11700 results. The first 30 articles in order of relevance were analysed for this review. Since the first search returned a large number of entries, item (iii) was included in the search. The number of entries has been reduced to approximately 435 articles. In this case, all entries were analysed. Only items (i), (iii) and (iv) were searched in the last survey, which returned approximately 436 entries. These resulting articles were analysed by removing the repeated entries.

By observing the results obtained in these surveys, a classification scheme (based on the analysed articles) was created to describe the content of this chapter, as illustrated in Figure 10.

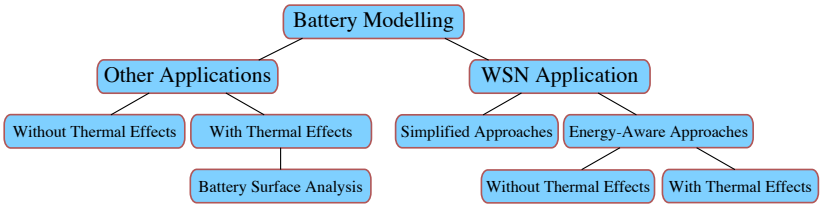

Figure 10 – Battery models and their applications.

3.2 BATTERY MODELLING: APPLICATIONS

Battery models can be used in a wide range of applications. In this section, the application of battery models is classified in two categories (cf. Figure 10): those used in WSN context and those used in other types of applications.

The use of battery models in the context of Electric Vehicles (EVs) and Hybrid Electric Vehicles (HEVs) is one of the most recurrent applications. This subject has been deeply studied in recent years by the scientific community since EVs/HEVs are expected to become popular in the near future. In this context, battery models can be divided in two ways: (i) temperature-independent battery models; and (ii) temperature-dependent battery models.

The first case deals with research papers that do not take into account the effects caused by temperature on battery behaviour (CHAN; SUTANTO, 2000; HU et al., 2009; HSIEH; CHIU; WU, 2016). For instance, Manwell and McGowan (MANWELL; MCGOWAN, 1993) proposed a battery model based on the concepts of chemical kinetics that addresses two intrinsic battery effects, i.e., rate capacity and recovery. However, the voltage model used is linear and valid only for Lead-Acid batteries. Tremblay et al. (TREMBLAY; DESSAINT; DEKKICHE, 2007) developed other relevant battery model. The proposed voltage model can be applied in dynamic simulation software since the results are valid for Lead-Acid, Ni-MH and Lithium batteries. Although modelling the discharge curve ($V \times t$) of these battery technologies adequately, the Tremblay model presents an imprecision in the final third of the discharge curve. This may lead to an error in estimating the battery lifetime, which is important for some applications.

The second case deals with research papers that consider the thermal effect, i.e., the influence of temperature on battery behaviour (GUASCH; SILVESTRE, 2003). Several studies have proposed temperature-dependent battery models in the context of EVs since this is a fundamental factor during the use of this type of vehicle (KROEZE; KREIN, 2008; AGARWAL et al., 2010; HU et al., 2011; BENABDE-

LAZIZ; MAAROUFI, 2017). Another important factor in an EV is the battery SoC, which is also influenced by temperature. In this context, the battery SoC allows the driver to determine the distance that can be travelled according to the current consumption profile of the vehicle (JIANI et al., 2014; GREENLEAF et al., 2015; CHEN et al., 2016; MOTAPON et al., 2016; GAO et al., 2017; BARCELLONA; GRILLO; PIEGARI, 2017). Some studies also evaluate other characteristics of batteries in EVs, such as the state of discharge and state of health (LIU et al., 2017; SANGWAN et al., 2016; LI; SOONG; TSENG, 2017).

Generally, batteries in EVs/HEVs occupy much space of the vehicle's chassis. The temperature in each part of the chassis tends to vary due to interactions with other components of the vehicle or to the environment itself (PESARAN, 2002). This may change the behaviour of the batteries in a distributed way, i.e., the batteries in the front of the vehicle behave differently from the batteries in the rear of the vehicle. Recent works propose battery models to deal with these issues (MAJDABADI et al., 2015), allowing to evaluate the influence of temperature along the entire surface of the battery (PANCHAL, 2016; ANYAEGBUNAM, 2016; ZHANG et al., 2016; ASHWIN; CHUNG; WANG, 2016; RAMOTAR et al., 2017; CICCONI; LANDI; GERMANI, 2017; MEHNE; NOWAK, 2017). However, the complexity of these battery models makes their use infeasible in the context of WSNs as several parameters must be used to treat the components of electrochemical cells. Thus, battery models with a balanced trade-off between complexity and accuracy should serve as an alternative for use in WSNs.

Battery models are also widely used in WSN applications. In this case, as shown in Figure 10, the applications can be divided into: (i) simplified approaches; and (ii) energy-aware approaches.

The simpler approaches use only linear battery models, i.e., those that do not consider the influences of the main intrinsic effects that can modify the behaviour of batteries, such as the rate capacity, recovery and temperature (ARON; GIRBAN; KILYENI, 2011). For example, Förster and Murphy (FÖRSTER; MURPHY, 2010) proposed a machine learning-based multicast routeing paradigm called FROMS. Ac-

cording to the authors, such an approach is flexible to optimise routeing over several properties, such as route length, battery level, and ease of recovery after sensor node failures. The work of Gaudette et al. (GAUDETTE et al., 2012) investigated the problems involved in controlling a WSN powered by secondary batteries and solar energy. In this case, the objective is to maximise the quality of network coverage. However, the battery model used is linear, both for charge and discharge of the battery, i.e., there is no loss or leakage of energy. Finally, Dron et al. (DRON; HACHICHA; GARDA, 2013) presented a power estimation technique for WSN nodes using a fixed sampling frequency with a linear battery model. As it can be observed, such approaches fail to present a more detailed analysis of the behaviour of the battery against the issues considered important for its use.

On the other hand, energy-aware approaches use more accurate battery models, such as in routing protocols (MA; YANG; ZHANG, 2005; PADMANABH; ROY, 2006; WATFA; YAGHI, 2010; RAO; FAPOJUWO, 2012; LI; YI; LI, 2013; POURAZARM, 2017), techniques to estimate the SoC of the battery via software (CUNHA; ALMEIDA; SILVA, 2009; MADUREIRA et al., 2011; HÖRMANN et al., 2012; VALLE et al., 2013; VASILEVSKI et al., 2015) or hardware (SOMOV et al., 2009; KERASIOTIS et al., 2010; DRON et al., 2014). While some papers evaluate the use of battery models in the context of WSNs (ROHNER; FEENEY; GUNNINGBERG, 2013; NIGHOT; LAMBOR; JOSHI, 2014; VERMA; SINGH; PATHAK, 2015; JIN et al., 2015; HUSSEIN; SAMARA, 2015; ZYTOUNE; ABOUTAJDINE, 2016), other studies propose new approaches for modelling the battery behaviour in this type of network. For example, Chau et al. (CHAU et al., 2010) proposed a battery model based on Markov chains to capture the occurrence of the recovery effect on batteries. Aron et al. (ARON; GÎRBAN; POP, 2011) analysed the properties of a differential system derived from an electrochemical battery model for Li-ion cells. Kim and Qiao (KIM; QIAO, 2011) proposed a hybrid battery model consisting of an analytical model and an electric circuit-based model. The developed model predicts the dynamic circuit character-

istics of the battery, providing a lifetime estimation and tracking the SoC of the battery. However, a clear disadvantage of using this hybrid model is the requirement to extract 28 parameters to model a Lead-Acid battery. Yang et al. (YANG; FAN; GAO, 2014) proposed an optimised control strategy for WSNs with a external power supply. In this case, the authors modified the KiBaM model to allow recovery of charge on the battery through an external solar panel. Antolín et al. (ANTOLÍN; MEDRANO; CALVO, 2016) proposed an empirical battery model capable of considering the decay of the battery voltage during its discharge process, allowing to estimate the lifetime of the WSN nodes. Note that the influence of temperature is not addressed in any of the above-mentioned works.

An experimentally proven fact is that temperature is one of the factors that can influence the behaviour of the battery over time, particularly, its lifetime (GUO; HEALY, 2014). Relevant works were developed between 2000 and 2010 including the influence of temperature on battery models. For example, Gao et al. (GAO; LIU; DOUGAL, 2002) introduced a dynamic model suitable for virtual prototyping of portable battery-powered systems that considers the main non-linear effects, such as rate capacity and temperature. However, it has not been validated in the context of low-power WSNs. In this case, Park et al. (PARK; LAHIRI; RAGHUNATHAN, 2005) assessed the impact of important parameters (e.g., ambient temperature) on WSN design. The authors used the Mica2dot platform to perform experiments and demonstrate how the characteristics of the batteries change the nature of the parameters at the network level. Dualfoil software was used to simulate the behaviour of CR2354 batteries. Expanding the application for portable electronic devices, Rong and Pedram (RONG; PEDRAM, 2006) presented a closed form analytical expression to predict the remaining charge capacity of a Li-ion battery, considering both the thermal and ageing effects of the battery. However, the model relies on on-line current and voltage measurements. In the same context, Chen and Rincón-Mora (CHEN; RINCÓN-MORA, 2006) proposed a battery model based on an electric circuit. The great advantage of this work

is that the model considers several dynamic characteristics of the battery, such as open circuit voltage, current, temperature, cycle count, etc. However, at least six parameters need to be extracted as a function of the battery SoC. Erdinc et al. (ERDINC; VURAL; UZUNOGLU, 2009) developed a dynamic model to investigate the output characteristics of Li-ion batteries. Briefly, this work extends the approach of Chen and Rincón-Mora by adding the extraction of the parameters for different temperatures. Recent work also deals with the thermal effect and its influence on the batteries (BEHRENS et al., 2007a; BEHRENS et al., 2007b; GÎRBAN; POPA, 2010; PENELLA-LÓPEZ; GASULLA-FORNER, 2011; FERRY et al., 2011b; FERRY et al., 2011a; DIDIOUI et al., 2013), as well as the estimate for its SoC (BUCHLI; ASCHWANDEN; BEUTEL, 2013; MENZEL; WOLISZ, 2013; PFLUG et al., 2013; SOMMER; KUSY; JURDAK, 2013) and remaining energy (KIM et al., 2015; JIN et al., 2015).

3.3 BATTERY MODELLING: WSN SIMULATORS

Battery models are widely used in WSN simulators, allowing the analysis of the influence of several network parameters on the behaviour of the batteries in the sensor nodes. Thus, this thesis includes a brief review on WSN simulators and the use of battery models in these virtual environments.

There are several WSN simulators available for both academic and commercial purposes. Many papers analyse the available simulators under different aspects (EGEA-LOPEZ et al., 2006; HAASE; MOLINA; DIETRICH, 2011; GARG et al., 2012; THANGARAJ; ANURADHA, 2014). Minakov et al. (MINAKOV et al., 2016) performed a comparative evaluation of six open-source simulators, analysing metrics such as runtime simulation, network throughput, packet loss at the MAC layer, packet delivery rate/delay, and accuracy of the power consumption estimation. The authors pointed out that three of these simulators (WSNet, Castalia and COOJA) are very efficient for dealing with large-scale networks, suggesting the use of Castalia or WSNet for

greater ease of use.

The search results has shown that simulators usually employ (i) linear battery models (NATAF; FESTOR, 2012; BRAMAS et al., 2015) or (ii) complex battery models (PERLA et al., 2008; LEVEQUE et al., 2010; LATTANZI et al., 2017). In the latter case, Mikhaylov and Tervonen (MIKHAYLOV; TERVONEN, 2012) presented a method for modelling the energy consumption in WSN nodes. Feeney and Rohner (FEENEY; ROHNER, 2017) presented a suite of simulation and measurement tools for the study of primary Li-ion batteries. A hybrid KiBaM battery model was implemented in the OMNeT++/INET simulator. Other works propose energy-aware frameworks for use in WSN simulators (MERRETT et al., 2009; MORA-MERCHAN et al., 2013; MINAKOV; PASSERONE, 2013). For example, Benedetti et al. (BENEDETTI; PETRIOLI; SPENZA, 2013) presented a framework for energy harvesting applications, mainly. In addition, such a framework was prepared to accept different battery models, facilitating the implementation of different energy-aware approaches.

Note that few simulators are concerned with properly modelling the behaviour of the batteries, mainly the influences caused by the temperature variation, since nodes are usually deployed in environments subject to thermal effects, e.g., outdoors, industrial, etc. Thus, there is the possibility of scientific contribution also in this context.

4 A BATTERY MODEL FOR WSN NODES

This chapter introduces the Temperature-Dependent Kinetic Battery Model (T-KiBaM), which considers the influence of temperature on the behaviour of batteries in WSN nodes. Some preliminary studies were carried out to reach the current stage of development of the proposed battery model. The assessments can be divided into two stages, briefly presented in the following. In a first step, an analytical evaluation of the KiBaM model was performed through simulation. In the sequence, a comparison between the analytical and experimental results was performed using a prototype of the battery discharge hardware (without temperature control in this case).

The objective of the analytical evaluation was to verify the behaviour of the KiBaM model regarding the battery recovery effect. The obtained results allowed to confirm that the recovery effect can influence the lifetime of the batteries according to the order of execution of the tasks in WSN nodes. Also, these experiments confirmed that there is a minimum period (threshold) in the low-power state (sleep time) to achieve a satisfactory charge recovery. For the parameters used in the simulations (discharge current, execution time, KiBaM constants), a time between 5 and 10 minutes was sufficient to reach the charge recovery threshold at a sensor node. Finally, the frequency of switching between tasks was evaluated to verify its impact on the execution time of the KiBaM model. The results showed that high exchange rates significantly increase the simulation time of the KiBaM model. The Appendix A of this thesis presents the full details of these evaluations.

The objective of the comparison between the analytical and experimental assessments was to analyse the error of the analytical model concerning the lifetime of real Ni-MH batteries. The results demonstrated that the KiBaM model could adequately estimate the lifetime of the batteries in WSN nodes as long as the values of its constants are correctly adjusted. The analysis performed on the charge capacity extracted from the battery in each test showed that the model is accurate. On the other hand, the tests pointed out errors of up to 8% when

considering the nominal capacity of the used battery. The Appendix B of this thesis presents the full details of these evaluations.

These studies have shown that KiBaM has the following benefits:

- It deals with both the rate capacity and recovery effects;
- It provides an estimate of the battery State of Charge (SoC);
- It estimates with good accuracy the battery lifetime;

However, KiBaM also has the following limitations:

- It does not address the thermal effect, which can influence the behaviour of the battery over time, particularly, its lifetime;
- It does not present an appropriate voltage model for batteries commonly used in WSN nodes, e.g., Li-ion and Ni-MH;
- To the best of our knowledge, its hardware implementation has never been assessed to verify the feasibility of running its analytical expressions on COTS WSN nodes.

The battery model proposed in this thesis, T-KiBaM, benefits from the main advantages of the KiBaM model, such as the accuracy regarding the battery lifetime estimation. Simultaneously, the T-KiBaM model addresses the main limitations of the KiBaM model, such as the lack of an appropriate voltage model and its inability to cope with the effects caused by temperature variations in battery behaviour.

The remainder of this chapter is organised as follows. Section 4.1 introduces the battery test platform used in the experimental assessments, which includes a device for discharging the batteries and another for temperature control. Section 4.2 presents the T-KiBaM model, which is based on the concepts of the Arrhenius equation to estimate its constant values and on the use of a function to adjust the battery charge capacity at each temperature. Section 4.3 presents the results of the first[1] validation regarding the T-KiBaM model. Section 4.4 presents the main considerations of the chapter.

[1] Chapters 5 and 6 of this thesis present further validations of the T-KiBaM model.

4.1 BATTERY TEST PLATFORM

The studies mentioned at the beginning of this chapter allowed observing that the temperature can, in fact, influence the behaviour of batteries, even when the discharge rate is low, as in the case of low-power WSN nodes. In this way, it was verified the need to use a sort of equipment with temperature control, which allows obtaining more reliable results. Thus, the Battery Test Platform (BTP) has been developed specifically for the experimental assessments performed in this project. The objective of this platform is to allow the realization of experiments both at constant and varying temperatures. This platform is used in the experiments presented here and in the next chapters of this thesis. Details on the used devices are shown below.

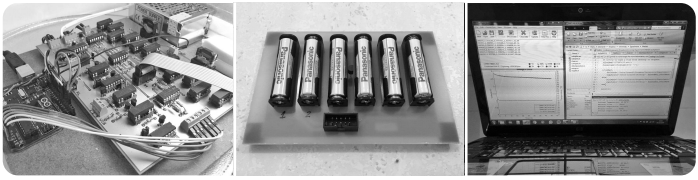

Figure 11 – BTP used for the experimental assessments.

The BTP includes a discharge-controlled circuit[2] and an Arduino UNO (ARDUINO, 2016), as well as a thermally insulated equipment with temperature control. This platform allows setting up controlled discharge currents to the batteries and collecting the experimental data for further analysis. Figure 11 presents a photo of the designed circuits, and Figure 12 illustrates the interconnection of its main blocks.

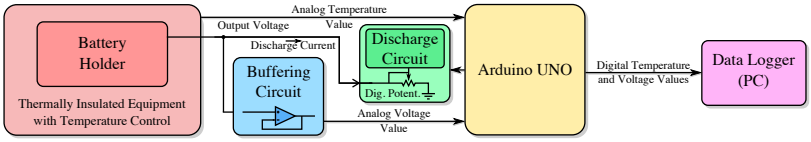

Figure 12 – Connectivity scheme of the BTP system.

[2] This device was designed in partnership with the University of Porto, Porto, Portugal.

The discharge-controlled circuit can consume currents in the range of 30 μA–30 mA, which represent values commonly found in COTS low-power WSN nodes, e.g., MICAz from Crossbow (CROSSBOW, 2016). It is possible to select among 256 discharge current values within this range by using a digital potentiometer (AD5206) (ANALOG DIGITAL INC, 2016). The discharge-controlled circuit guarantees a constant discharge current from the batteries by using a controlled current source. The batteries' board also includes a temperature sensor (Maxim 18B20) (MAXIM, 2016) for temperature measurements.

An Arduino UNO controls all circuit components and collects the experimental data from the batteries' board: battery voltage and temperature. The UNO board has analogue inputs with 10-bit resolution. The data log interval is adjustable. However, the data is recorded every 10 s for the performed assessments. A computer receives the collected data from the UNO board through a USB connection using CoolTerm (MEIER, 2016), which stores all information in a text file.

A thermally insulated equipment with temperature control is also used in the experimental assessments of this project. The developed solution includes the following items: (i) wood base; (ii) a glass tank with Styrofoam coating; (iii) power resistors; (iv) temperature sensor (Maxim 18B20); (v) relay; and an (vi) Arduino UNO. The temperature control is performed by the UNO board, which reads the internal temperature of the device and activates the power resistors when the temperature reaches a value outside the pre-programmed range. The implemented firmware allows the configuration of several temperature profiles, e.g., constant or variable profiles.

A set of twelve new Panasonic batteries, model HHR-4MRT/2BB (2xAAA, Ni-MH, 2.4 V, 750 mAh), was used in all experimental assessments. These batteries need to be fully charged at the beginning of the experiments, being discharged until reaching the cut-off value of 2.0 V. Note that this cut-off value is commonly used in experimental tests with Ni-MH batteries to prevent the cell-internal damage that could occur if the voltage level falls below 2.0 V (PANASONIC, 2016). The time required for reaching this voltage level defines the battery lifetime

in each experimental assessment. The recharging time is around eight hours by using a standard Ni-MH battery charger (output: 1.2 V_{DC}, 250 mA). Besides, the batteries need to stay at rest during, at least, 60 minutes before the start of each experiment.

4.2 TEMPERATURE-DEPENDENT KINETIC BATTERY MODEL

The target of this section is to detail the integration of the Arrhenius equation with the original KiBaM model. The resulting analytical model, Temperature-Dependent Kinetic Battery Model (T-KiBaM), is able to combine the effect of temperature on the battery operating behaviour, particularly, its voltage behaviour and its lifetime.

4.2.1 Arrhenius Equation

As noted by Manwell and McGowan (MANWELL; MCGOWAN, 1993), most chemical processes are sped up at higher temperatures, which corresponds to a higher k value in KiBaM. This behaviour is consistent with the higher battery capacities observed at higher temperatures, suggesting that it may be appropriate to use a chemical kinetics analysis based on the Arrhenius equation to model the influence of temperature on batteries.

Svante August Arrhenius (1859–1927) has contributed to the development of classical chemical kinetics. His contribution refers to the influence of temperature on the rate of a chemical reaction, which follows an empirical law known as the Arrhenius equation:

$$k = A \cdot e^{-\frac{E_a}{R \cdot T}}, \tag{4.1}$$

where k is the constant rate of a reaction, A is the pre-factor (in s^{-1}), E_a is the activation energy (in KJ/mol), R is the universal gas constant (8.314×10^{-3} KJ/mol·K) and T is the temperature (in Kelvin).

Equation (4.1) indicates that the increase of the reaction rate occurs either by increasing the temperature or by decreasing the activation energy (i.e., using a catalyst). In an extreme situation, i.e., an infinite temperature or the activation energy equal to zero, $e^{-\frac{E_a}{R \cdot T}} = 1$.

The result leads to $k = A$, which means that the value of A is an upper-bound for the reaction rate. Equation (4.1) can be written in a more convenient form by applying a natural logarithm:

$$ln(k) = ln(A) - \frac{E_a}{R \cdot T}. \tag{4.2}$$

Typically, the activation energy (E_a) definition refers to the minimum energy required to start a chemical reaction. Experiments at two different temperatures allow to obtain the value of the activation energy. Equation (4.2) can be used for both experiments. In this case, consider the following:

$$ln(k_1) = ln(A) - (E_a/R \cdot T_1)$$
$$ln(k_2) = ln(A) - (E_a/R \cdot T_2).$$

It is possible to re-write the above equations as follows:

$$ln(k_1) + \frac{E_a}{R \cdot T_1} = ln(k_2) + \frac{E_a}{R \cdot T_2}$$
$$ln(k_2) - ln(k_1) = \frac{E_a}{R}\left(\frac{1}{T_1} - \frac{1}{T_2}\right).$$

By solving the equation with respect to E_a, it is obtained:

$$E_a = \frac{R \cdot \ ln\left(\frac{k_2}{k_1}\right)}{\frac{1}{T_1} - \frac{1}{T_2}}. \tag{4.3}$$

Furthermore, by determining the value of k at different temperatures, it becomes possible to find the upper-bound value for the reaction rate (A) through the Arrhenius plot (Equation (4.1)).

4.2.2 Integrating Arrhenius Equation With KiBaM

Proposition 1. *Both k parameters from KiBaM and the Arrhenius equation refer to a constant reaction rate, which models the rate of a chemical diffusion/reaction process (in KiBaM, this rate is represented by the charge rate between both tanks). Thus, considering that* $k_{KiBaM} = k_{Arrhenius}$*:*

$$k_{KiBaM} = A \cdot e^{-\frac{E_a}{R \cdot T}}. \tag{4.4}$$

Therefore, the constant rate parameter of KiBaM (Equation (2.5)) are now re-defined to consider the activation energy (E_a) and the temperature (T), as defined in Equation (4.1), i.e., $k = A \cdot e^{-\frac{E_a}{R \cdot T}}$.

A set of assessments was experimentally performed to validate this procedure and to illustrate how to use the proposed T-KiBaM. Briefly, a set of experiments with Ni-MH batteries were conducted to obtain the T-KiBaM parameters, c and k. Then, the described methodology was applied to obtain the Arrhenius constants, E_a and A. Finally, the proposed approach was validated by comparing the experimental results against the results obtained with the analytical T-KiBaM. This methodology is presented below. Note that, except when explicitly stated, all presented graphs contain interpolated voltage curves upon the experimental data, in order to clearly present the obtained results.

4.2.3 Finding Arrhenius Constants (E_a and A)

The experiments were performed at a set of different temperatures, with a 15 °C step, −5, 10, 25 and 40 °C, using the thermally-insulated equipment with temperature control. A complementary full experiment was performed for 32.5 °C, as this temperature was found to be the most relevant outlier between the assessed temperature values. For all of the experiments, only the batteries (including the temperature sensor) remained inside the thermally-insulated equipment, at a controlled temperature.

Three experimental assessments were performed for each of the above-mentioned temperature values and for each of the following discharge current values: 10, 20 and 30 mA[3]. A total of 45 experiments were performed, three for each current/temperature pair. Thus, the average lifetime/voltage values from three experiments were considered for each measurement presented in this thesis.

The estimation of the T-KiBaM parameters requires experiments in at least two temperatures. Thus, only the measurements for −5 and

[3] Actually, due to the 256 available resistance values, obtained from the digital potentiometer, the considered current values were: 10.424, 20.303 and 30.242 mA.

Table 3 – Experimental results.

Discharge Current (mA)	–5 °C		25 °C	
	Lifetime (h)	Capacity (mAh)	Lifetime (h)	Capacity (mAh)
10	72.31	753	73.88	770
20	36.54	741	37.36	758
30	23.99	725	24.63	744

25 °C were considered as this range represent conditions typically found in WSNs (ALIPPI et al., 2007; RUIZ-GARCIA et al., 2009). It is possible to obtain the capacity provided by the battery using $\int Idt$. As the discharge current is constant, the battery capacity is obtained by just multiplying the discharge current value by the experimental lifetime, i.e., $I \cdot t_I$. Table 3 shows the obtained results for both temperature ranges. Figure 13 (a) depicts the discharge curves separated by temperature (−5 and 25 °C). Figure 13 (b) depicts a pairwise comparison of each discharge current at the two temperatures.

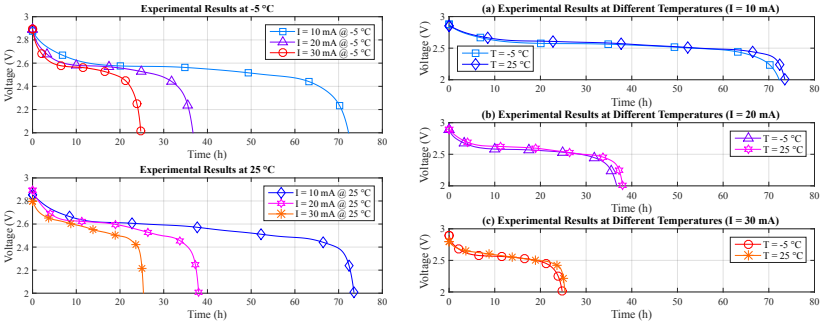

(a) Results separated by temperature. (b) Results paired by discharge current.

Figure 13 – Experimental results at different temperatures.

The obtained set of experimental measurements (numerical values are represented with up to five significant figures, whenever available) allows the evaluation of the T-KiBaM parameters, as explained by Manwell and McGowan (MANWELL; MCGOWAN, 1994):

$$T_1 = 268.15\ \text{K}: \quad c_1 = 0.56350, \quad k_1 = 0.56401;$$
$$T_2 = 298.15\ \text{K}: \quad c_2 = 0.56486, \quad k_2 = 0.59526.$$

Note that $k_1 < k_2$ indicates that the reaction rate is slower at lower temperatures. By using Equation (4.3), it is possible to obtain the activation energy value, E_a, which is equal to 1.1949 KJ/mol. Through the activation energy (E_a), k_2 and temperature (T_2) values, it is possible to obtain an upper-bound for the reaction rate (A):

$$\begin{aligned} k_2 &= A \cdot e^{-\frac{E_a}{R \cdot T_2}} \\ A &= 0.96397\ \text{s}^{-1}. \end{aligned} \tag{4.5}$$

The new values for k are then obtained by combining Equation (4.4) with the obtained values of A, E_a, R and T. Thus, k values vary with temperature, defining the T-KiBaM dependence on temperature as shown by Proposition 1. Finally, A and E_a values are constant values for a given battery type and do not depend on the temperature value. Table 4 depicts the relationship between k and temperature.

Table 4 – Variation of k according to temperature.

Temperature (°C)	k **Value (s^{-1})**	**Temperature (°C)**	k **Value (s^{-1})**	**Temperature (°C)**	k **Value (s^{-1})**
−12.5	0.55538	10.0	0.58025	32.5	0.60234
−5.0	0.56401	17.5	0.58790	40.0	0.60917
2.5	0.57229	25.0	0.59526	47.5	0.61574

Note that it is possible to extrapolate the values of k beyond the temperature range at which the parameters were obtained due to the chemical kinetics concepts modelled by the Arrhenius equation. Table 4 shows the behaviour of the reaction rate (k) between −12.5 and 47.5 °C. However, it is also worth mentioning that the operating limits of the battery must be taken into account for these extrapolations. The indicated temperature range for the discharge of Ni-MH batteries varies from −10 to 45 °C (PANASONIC, 2016).

4.2.4 Calibrating Battery-Specific Characteristics

Temperature also affects the battery capacity. Typically, batteries provide higher effective capacities at higher temperatures (CHEN; RINCÓN-MORA, 2006) and lower effective capacities when used at low-temperatures (JAGUEMONT et al., 2016). In this context, it is crucial to adjust T-KiBaM to the battery technology (e.g., Ni-MH or Li-ion). Thus, this section presents a method for adjusting the T-KiBaM parameter related to the initial battery capacity, q_0. Briefly, through a set of experimental assessments, it is possible to evaluate the losses and gains of the battery capacity according to the temperature variation. Such knowledge is incorporated in T-KiBaM to model the initial battery capacity under different temperature conditions.

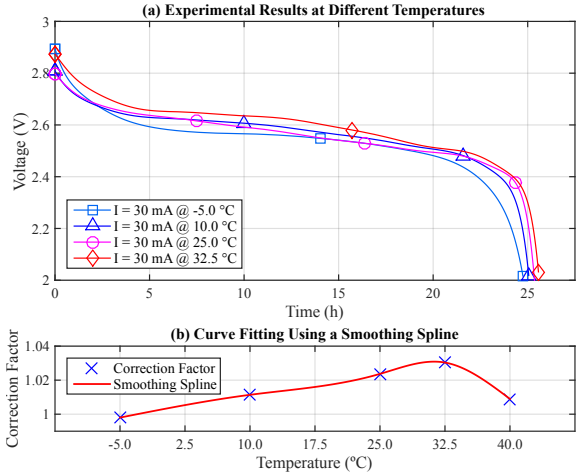

Figure 14 – The battery-specific behaviour.

First, fifteen experiments were performed with the same discharge current, 30 mA, under five different temperatures: −5, 10, 25, 32.5 and 40 °C (i.e., three experiments for each temperature, to provide greater confidence on the obtained results). Each of the following average lifetimes was obtained from three battery pairs: 24.749, 25.087, 25.385, 25.560 and 25.022 h, respectively. Figure 14 (a) illustrates the related discharge curves, $V \times t$ (for the sake of clarity, the results

at 40 °C were not included). Note the non-linearity of these voltage curves throughout the experiments with different curves for different temperatures, even using the same discharge current.

As previously mentioned, the capacity provided by the battery can be obtained by integrating its discharge current over time. From the obtained results, it becomes possible to evaluate the losses and gains of the battery capacity at different temperatures to establish the Correction Factor (CF) of the initial battery capacity (q_0) for each situation. The losses and gains of the battery capacity are evaluated with respect to the nominal battery capacity, which was 750 mAh for this case. Table 5 presents the obtained results.

Table 5 – Correction Factor at different temperatures.

TEMP (°C)	Time (h)	Capacity (mAh)	Loss or Gain (%)	Correction Factor
−5.0	24.749	748.5	−0.2	0.9980
10.0	25.087	758.6	1.14	1.0114
25.0	25.385	767.7	2.36	1.0236
32.5	25.560	772.9	3.05	1.0305
40.0	25.022	756.7	0.89	1.0089

Discharge current equal to 30 mA.

After establishing the correction factor, which indicates the gain or loss of the initial battery capacity (q_0) at different temperatures, it is possible to find a function that properly fits the data. Figure 14 (b) depicts the CF data points and the fitted curve. A smoothing spline (piecewise polynomial function of degree three) (MATHWORKS INC, 2016) with $p = 0.6$ and $w = [1,1,1,1,1]$ fits the obtained data points:

$$CF(T) = a \cdot (T - T_1)^3 + b \cdot (T - T_1)^2 + c \cdot (T - T_1)^1 + d,$$

where $T_1 \leq T < T_2$. Table 6 presents the coefficients for each segment. This function enables the adjustment of the initial battery capacity according to the selected temperature, being valid only within the range from −5 to 40 °C. This temperature range represents the case for the

most part of the WSN applications, e.g., from snow (KERKEZ et al., 2012) to industrial (BOANO et al., 2010) monitoring applications.

Table 6 – Smoothing spline coefficients.

a	b	c	d	Segment
$-5.1170 \cdot 10^{-7}$	0	$1.0076 \cdot 10^{-3}$	0.9980	$-5.0 \leq T < 10.0$
$2.2375 \cdot 10^{-6}$	$-2.3027 \cdot 10^{-5}$	$6.6220 \cdot 10^{-4}$	1.0114	$10.0 \leq T < 25.0$
$-2.0925 \cdot 10^{-5}$	$7.7663 \cdot 10^{-5}$	$1.4817 \cdot 10^{-3}$	1.0237	$25.0 \leq T < 32.5$
$1.7473 \cdot 10^{-5}$	$-3.9315 \cdot 10^{-4}$	$-8.8444 \cdot 10^{-4}$	1.0303	$32.5 \leq T < 40.0$

4.2.5 Temperature-Dependent Voltage Model (TVM)

The TVM model is presented in this section. This voltage model is an extension of the Battery Dynamic Model (BDM) model, which is able to attenuate the P1 and P2 problems (cf. Section 2.3.4.3) and appropriately represent the influence of the temperature on the $V \times t$ curve during the battery discharge.

In order to increase the accuracy of the BDM voltage model, i.e., attenuating P1 and P2 problems, a smoothing constant, τ_b, has been added to the model. This τ_b value multiplies the terms that relate current and time, i.e., it and $\dot{Exp}(t)$. Therefore, Equations (2.13) and (2.14) should be rewritten as follows:

$$\dot{Exp}(t) = \tau_b \cdot B \cdot |i(t)| \cdot (-Exp(t) + A_b \cdot u(t)), \tag{4.6}$$

$$V_b = E_0 - R_b \cdot i - K_b \cdot \frac{Q}{Q - it \cdot \tau_b} \cdot (it \cdot \tau_b + i^*) + Exp(t). \tag{4.7}$$

All parameters (A_b, B, E_0, $Exp(t_0)$, K_b, Q, R_b and τ_b) can be obtained by using the battery data-sheet or by performing experimental measurements (TREMBLAY; DESSAINT, 2009). Considering an experiment at -5 °C, for example, the following values can be obtained:

$A_b = 0.2831$ V	$\tau_b = 0.954$	$K_b = 0.0375\ \Omega$	$Exp(t_0) = 0.280$ V
$E_0 = 2.570$ V	$B = 18\ (\text{Ah})^{-1}$	$R_b = 0.070\ \Omega$	$Q = 0.75\ \text{Ah} \cdot CF(-5)$

Figure 15 compares data obtained through the experimental assessment ($T = -5$ °C, $I = 30$ mA) with the T-KiBaM (Equation (4.7)), the BDM (Equation (2.14)) and the original KiBaM analytical results (Equation (2.10)). The raw experimental data are then used to make a point-to-point comparison with just the T-KiBaM analytical curve, as the original KiBaM linear results are clearly inaccurate along the time scale. Note that a reduced steady-state relative error is obtained for most of the T-KiBaM analytical results. The following absolute errors were obtained for T-KiBaM values: 3.1% (max) and 0.6% (mean).

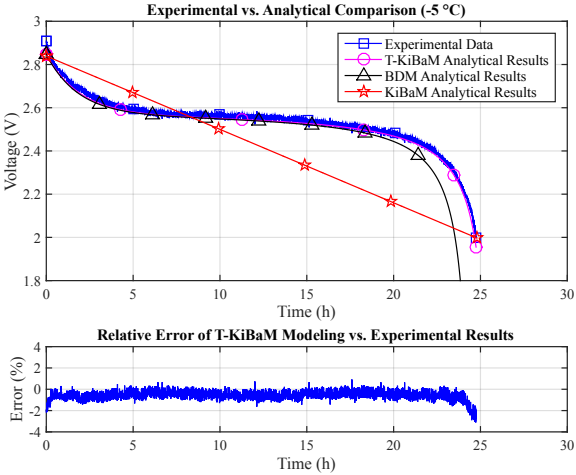

Figure 15 – Experimental vs. analytical results.

Experiments performed for different temperature values enabled the extraction of the voltage model parameters. Table 7 illustrates the Arrhenius constants obtained for each parameter, as well as the values of all parameters at each temperature.

Finally, it becomes possible to represent the values obtained from the T-KiBaM analytical voltage model adapted to different temperatures, using the set of parameters described in Table 7, along with their respective constants A and E_a, using the Arrhenius equation. Figure 16 depicts the voltage results for the different temperatures using Arrhenius constants. The absolute errors are: (a) $T = -5$ °C: 3.1% (max)

Table 7 – TVM parameters at different temperatures.

TVM	Temperature (°C)					Arrhenius Constants	
Parameter	–5	10	25	32.5	40	A	E_a
E_0	2.5700	2.5850	2.6000	2.6060	2.6120	2.884200	0.25714
R_b	0.0700	0.0480	0.0350	0.0300	0.0260	0.000071	−15.358
K_b	0.0375	0.0286	0.0225	0.0201	0.0180	0.000234	−11.318
B	18.000	15.010	12.750	11.820	11.000	0.584660	−7.6403
$Exp(t_0)$	0.2800	0.2620	0.2470	0.2410	0.2350	0.082728	−2.7181
τ_b	0.9540	0.9630	0.9706	0.9742	0.9776	1.126800	0.36978

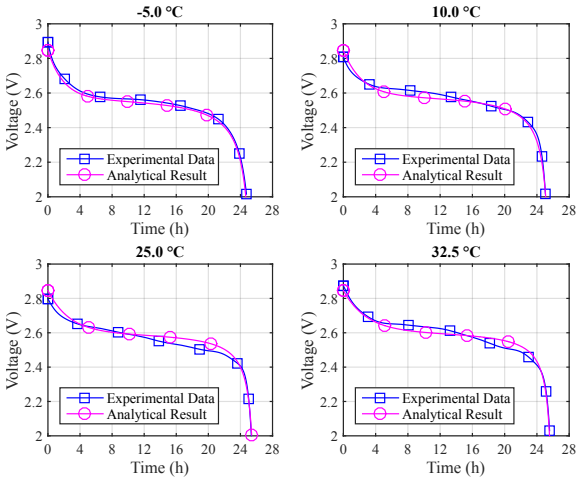

Figure 16 – Results at different temperatures.

and 0.6% (mean); (b) $T = 10$ °C: 2.9% (max) and 0.7% (mean); (c) $T = 25$ °C: 2.0% (max) and 0.9% (mean); (d) $T = 32.5$ °C: 6.7% (max) and 1.2% (mean). Figure 17 (a) depicts the obtained results regarding the voltage levels for both experimental (top) and analytical (bottom) assessments. Figure 17 (b) depicts a comparison between experimental and T-KiBaM analytical results (the same as in Figure 17 (a)), regarding the voltage levels, at each temperature.

The modified voltage model, which is called TVM, was integrated into T-KiBaM, as it satisfactorily represents the battery discharge behaviour regarding the battery voltage level for the case of Ni-MH batteries at different temperatures.

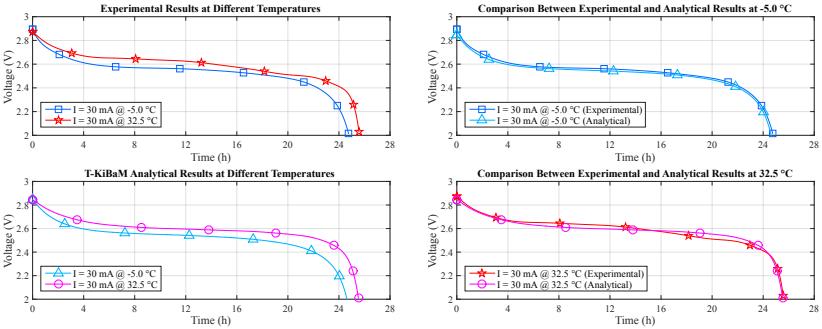

(a) Results separated by type.

(b) Results paired by temperature.

Figure 17 – Experimental vs. Analytical comparison.

4.2.6 T-KiBaM Summary

This section summarizes the parameters of the T-KiBaM model for Ni-MH batteries. Table 8 illustrates the experimentally-obtained values, as described in the previous sections (in Table 8, T_c and T_k are the temperatures in degrees Celsius and Kelvin, respectively).

Table 8 – T-KiBaM parameters for a Ni-MH battery.

Model	Parameter	Value
Arrhenius	E_a	1.1949
	A	0.96397
	R	0.008314
CF (T_c)	a, b, c, d	cf. Table 6
T-KiBaM	c	0.56418
	k	$A \cdot e^{\frac{-E_a}{R \cdot T_k}}$
	q_0	$750 \cdot CF\ (T_c)$
TVM	A_b, B, E_0, $Exp(t_0)$, K_b, Q, R_b, τ_b	cf. Table 7

4.3 ANALYTICAL AND EXPERIMENTAL VALIDATION

This section aims to present the performed T-KiBaM validation. Briefly, Matlab was used to implement the T-KiBaM analytical model (Equations (2.7) and (4.4)). Then, both analytical and experimental results were compared regarding the battery lifetime. The details of the implementation of the analytical set-up are shown below.

4.3.1 Implementing T-KiBaM

First, the following steps must be performed to find the function that allows calculating the Correction Factor (CF) with respect to the initial battery capacity, according to the temperature (TEMP):

1. Perform at least four experiments at distinct temperatures using the same constant discharge current, whose value should be within the interest range of the supported WSN application.

2. From the obtained results in Step 1, extract the charge losses/-gains according to the nominal battery capacity.

3. From TEMP vs. CF data, it is possible to determine a function that properly fits the data behaviour.

4. Add such a function to the T-KiBaM implementation.

Next, there is the need to implement the T-KiBaM function to estimate both the SoC and voltage level of the battery over time, at different temperatures. Therefore, it becomes possible to obtain the estimated battery lifetime according to the discharge profile and the used temperature. The implementation presented in this section is divided into two stages: (i) the call to the T-KiBaM function; and (ii) the T-KiBaM function itself. Such stages are described below.

The first stage implements the call to the T-KiBaM function, that has as input the discharge profile. Such Discharge Profile (DP) is defined by a set of pairs (I_x, t_x), where I_x represents the discharge current and t_x represents its operating time (or time step), with $x = 1, 2, 3, \ldots, n$.

For example, $DP_{set} = [(I_1,t_1);(I_2,t_2);\ldots;(I_n,t_n)]$. Therefore, this stage returns the updated values regarding the T-KiBaM and TVM functions. Algorithm 1 shows the implementation of the function call that uses Equations (2.7) and (4.7) to update the battery data.

Algorithm 1: T-KiBaM_call.

Input: $E_a, A, R, T, q_0, c, k, t_0, DP_{set}$, $E_0, R_b, K_b, \tau_b, B, prExp$
Output: q_1, q_2, t_0, V_b

$q_0 = q_0 \cdot CF(T)$;
$q_1 = (c) \cdot q_0$;
$q_2 = (1-c) \cdot q_0$;
$k = A \cdot e^{-Ea/(R \cdot T)}$;
$It = 0$;
foreach $(I_x, t_x) \in DP_{set}$ **do**
  $It = It + (I_x \cdot t_x)$;
  if $q_1 > 0$ **then**
    $[q_1, q_2, t_0]$ = T-KiBaM_function $(c, k, q_1, q_2, t_0, I_x, t_x)$;
    $Exp = (1/(1 + (B \cdot I_x \cdot t_x \cdot \tau_b))) \cdot prExp$;
    V_b = TVM_function $(E_0, R_b, K_b, \tau_b, B, q_0, I_x, It, Exp)$;
    $prExp = Exp$;
  end
end
return (q_1, q_2, t_0, V_b);

The input parameters at this stage are related to the Arrhenius equation (E_a, A, R, T), to T-KiBaM (q_0, c, k, t_0, DP_{set}) and TVM (E_0, R_b, K_b, τ_b, B, $prExp$). In T-KiBaM parameters, note that q_0 represents the initial battery capacity. In this case, this parameter receives the nominal capacity of the battery used as reference. The values of c and k are dependent on the battery technology. In this case, these three values were obtained from a Panasonic battery, model HHR-4MRT/2BB (2xAAA, 2.4 V, 750 mAh). Next, parameter t_0 represents the total battery lifetime. Besides, parameter DP_{set} may contain one or more pairs (I_x, t_{I_x}) to indicate the use of a set of tasks (i.e., a discharge profile as depicted in Figure 19). This feature is useful as a WSN node usually has different discharge currents for different operating states, e.g., Tx, Rx and Sleep. Using the DP_{set} definition, duty cycles can also

be used in the T-KiBaM implementation. In the TVM parameters, $prExp$ represents the initial value of the exponential voltage, $Exp(t_0)$, which is used for the calculation of $Exp(t)$ in each iteration.

In Algorithm 1, the CF function is applied in Line 1, as described in Section 4.2.4. Also, the definition of k (Line 4) considers the Arrhenius equation values (E_a, A, R and T), which can be obtained through experiments, as described in Section 4.2.3. Through the `for` loop (Line 6), it is possible to call the T-KiBaM function according to the used discharge profile. As presented in Line 8, the user of T-KiBaM should check the content of the Available Charge tank, which needs to be greater than zero. This is a necessary condition for the battery operation, even if there is charge at the Bound Charge tank. Note that the battery voltage level is obtained in Line 11, which performs the calculations corresponding to Equation (4.7). Finally, the algorithm returns some additional information about the battery, such as remaining battery charge in both tanks (q_1 and q_2), battery run time (t_0), and voltage level (V_b) when executing the discharge profile DP_{set}.

The T-KiBaM function returns the updated values in relation to the battery charge and its time of use, as shown in Algorithm 2.

Algorithm 2: T-KiBaM_function.

Input: c, k, $q_{1,0}$, $q_{2,0}$, t_0, I, t_I
Output: q_1, q_2, t
1 $q_0 = q_{1,0} + q_{2,0}$;
2 $t = t_0 + t_I$;
3 q_1 = compute-q1 $(c, k, q_0, q_{1,0}, q_{2,0}, I, t_I)$;
4 q_2 = compute-q2 $(c, k, q_0, q_{1,0}, q_{2,0}, I, t_I)$;
5 **return** (q_1, q_2, t);

T-KiBaM function has the following input parameters: c, k, $q_{1,0}$, $q_{2,0}$, t_0, I and t_I. The values of I and t_I represent a task in the DP_{set}. Lines 3 and 4 perform the calculations corresponding to Equation (2.7). The output values of q_1 and q_2 represent the actual SoC in the Available and Bound Charge tanks, respectively. Finally, t represents a time accumulator that is used to compute the total time of battery usage.

The knowledge about the SoC of the battery is essential for the development of energy-aware strategies. In this approach, during the node duty cycle, for example, it is possible to perform an iteration of T-KiBaM for each performed task (e.g., Tx, Rx, Sleep) in order to update the battery status (SoC and voltage level). Thus, the node can take different decisions according to the battery state. Although the proposed approach is flexible in several aspects, the following assumptions should be considered when running the T-KiBaM model:

1. The node initializes its operating cycle with a fully charged battery, i.e., SoC = 100%. Also, the T-KiBaM model is adjusted for the used battery technology. Therefore, it is not necessary to measure any battery information over time (e.g., voltage level);

2. The node knows the discharge profile for all tasks that need to be performed during its operation. Knowing the discharge current in the transition between states, as well as the time it takes to perform such action, makes the T-KiBaM even more accurate. Thus, it is possible to parametrize T-KiBaM with the measured values and the time spent in each state/transition. The better the discharge profile definition, the greater the accuracy of the estimates. Note that the DP can be obtained from an analysis of the hardware power consumption (e.g., MCU, sensors, transceiver);

3. The duty cycle of the node does not have to be constant since T-KiBaM supports different operating times (t_x) for each task (I_x), allowing the configuration of any combination of tasks;

4. The node can obtain the environment temperature, which increases the accuracy of the estimate on the battery behaviour.

4.3.2 Validating T-KiBaM

The T-KiBaM analytical evaluation involves the use of Algorithms 4 and 5. The following discharge currents are used for this analysis: 20 and 30 mA, which represent the same current values used

for the experimental assessments. The input parameters are the same as those mentioned in Algorithm 5. However, note that the initial battery capacity (q_0) is set according to the values returned by the CF function. Besides, the value $c = 0.56418$ is used, which represents the average of c_1 and c_2 values (mentioned in Section 4.2.3).

Table 9 illustrates the results of the analytical evaluations using T-KiBaM. The EXP, T-KiBaM and ERR columns represent, respectively, the experimental average lifetime of three battery measurements, the lifetime using T-KiBaM and the relative error between EXP and T-KiBaM. Note that the adapted model performs the battery lifetime estimation with an average relative error of 0.21% for low temperatures (−5 °C) and 0.23% for room temperatures (25 °C).

Table 9 – T-KiBaM analytical results.

	–5 °C			25 °C		
Discharge Current (mA)	**EXP (h)**	**T-KiBaM (h)**	**ERR (%)**	**EXP (h)**	**T-KiBaM (h)**	**ERR (%)**
20	36.714	36.866	0.41	37.984	37.815	0.44
30	24.749	24.750	0.00	25.385	25.386	0.01
Average			0.21			0.23

EXP: Experimental result; ERR: Relative error.

These results demonstrate that T-KiBaM can estimate the battery lifetime of WSN nodes accurately, presenting average accuracy errors smaller than 0.25% when using the nominal battery capacity. Our rationale is that, if all 45 tests (with one pair of batteries each) are started exactly with the same battery capacity, even better results would have been achieved using T-KiBaM. However, this is an assumption that is difficult to hold as, due to electrochemical reactions inside the batteries, it is not possible to guarantee the same value with respect to the initial battery capacity for each test.

4.3.3 Model Comparison: KiBaM vs. T-KiBaM

This section compares the original KiBaM and T-KiBaM according to the expected battery lifetimes for five different temperatures.

The target is to perform an experimental validation of T-KiBaM. The analytical evaluations consider the following details.

The constants used for setting up KiBaM are the ones that were obtained at 25 °C, i.e., $c_2 = 0.56486$ and $k_2 = 0.59526$. For T-KiBaM, $c = 0.56418$, and the value of k varies according to the evaluated temperatures (cf. Table 4). The initial battery capacity is the same for both models, $q_0 = 2700$ As (750 mAh). Nevertheless, T-KiBaM adjusts this value after the start of the analytical evaluation, in accordance with the related Correction Factor (CF). The evaluated temperatures (TEMP) were the following: −5, 10, 25, 32.5 and 40 °C. The battery is drained until the end of the available charge in all of the analytical evaluations. Table 10 presents the results obtained using both models.

Table 10 – Model comparison.

TEMP (°C)	EXP† (h)	KiBaM (h)	ERR (%)	T-KiBaM (h)	ERR (%)
−5.0	24.749	24.799	0.20	24.750	0.00
10.0	25.087	24.799	1.15	25.082	0.02
25.0	25.385	24.799	2.31	25.386	0.01
32.5	25.560	24.799	2.98	25.552	0.03
40.0	25.022	24.799	0.89	25.022	0.00
Average			1.50		0.01

EXP: Experimental Result; ERR: Relative Error.
† Discharge current equal to 30 mA.

As expected, KiBaM presents the same battery lifetimes for all situations, regardless of the evaluated temperature. In the KiBaM analytical evaluation, the average relative error is 1.50%, with a standard deviation of 1.12%. The largest error occurs at 32.5 °C, where a difference of 2.98% (45 min.) is achieved between the experimental assessment and the analytical evaluation. This error would generate a difference in the battery lifetime of 10.8 days in a period of 365 days (one year). On the other hand, T-KiBaM presents different battery lifetimes according to the assessed temperatures. For this case, the average relative error is 0.01%, with a standard deviation of 0.01%. The largest error also occurs at 32.5 °C, where it is possible to observe a

difference of 0.03% (29 s). In one year, this error would represent a difference of 0.1095 days (NAVARRO et al., 2013; LAZARESCU, 2015). Table 11 (at the end of this section) presents a full comparison between experimental and analytical results for each of the assessed temperatures. The EXP column represents the average discharge time of three discharge experiments using different batteries of the same model.

The results obtained when using using Peukert's Law (RAKHMATOV; VRUDHULA; WALLACH, 2003; DOERFFEL; SHARKH, 2006; RUKPAKAVONG; GUAN; PHILLIPS, 2014) were also included for comparative purposes. As explained in Section 2.3.1, this is a simpler battery model, which can capture part of the non-linear properties of the batteries. In this comparison, the value of a was set at 0.75 Ah, which corresponds to the nominal battery capacity, and b was adjusted according to the experimental results at 25 °C using the discharge current $I = 30$ mA. Thus, $b = 1.0067$.

Table 11 also contains the results of T-KiBaM when the discharge current of 20 mA is used to calculate the function that returns the correction factor for each temperature. In this case, the same methodology mentioned in Section 4.2.4 was followed to generate the function parameters.

The behaviour of the battery voltage over time is also assessed in this work. In this case, the experimental results are compared with the analytical results using both KiBaM and T-KiBaM. Figure 18 depicts some examples of voltage tracking at different temperatures.

Note that KiBaM presents the same results in all analytical assessments since this model is not able to handle different temperatures. Also, KiBaM represents linearly the voltage behaviour, which causes a significant error in relation to the experimental data when analysing different cut-off points, as in the range between 2.0 and 2.5 V. On the other hand, T-KiBaM is able to deal more accurately with voltage tracking at different temperatures. For instance, at $T = -5$ °C (Figure 18 top-left), analysing the voltage level equal to 2.4 V, the relative error to the experiment of KiBaM is 37.53%, while in T-KiBaM is 0.73%.

Finally, it is possible that thermal effects will have an even

greater impact when applying intermittent discharge currents to the battery, e.g., WSN nodes operating in a duty cycle scheme. Our rationale is that, by taking advantage of the radio sleep periods at different temperatures, the transfer rate from the bound charge tank to the available charge tank (recovery effect) will also be variable. In other words, the parameter k will have different values according to the temperature (cf. Table 4). It means that a smaller value of k implies a slower rate to the charge recovery. This behaviour may have a substantial impact on the battery lifetime for different temperatures, particularly when long periods of time are evaluated, e.g., weeks or months. Therefore, this issue is partially addressed in next chapters of this thesis.

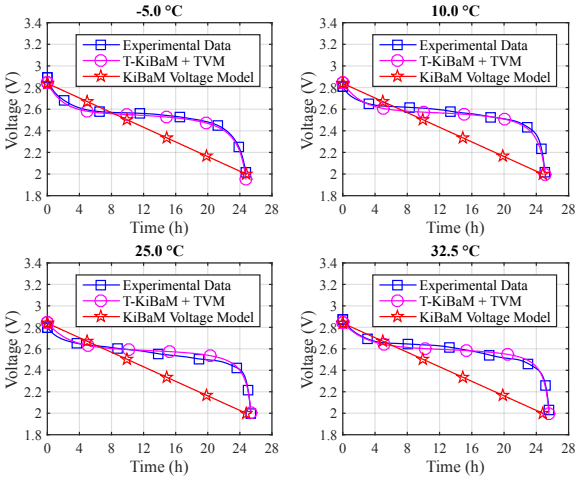

Figure 18 – Voltage level tracking comparison.

Table 11 – Comparison between experimental and analytical results.

	Temperature (°C)														
	−5			10			25			32.5			40		
Discharge Current (mA)	**EXP (h)**	**Peukert's Law (h)**	**ERR (%)**	**EXP (h)**	**Peukert's Law (h)**	**ERR (%)**	**EXP (h)**	**Peukert's Law (h)**	**ERR (%)**	**EXP (h)**	**Peukert's Law (h)**	**ERR (%)**	**EXP (h)**	**Peukert's Law (h)**	**ERR (%)**
20	36.714	37.91	3.27	37.402	37.91	1.37	37.984	37.91	0.19	37.835	37.91	0.21	37.133	37.91	2.10
30	24.749	25.39	2.57	25.087	25.39	1.19	25.385	25.39	0.00	25.560	25.39	0.68	25.022	25.39	1.45
Average			2.81			1.51			0.34			0.74			2.07
Discharge Current (mA)	**EXP (h)**	**KiBaM (h)**	**ERR (%)**	**EXP (h)**	**KiBaM (h)**	**ERR (%)**	**EXP (h)**	**KiBaM (h)**	**ERR (%)**	**EXP (h)**	**KiBaM (h)**	**ERR (%)**	**EXP (h)**	**KiBaM (h)**	**ERR (%)**
20	36.714	36.940	0.62	37.402	36.940	1.24	37.984	36.940	2.75	37.835	36.940	2.37	37.133	36.940	0.52
30	24.749	24.799	0.20	25.087	24.799	1.15	25.385	24.799	2.31	25.560	24.799	2.98	25.022	24.799	0.89
Average			0.41			1.19			2.53			2.67			0.71
Discharge Current (mA)	**EXP (h)**	**T-KiBaM† (h)**	**ERR (%)**	**EXP (h)**	**T-KiBaM† (h)**	**ERR (%)**	**EXP (h)**	**T-KiBaM† (h)**	**ERR (%)**	**EXP (h)**	**T-KiBaM† (h)**	**ERR (%)**	**EXP (h)**	**T-KiBaM† (h)**	**ERR (%)**
20	36.714	36.711	0.01	37.402	37.398	0.01	37.984	37.978	0.02	37.835	37.828	0.02	37.133	37.133	0.00
30	24.749	24.646	0.42	25.087	25.107	0.08	25.385	25.497	0.44	25.560	25.396	0.64	25.022	24.929	0.37
Average			0.21			0.05			0.23			0.33			0.19
Discharge Current (mA)	**EXP (h)**	**T-KiBaM‡ (h)**	**ERR (%)**	**EXP (h)**	**T-KiBaM‡ (h)**	**ERR (%)**	**EXP (h)**	**T-KiBaM‡ (h)**	**ERR (%)**	**EXP (h)**	**T-KiBaM‡ (h)**	**ERR (%)**	**EXP (h)**	**T-KiBaM‡ (h)**	**ERR (%)**
20	36.714	36.866	0.41	37.402	37.361	0.11	37.984	37.815	0.44	37.835	38.061	0.60	37.133	37.271	0.37
30	24.749	24.750	0.00	25.087	25.082	0.02	25.385	25.386	0.01	25.560	25.552	0.03	25.022	25.022	0.00
Average			0.21			0.07			0.23			0.31			0.19

† Adjust using discharge current equal to 20 mA; ‡ Adjust using discharge current equal to 30 mA.

4.4 CHAPTER REMARKS

Estimating battery lifetimes is a complex task as multiple factors influence the battery behaviour. The most studied factors are both the rate capacity and recovery effects. However, the thermal effect also plays an important role as it concerns the evaluation of battery lifetime. Thermal effects can modify the electrochemical reaction rate and/or impair the battery operation. In the case of WSNs, battery-powered nodes are prone to the influences of temperature variations, particularly in outdoor or industrial environments.

Within this context, the availability of adequate battery models able to encompass thermal effects would be of utmost importance. This chapter proposed an extension to the widely-used analytical KiBaM to cover thermal effects. As a consequence, it provides a valuable tool for the battery lifetime estimation at different temperatures. The proposed model extension was validated through an extensive experimental assessment, using Ni-MH batteries operating at different temperatures. The achieved results show that the proposed T-KiBaM extension presents an average accuracy error smaller than 0.33% when estimating the lifetime of batteries for various temperature conditions. This result significantly improves the accuracy of KiBaM for the same operating conditions, which is slightly smaller than 2.7% in this work.

5 T-KIBAM MODEL IN MICRO-CONTROLLERS

The estimation of both the battery SoC and its lifetime according to the set of tasks performed by the nodes (e.g., data reception/transmission/processing tasks) can become a valuable data for the WSN management. This type of information can be employed in energy-aware approaches and protocols, for example. However, estimating the battery lifetime in WSN nodes is a challenging task, since several factors influence their operation (e.g., the chemical composition of the battery, operating temperature and discharge current) (KIM; QIAO, 2011), resulting in a non-linear behaviour over time (WANG; ZHANG; CHEN, 2015; LAJARA; PEREZ-SOLANO; PELEGRÍ-SEBASTIA, 2015; GANDOLFO et al., 2015).

There are two primary options to estimate the battery operating behaviour (BUCHLI; ASCHWANDEN; BEUTEL, 2013): (i) hardware-based solutions, which involve the use of Integrated Circuits (ICs) that provide the relevant battery data; and (ii) software-based solutions, which usually require the use of adequate mathematical models. These two options are briefly discussed below.

Smart batteries use ICs along with the electrochemical cell(s) to provide relevant data about the battery behaviour (e.g., voltage, temperature, current) (JIN et al., 2015) and, in some cases, estimations about its operating behaviour (e.g., SoC and remaining lifetime (WANG et al., 2016)) to the connected device (e.g., laptops, smartphones, cameras) (RAHIMI-EICHI et al., 2013; SBS IMPLEMENTERS FORUM, 2007). However, the use of these hardware-based approaches increases the cost of producing batteries by approximately 25% (fuel gauge ICs costs about $2–3) (CADEX ELECTRONICS INC, 2017). In the context of WSNs, where the deployment of a vast number of nodes may be required, such a solution may become economically infeasible. Besides, hardware-based solutions involving the use of ICs are often adapted to the integrated battery technology, where lookup tables are used to reconstruct the characteristics of the used cell(s) under different operating conditions (MAXIM, 2007). Thus, it would

be relevant to adopt software-based solutions able to accurately estimate the battery behaviour of WSN nodes, without requiring the use of dedicated hardware. An essential requirement is that whatever the estimation approach, it must (i) be flexible enough to support different battery technologies; and (ii) present low computational cost due to the hardware constraints of sensor nodes.

Analytical battery models typically rely on a set of differential equations to estimate the battery behaviour. Usually, these models are implemented in WSN simulators to predict the operating behaviour of the sensor nodes before their actual deployment. Within this context, the current battery condition is mathematically estimated to enable the implementation of energy-aware algorithms and protocols (RAZAQUE; ELLEITHY, 2014; JABBAR et al., 2015; MAMMU et al., 2015). However, it is necessary to evaluate whether it is possible (or not) to implement similar differential equations-based models in real-world WSN nodes. It would also be a need to assess the impact of implementing such mathematical models upon COTS low-power hardware. A pertinent question in this scenario is "how does the computation of battery models may affect the lifetime of WSN nodes, which are usually based on low-power micro-controllers to save energy?" In other words, and regarding the computational cost, "is it feasible to perform a battery model computation on a sensor node to implement an on-line SoC determination and the related voltage level tracking functions?"

The objective of this chapter is to assess the usability of a low complexity analytical battery model (JONGERDEN; HAVERKORT, 2008), the T-KiBaM, which is implemented on MCUs with low computational power, e.g., ATmega328P and ATmega128RFA1 (ATMEL, 2016). These MCUs are similar to those found in low-power COTS WSN nodes (e.g., the MICAz, which is based on the ATmega128L). Both ATmega-328P/-128RFA1 MCUs are widely available as the processing units of low-cost WSN nodes. The main advantage of the methodology proposed in this chapter is related to the implementation of a temperature-dependent battery model, which can be used to predict the battery behaviour of low-power WSN nodes in environ-

ments with temperature variations, regardless of the associated hardware. The proposed methodology assumes that there is a cyclical operation pattern for the WSN nodes (e.g., a duty cycle), so that the discharge profile can be used as input parameter to compute the battery behaviour over time (open-loop computation). Figure 19 depicts an example of a discharge profile based on a MICA2DOT WSN node (PARK; LAHIRI; RAGHUNATHAN, 2005). By using this type of discharge profiles, it becomes possible to obtain two information about the battery: (i) the SoC, which is obtained through the analytical battery model proposed in Section 4.2; and (ii) the voltage level, which is concurrently obtained through the execution of the voltage model presented in Section 4.2.5.

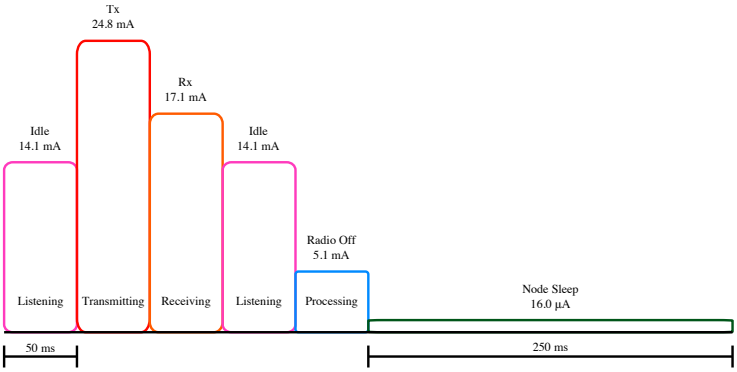

Figure 19 – A discharge profile. Tx = Transmitting; Rx = Receiving.

The remainder of this chapter is organized as follows. Section 5.1 includes the results of some experimental assessments, which are used to validate the T-KiBaM model for duty cycle operation mode. Section 5.2 presents the achieved results when running T-KiBaM on low-power MCUs, considering metrics such as the model execution time, memory usage and energy consumption. Section 5.3 extends the previous section by adding a proof-of-concept application example, where other metrics are evaluated in an emulated operating scenario. Section 5.4 presents the main considerations of the chapter.

5.1 T-KIBAM VALIDATION IN DUTY CYCLE SCHEME

This section aims to validate and compare the analytical results obtained from the T-KiBaM model with some experimental results. The error between the two approaches is compared regarding the battery lifetime estimation. The values of all the constants of the T-KiBaM model were obtained previously in Section 4.2.3. In addition, the model implementation is in accordance with the pseudo-codes presented in Section 4.3.1. Finally, all the analytical evaluations use the same experimental characteristics, e.g., discharge profile and temperature.

Some experiments using a Duty Cycle (DC) scheme are carried out to evaluate the ability of the T-KiBaM model to handle typical WSN scenarios. The discharge current in the active part of the DC is set at 30 mA, which is the highest value among the tested currents in order to decrease the time of the experiments. The following duty cycle schemes are evaluated in this section:

$$DC_{75\%} = [(I_1 = 30\text{ mA}, t_1 = 3\text{ s}); (I_2 = 0.0\text{ mA}, t_2 = 1\text{ s})];$$
$$DC_{50\%} = [(I_1 = 30\text{ mA}, t_1 = 1\text{ s}); (I_2 = 0.0\text{ mA}, t_2 = 1\text{ s})];$$
$$DC_{25\%} = [(I_1 = 30\text{ mA}, t_1 = 1\text{ s}); (I_2 = 0.0\text{ mA}, t_2 = 3\text{ s})].$$

Note that the duty cycle period is 4 s for $DC_{75\%}$ and $DC_{25\%}$, and 2 s for $DC_{50\%}$. In addition, only the temperature at 25 °C is used in the experiments. Table 12 presents the results of this evaluation, including the relative error for each situation.

Table 12 – Battery lifetime using duty cycle schemes.

		25 °C	
Duty Cycle (%)	**EXP (h)**	**T-KiBaM (h)**	**ERR (%)**
75	33.524	33.849	0.97
50	51.229	50.774	0.89
25	102.547	101.549	0.97
AVG			0.94

EXP: Experimental result; ERR: Relative error.

These results demonstrate that T-KiBaM can accurately estimate the battery lifetime of WSN nodes, presenting an average relative error value of 0.94% for duty cycle schemes.

5.2 RUNNING T-KIBAM IN LOW-POWER MCUs

This section presents the experimental results obtained when implementing the T-KiBaM model in some WSN-compatible MCUs. The objective is to check if analytical battery models, embedded in a low computational capacity hardware, can be used to track both the SoC and voltage level of the battery over time. Briefly, the basic characteristics of each MCU used in this work are presented first. Then, it is included a discussion regarding the selected metrics utilized for the experimental assessments. The results obtained from the experimental evaluations are shown at the end of this section.

As the analytical results presented in Sections 4.3 and 5.1 are consistent with those found in the experimental assessments, a PC with a 2.9 GHz Intel Core i5 processor running Matlab is used as the basis of the comparisons regarding the battery lifetime estimation. Matlab is considered a reliable platform for the execution of this algorithm as it presents a high precision regarding the number of significant figures.

5.2.1 MCUs and Related Hardware Platforms

Arduino[1] is an open-source platform that has been designed to facilitate electronic circuits prototyping. Arduino boards support the addition of sensors and/or actuators to existing designs, allowing the interaction with the physical environment. The use of this platform is highly popular due to its low cost, compatibility among operating systems, as well as the easy extensibility of both software and hardware. There are multiple Arduino board types. This work focuses on the UNO version that includes an Atmel ATmega328P low-power AVR 8-bit MCU, which has 32 KB of integrated Flash memory, as well as 2

[1] <https://www.arduino.cc>

KB of SRAM and 1 KB of EEPROM. This MCU operates at 16 MHz on the UNO board. The current consumption at 1 MHz is 0.2 mA in active mode (ATMEL, 2017a). Other MCUs are also used in the experimental assessments. These MCUs are programmed in C language with specific manufacturer library[2]. The specifications of each used MCU are summarized in Table 13 (at the end of this section).

The Atmel ATmega128RFA1 is an 8-bit AVR MCU, which has a built-in 128 KB of Flash memory, as well as 16 KB of SRAM and 4 KB of EEPROM. The MCU can operate up to 16 MHz (ATMEL, 2017b). The Atmel ATxmega256A3U is an 8/16-bit AVR XMEGA low-power MCU that features 256 KB of Flash memory, as well as 16 KB of SRAM and 4096 bytes of EEPROM. This MCU can run at 32 MHz (ATMEL, 2017c). The Atmel SAMR21G18A MCU uses a low-power 32-bit ARM Cortex-M0+ processor. This chip has a 256 KB of Flash memory, plus 32 KB of SRAM (ATMEL, 2017f). The Atmel SAMG55 is based on the ARM architecture. This MCU has a 32-bit Cortex-M4 core that can reach speeds up to 120 MHz with a Floating Point Unit (FPU). In addition, this chip has 512 KB Flash Memory and 160 KB SRAM plus up to 16 KB (cache + I/D RAM) (ATMEL, 2017d). The Atmel SMART SAMV71Q21 is based on the ARM architecture, featuring a Cortex-M7 RISC 32-bit processor with a FPU. This MCU can reach speeds up to 300 MHz, featuring 2048 KB of Flash memory, as well as a dual 16-KB cache and 384 KB of SRAM memories (ATMEL, 2017e).

[2] <http://www.atmel.com/tools/avrsoftwareframework.aspx>

Table 13 – Specifications of the used MCUs.

MCU	Platform	Clock (MHz)	Wait State	FPU	Flash (KB)	SRAM (KB)	EEPROM (KB)	Typical Current (mA)
ATmega328P	8-bit AVR	16	0	no	32	2	1	0.2
ATmega128RFA1	8-bit AVR	16	0	no	128	16	4	4.1
ATxmega256A3U	8/16-bit AVR	32	0	no	256	16	4	9.5
SAMR21G18A	32-bit ARM Cortex-M0+	48	1	no	256	32	0	6.7
SAMG55	32-bit ARM Cortex-M4	120	5	yes	512	160	0	24.2
SAMV71Q21	32-bit ARM Cortex-M7	300	6	yes	2048	384	0	83.0

5.2.2 Performance Metrics

The set of tasks includes the same continuous discharge currents used in the experimental assessments, as well as a variety of other discharge current values. Such set comprises the following currents: 5, 10, 20, 30, 40, 50, 60, 70, 80, 90, and 100 mA. The following metrics are used for this experimental assessment: (i) algorithm execution time; (ii) memory usage; (iii) energy consumption; (iv) number of algorithm iterations for different tasks; and (v) estimated battery lifetime.

5.2.3 Experimental Results Using Low-Power MCUs

The results shown in this section were obtained by running the T-KiBaM functions on different low-power MCUs. Note that, when using continuous discharge currents in the analytical evaluations, the T-KiBaM function requires an operating time t_I (or time step) as input to run the battery model. Hereafter, a 1-second step is assumed between consecutive executions as it represents a relevant low granularity when continuous discharge currents are used to feed the model (if compared to the total battery discharge time). A discussion regarding the time step size is performed in Section 5.3.3 of this manuscript.

5.2.3.1 Execution Time

The first evaluated metric is the function Execution Time (ET) when running T-KiBaM in low-power MCUs. The objective is to compare the performance of the algorithm in platforms with different characteristics to verify the possibility of its implementation in WSN nodes.

It is important to note that the results presented in this section consider the average of three executions of the algorithm. The execution times are collected from checkpoints at the beginning and at the end of the T-KiBaM function call. In addition, all MCUs can only access the flash memory with a maximum clock of 32 MHz and, after that speed, wait-states must be inserted. All the performed experiments used the best configuration to achieve the fastest results. Note

that the focus of this work is not in the evaluation of the faster MCU, therefore, the source code is compiled with `-O2` option and no specific optimization is performed in the available libraries. The FPU has been enabled on all MCUs that have this option. The instruction cache has been enabled in SAMG55 and the instruction/data cache has been enabled in SAMV71. The use of same MCU manufacturer allowed both to unify code and test the same library for all MCU models. Table 14 presents the average execution times achieved by each platform.

Table 14 – Execution times (average) on all platforms[†].

	ATmega 328P	**ATmega 128RFA1**	**ATxmega 256A3U**	**SAMR 21G18A**	**ATSAM G55**	**SAMV 71Q21**
Execution Time (μs)	549.02	499.86	259.10	1311.65	164.87	5.33

[†] Results using the clock frequencies shown in Table 13.

The results point to average execution times of less than 1.4 ms on all platforms. The SAMV71Q21 MCU presented an average execution time close to 5.3 μs. This result is within the expected range, since this MCU operates at a higher frequency, i.e., 300 MHz. On the other hand, the SAMR21G18A MCU delivers a poor performance for a MCU from its category. The average execution time around 1.3 ms, even when operating at 48 MHz, could be related to lack of code optimization of GCC compiler (LAUNCHPAD.NET, 2017) that increases code size and, consequently, slows down the code execution considerably. The performed experiments clarified that optimization should be mandatory to achieve better results. Tests also have shown that ARM and AVR produce similar results when using soft float ABI (Application Binary Interface) and no cache since ARMs, probably, are stalled waiting for new instruction due to wait-states. Despite this, the rational indicates that the obtained values are feasible when compared with real-world applications, such as the use of encryption algorithms in WSNs with low-power MCUs, which presents execution times between 1.53 and 7.41 ms (OTHMAN; TRAD; YOUSSEF, 2012).

5.2.3.2 Memory Usage

The second evaluated metric is memory usage. Analysing the amount of Flash memory occupied by the T-KiBaM model is an important metric, as the MCUs used in WSN nodes usually have very little available memory. In this sense, it is possible to establish the spatial cost of implementing an analytical battery model in a low-power MCU.

Note that the results presented in this section consider only the memory usage relative to the T-KiBaM model source code implementation and the essential compiled components on each platform. In other words, libraries and debugging codes are not considered in this analysis. Table 15 presents the memory usage on all platforms, including the percentage of total available memory.

Table 15 – Memory usage on all platforms.

	ATmega 328P	**ATmega 128RFA1**	**ATxmega 256A3U**	**SAMR 21G18A**	**ATSAM G55**	**SAMV 71Q21**
Memory usage (KB)	7.444	11.384	19.254	40.376	39.136	25.712
Total Available (KB)	32	128	256	256	512	2048
Percentage of total (%)	23.2	8.9	7.5	15.7	7.6	1.2

According to Table 15, the implementation of T-KiBaM on the SAMR21G18A occupies approximately 40.3 KB, the highest memory occupancy among all platforms. On the other hand, the ATmega328P presents the lowest memory occupancy, with only 7.4 KB. However, in relation to the total Flash memory availability, this MCU has the highest occupancy, about 23.2% of 32 KB in total. The SAMV71Q21 has the lowest memory occupancy rate in percentage terms. Note that four of the six tested platforms have memory occupancy rates of less than 10%. Thus, these results show that it is feasible to implement an analytical battery model on a low-power WSN node, such as the iLive node, which features 128 KB of Flash memory (LIU et al., 2014).

5.2.3.3 Power Consumption

The power consumption is the third metric evaluated in this thesis. The objective is to assess how much energy consumes an iteration of the T-KiBaM algorithm. For this, it is necessary to measure the current consumed by each MCU first. Further details are given below.

A multimeter (MD-6450 True-RMS) is used to measure the current on each platform. All measurements are taken with the board of each MCU connected via USB while running the T-KiBaM model. Voltage variations are not considered since the algorithm execution time is minimal (<1.4 ms). Thus, the average values for voltage (≈5.05 V) and current are considered in the calculations of this section. Table 16 shows the measured current values as well as the electrical power for each MCU, calculated through the relation $P = V \times I$.

Table 16 – Power consumption in each platform.

	ATmega 328P	ATmega 128RFA1	ATxmega 256A3U	SAMR 21G18A	ATSAM G55	SAMV 71Q21
Power Supply (V)	5.05	5.05	5.05	5.05	5.05	5.05
Current (mA)	49.3	77.1	18.9	12.0	30.2	82.6
Power (mW)	248.9	389.3	95.4	60.6	52.5	417.1

From these results, it is possible to obtain the energy spent according to the ET of an iteration of T-KiBaM algorithm in each MCU through the relation $E_n = P \times \Delta t$. In this case, Δt is obtained from the execution time in each platform. Thus, the energy spent is directly related to the first metric, the ET. Table 17 shows the average energy spent when running a single iteration of T-KiBaM on each platform. Note that these results are compatible with those obtained when performing the steps of encryption algorithms on a WSN node (TelosB), where the power consumptions vary between 0.033 and 0.116 mJ (OTHMAN; TRAD; YOUSSEF, 2012).

Table 17 – Energy spent (average) on a single iteration.

	ATmega 328P	ATmega 128RFA1	ATxmega 256A3U	SAMR 21G18A	ATSAM G55	SAMV 71Q21
Energy Spent (mJ)	0.1366	0.1945	0.0247	0.0794	0.0086	0.0022

5.3 APPLICATION EXAMPLE

WSN nodes usually perform several tasks during their operation, including data transmission (Tx), reception (Rx) and processing (Pr). It is also possible to save energy during certain intervals of time by putting the nodes in sleep mode (Sl). Generally speaking, such nodes operate in duty cycle scheme, i.e., cyclically repeating a sequence of tasks over time, until their battery power runs out. The objective of this section is to illustrate the usage of T-KiBaM in a real application, considering the operating characteristics of real-world WSN nodes. With this, other performance metrics can be assessed regarding the execution of the T-KiBaM model in low-power MCUs. Finally, the presented application example is used in a sensitivity analysis, where variations are applied to the input parameters of the T-KiBaM model.

5.3.1 Scenario Description

The situations described in this section covers the mode of operation of most WSN applications. Two scenarios are described: (i) the node remains 100% of the time in the active mode; and (ii) the node operates in a duty cycle scheme, i.e., inserting periods in sleeping mode alternately with its active period. Further details are given below.

A set of tasks (discharge profile) can be used to emulate the operation of the nodes correctly, i.e., discharge the battery charge when performing different tasks. However, for the sake of simplicity, it is assumed that the node performs only one useful task (e.g., Rx, Tx, or Pr) in both scenarios. A task is defined by the discharge current and its operating time (I_x, t_x), including periods in sleeping mode. The node

executes the T-KiBaM algorithm at the end of each task to update its battery SoC. Although it may play a significant role in energy consumption, the node initialization process is not considered in these analyses, since it runs only once during its entire life cycle. Figure 20 depicts a schematic summarizing the two presented scenarios.

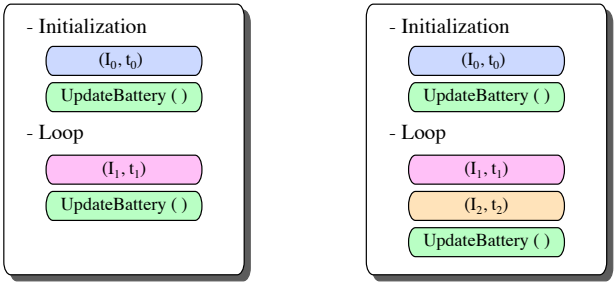

(a) Scenario 1 (b) Scenario 2

Figure 20 – Node activity modes. (**a**) Active; (**b**) Active + Inactive.

As depicted in Figure 20 (a), Scenario 1 presents the behaviour of a node operating 100% of the time in active mode. Note that the main loop considers only the performed task, represented by (I_1,t_1), and the update of the battery state of charge and voltage level. On the other hand, Figure 20 (b) presents Scenario 2, which adds a sleep mode period, represented by (I_2,t_2), at each duty cycle. In this sense, the node performs its main task, goes into a low-power mode (Sl), and then updates the battery state of charge and voltage level.

5.3.2 Estimating the Battery Lifetime

The fourth metric assessed is the battery lifetime estimation. One of the main features of T-KiBaM model is to provide this information according to the used discharge profile. Thus, a modified version of Algorithm 5 is considered to allow the cyclic execution of the discharge profile, i.e., as a duty cycle scheme, until the battery charge runs out. Through this simple modification, it becomes possible to predict the total battery lifetime according to both the discharge profile and operating temperature. Scenarios 1 and 2 are used in these assessments

as they depict the operating mode of traditional WSN nodes. The evaluations performed in this section consider the aspects below.

The first requirement to evaluate the battery lifetime estimation is to run the T-KiBaM model until the battery charge runs out. In these evaluations, the selected cut-off point occurs when the T-KiBaM algorithm indicates SoC $= 0\%$ ($\approx$2.0 V). Note that other cut-off points can be selected depending on the hardware requirements (e.g., 2.1 V or 2.2 V). The second aspect concerns the tested set of tasks, which is the same as mentioned in Section 5.2.2 for Scenario 1. For simplification purposes, the experiments using Scenario 2 assume that the sleep mode does not consume energy (i.e., $I_2 = 0.0$ mA), although it is recognized that there is a small discharge current in this state, usually in the range of μA (MIKHAYLOV; TERVONEN, 2012). The last aspect concerns the number of iterations required for the algorithm to complete the estimation regarding the battery lifetime. The lower the granularity of the operating times (t_x) of the discharge currents (I_x), the greater the number of iterations of the algorithm and, consequently, the longer its computation time. Figure 21 (a) depicts the number of iterations, after performing the T-KiBaM model until the battery charge runs out, for each discharge current presented in the mentioned set of tasks.

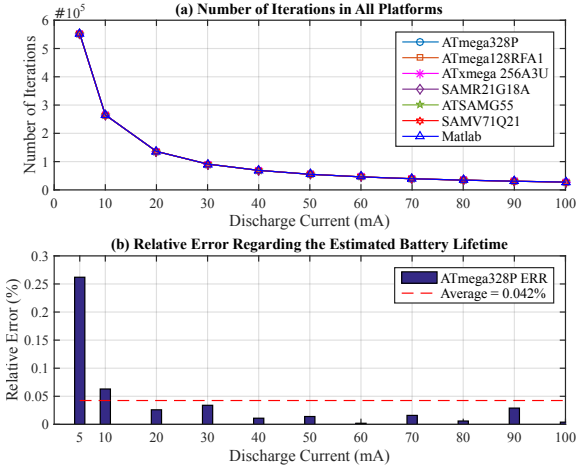

Figure 21 – Results. (**a**) Number of iterations; (**b**) Relative Error.

Considering the previously mentioned aspects, the challenge of this evaluation is to assess how close the estimates of the battery lifetime are from the results obtained when executing the T-KiBaM model on a PC. The assessments for Scenarios 1 and 2 are presented below.

For the Scenario 1 assessments, the entire set of tasks (i.e., $I_1 =$ 5, 10, 20, 30, 40,..., 100 mA) is executed with $t_1 = 1$ s. Table 19 (at the end of this section) presents the results regarding the estimated battery lifetime obtained when running the T-KiBaM algorithm on all platforms using Scenario 1. Note that the EXP column represents the results obtained when using real batteries at 25 °C, when available.

The results indicate small Relative Errors (ERRs) when compared to the estimated battery lifetime on a PC running Matlab. For instance, considering all tested discharge currents, the average deviation between the ATmega328P and Matlab is 0.042%. In this case, the minimum ERR is 0.002% and the maximum ERR is 0.262% (when $I_1 = 5$ mA). Figure 21 (b) depicts the ERR of the ATmega328P with respect to the estimated battery lifetime when using T-KiBaM on Matlab for the entire set of discharge currents. The other MCUs present the following average ERRs: 0.042% (ATmega128RFA1), 0.042% (ATxmega-256A3U), 0.023% (SAMR21G18A), 0.023% (ATSAMG55) and 0.023% (SAMV71Q21).

The evaluations for Scenario 2 consider the insertion of sleeping periods between the activities of the node (DC scheme). The evaluated DCs are as follows: 100%, 75%, 50%, 25%, 10%, and 5%. The discharge current (I_1) has its value set at 30 mA to allow comparison with the experimental results. Thus, the current profiles are as follows:

$$
\begin{aligned}
DC_{100\%} &= [(30\text{ mA}, 1\text{ s}); (0.0\text{ mA}, 0\text{ s})],\\
DC_{75\%} &= [(30.0\text{ mA}, 3\text{ s}); (0.0\text{ mA}, 1\text{ s})],\\
DC_{50\%} &= [(30.0\text{ mA}, 1\text{ s}); (0.0\text{ mA}, 1\text{ s})],\\
DC_{25\%} &= [(30.0\text{ mA}, 1\text{ s}); (0.0\text{ mA}, 3\text{ s})],\\
DC_{10\%} &= [(30.0\text{ mA}, 1\text{ s}); (0.0\text{ mA}, 9\text{ s})],\\
DC_{5\%} &= [(30.0\text{ mA}, 1\text{ s}); (0.0\text{ mA}, 19\text{ s})].
\end{aligned}
$$

Since the results between platforms for Scenario 1 are very similar, the evaluations for Scenario 2 are performed only with the ATmega328P MCU. Table 18 presents the results obtained after running the T-KiBaM algorithm on this platform using Scenario 2. Again, the EXP column represents the results obtained from experiments with Ni-MH batteries at 25 °C, when available.

Table 18 – Estimated Battery Lifetime (ELT)†.

Duty Cycle (%)	**ATmega 328P ELT (h)**	**MATLAB ELT (h)**	**EXP (h)**
100	25.3956	25.3869	25.385
75	33.8533	33.8489	33.524
50	50.7678	50.7744	51.229
25	101.6122	101.5489	102.547
10	253.8528	253.8722	-
5	507.3667	507.7444	-

EXP: Experimental time.

† Results considering Scenario 2 in ATmega328P.

The results illustrated in Table 18 demonstrate that the estimates for the battery lifetime are compatible on both platforms. The variations in the results arise by virtue of the accuracy of the numerical representation in each platform. Regarding the voltage level tracking, Figure 22 depicts the behavior of the battery discharge curves for duty cycles of 75%, 50% and 25% at 25 °C. The experimental data represents the average behaviour obtained in the experimental assessments, being presented as fitted curves. The analytical results are obtained through data prints during the execution of the T-KiBaM algorithm. However, only the fitted curves are presented for easy viewing.

Table 19 – Estimated Battery Lifetime (ELT)† in all platforms.

I_1 (mA)	ATmega 328P ELT (h)	ATmega128 RFA1 ELT (h)	ATxmega256 A3U ELT (h)	SAMR21 G18A ELT (h)	ATSAM G55 ELT (h)	SAMV71 Q21 ELT (h)	MATLAB ELT (h)	EXP (h)
5	153.1517	153.1517	153.1517	153.4969	153.4969	153.4969	153.5533	-
10	73.7003	73.7003	73.7003	73.6264	73.6264	73.6264	73.6536	73.557
20	37.8050	37.8050	37.8050	37.8028	37.8028	37.8028	37.8150	37.984
30	25.3956	25.3956	25.3956	25.3764	25.3764	25.3764	25.3869	25.385
40	19.1914	19.1914	19.1914	19.1850	19.1850	19.1850	19.1936	-
50	15.3572	15.3572	15.3572	15.3575	15.3575	15.3575	15.3550	-
60	12.7958	12.7958	12.7958	12.7947	12.7947	12.7947	12.7956	-
70	10.9658	10.9658	10.9658	10.9667	10.9667	10.9667	10.9675	-
80	9.5961	9.5961	9.5961	9.5953	9.5953	9.5953	9.5967	-
90	8.5328	8.5328	8.5328	8.5300	8.5300	8.5300	8.5303	-
100	7.6775	7.6775	7.6775	7.6778	7.6778	7.6778	7.6772	-

EXP: Experimental time.

† Results considering Scenario 1 in all platforms.

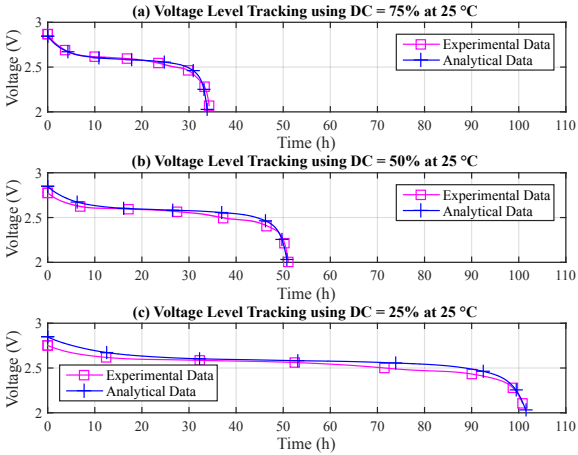

Figure 22 – Results regarding the voltage level tracking.

5.3.3 Sensibility Analysis of T-KiBaM Model

Finally, this section presents an assessment of the same application example, when different values are considered for the time step (t_x) of the discharge current (I_x) in the T-KiBaM function. The purpose is to assess the relationship between the execution time of the algorithm for different tasks and the quality of the estimation-prediction concerning the battery operating behaviour, i.e., its lifetime and voltage level over time, in Scenario 1. Note that the time step value corresponds to the interval between two consecutive invocations of the battery update function. The following time steps are used for this assessment: 1, 2, 5, 10 and 60 s. This evaluation is performed only for the ATmega328P, as this MCU presents the hardware with the least amount of available resources among all the previously assessed devices. Thus, these results can be similarly extended to the other platforms.

First, the quality of the estimated battery lifetime is evaluated for different time steps. The following metrics are evaluated: (i) execution time; (ii) number of iterations; and (iii) estimated battery lifetime. The assessments considering Scenario 1 are performed below.

The first evaluated metric is the execution time for the entire set of tasks when different time steps are used as input to the T-KiBaM function. Figure 23 (a) depicts the results obtained for the set of discharge currents (cf. Section 5.2.2). Note that the execution time of each task (I_x, t_x) reduces significantly, as the discharge current time step increases. For example, by comparing the time steps of 1 s and 10 s when $I_1 = 5$ mA, the execution time falls from 303.98 s to 32.227 s when the algorithm is executed until the battery charge runs out. Considering the entire set of tasks, it is possible to observe an execution time 9.5 times faster, on average. The same behaviour is observed for the second metric, i.e., the number of iterations, as shown in Figure 23 (b). Using the same previously-mentioned time steps, 1 s and 10 s, the number of iterations drops from 551,347 to 55,320, respectively. Considering the entire set of tasks, it is possible to observe a reduction in the number of iterations equivalent to 10 times, on average.

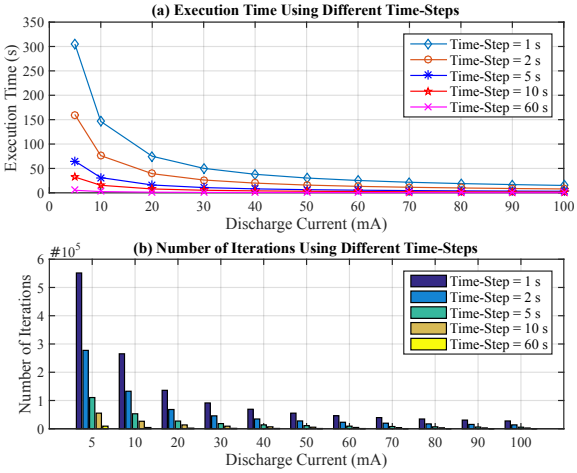

Figure 23 – Results using different time steps.

The third evaluated metric is the estimated battery lifetime when different time steps are used as input to the T-KiBaM function. Figure 24 (a) depicts the results for the same set of discharge currents. As expected, battery lifetimes have small variations for all cases.

Clearly, in terms of resource savings and performance, WSN designers should select the highest time step values. However, this selection must also take into account the imprecision introduced in the estimation when large time intervals are used to make the measurements. Figure 24 (b) depicts the relative error for each time step considering the results obtained in a PC regarding the selected set of discharge currents. Note that the relative error is less than 0.4% for all the assessed cases. Particularly, the time step equal to 2 s has the highest relative errors for tasks with low discharge currents (<50 mA). On the other hand, the time step equal to 60 s presents highest relative error for tasks with larger discharge currents (>50 mA). Thus, the time step equal to 10 s is most indicated when continuous discharge currents are evaluated by the T-KiBaM model. In this case, both the execution time and the number of iterations are significantly smaller and, at the same time, both the average relative error and the standard deviation compared to the values estimated in the PC are the lowest.

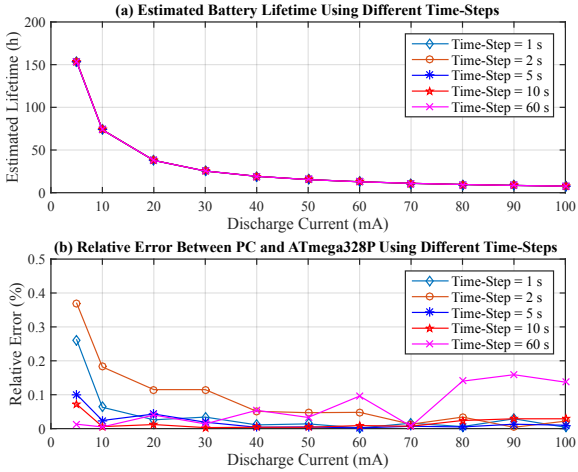

Figure 24 – Results using different time steps.

Finally, the voltage level estimation provided by the T-KiBaM model is evaluated over time, using different time steps (Scenario 1). Again, a comparison of the experimental and analytical results is per-

formed using the results provided by the ATmega328P MCU at the mentioned time steps. Figure 25 depicts the behaviour of the estimation of the voltage curve at each update of the T-KiBaM model, under a continuous discharge current of 30 mA at -5 °C. The experimental data are adjusted according to the average behaviour of three tests.

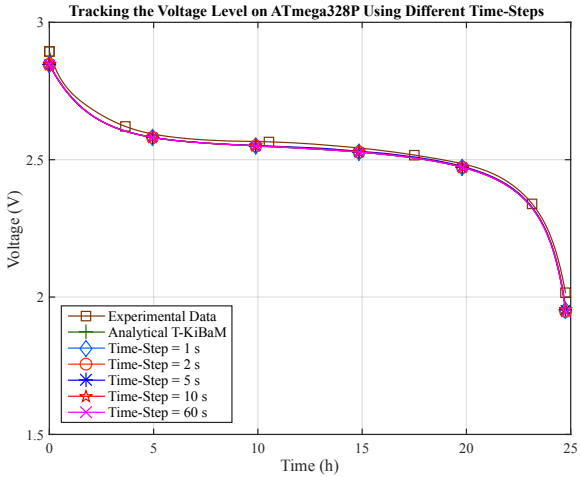

Figure 25 – Results using different time steps for voltage tracking.

The assessments made for the ATmega328P present the same results of the analytical evaluation performed on the PC, regardless the used time step. Thus, it is clear that the T-KiBaM model generates compatible results for both low-power and robust platforms regarding the voltage level tracking. This is a major result, since estimating the voltage level over time is required to ensure the operation of any sensor node, allowing for optimizations in the WSN management policies.

5.4 CHAPTER REMARKS

Analytical battery models can assist in estimating the battery lifetime, achieving results close to reality. However, two problems may arise within the WSN context. Firstly, the implementation of complex analytical models on low-capacity hardware platforms is not an easy

task, due to their low processing capabilities, memory constraints and the high accuracy required to represent low varying analogue values. Secondly, the execution of this type of models by real-world nodes may influence its energy consumption. Thus, the required effort to estimate the network lifetime may reduce the lifetime of the network itself.

The study performed in this chapter evaluated the cost of executing the T-KiBaM model in low-power MCUs. The model validation took into account experimental data. As shown in Sections 4.3 and 5.1, the T-KiBaM model can accurately estimate the lifetime of Ni-MH batteries and is also able to predict the voltage behaviour over time at different temperatures, which is an important issue when considering devices (sensor nodes) that require a minimum voltage value to maintain their operation. The analytical models were implemented upon different MCUs. As a result, although running T-KiBaM on low-power MCUs requires long computing times, such computing times do not represent a significant slice of the estimated battery lifetime. Therefore, the time required to estimate the battery behaviour (which includes tracking both its SoC and voltage level over time) is feasible.

6 USING T-KIBAM MODEL IN A WSN SIMULATOR

WSNs can be used in many types of environments due to the flexibility offered by sensor nodes. Regardless of whether the environment is indoor or outdoor, WSNs are subject to local operating conditions, and they can be influenced by several factors (e.g., pressure, temperature, and humidity). Particularly, the thermal effect can influence the operation of the embedded hardware in the sensor nodes (BANNISTER; GIORGETTI; GUPTA, 2008; BOANO et al., 2010), mainly their batteries. These electrochemical devices are very sensitive to temperature variations, which impairs the offered effective charge capacity. This unpredictability makes it difficult to obtain important information for energy-aware approaches, such as the battery SoC and lifetime (HÖRMANN et al., 2012).

WSN simulators are often used before the deployment of the physical network in order to analyse the behaviour of the sensor nodes in the context of the implemented application. Regarding the energy, such simulators use battery models to estimate both the SoC and the lifetime of the sensor nodes. However, most WSN simulators use simplistic battery models that do not consider important effects on battery behaviour (STETSKO; STEHLÍK; MATYAS, 2011; KHAN et al., 2011; MORAVEK; KOMOSNY; SIMEK, 2011; HAASE; MOLINA; DIETRICH, 2011; STETSKO; STEHLÍK; MATYAS, 2011; MUSZNICKI; ZWIERZYKOWSKI, 2012; PEREIRA; RUIZ; GHIZONI, 2015), such as the thermal effect, which can change the lifetime of the sensor nodes. This situation deviates the result of simulations concerning the network lifetime in environments with temperature variations, affecting both the management and maintenance of the WSN after its deployment.

The objectives of this chapter are as follows: (i) extend the T-KiBaM model to increase the accuracy of estimates on battery behaviour in scenarios with temperature variations; and (ii) integrate this extended T-KiBaM model in a WSN simulator widely used by the scientific community. Thus, designers can simulate the lifetime of WSNs in environments with variable temperatures.

The remainder of this chapter is organized as follows. Section 6.1 presents the experiments performed to validate the T-KiBaM model with respect to different temperature profiles. This section also includes a new algorithm that allows use the T-KiBaM model in environments with temperature variations. Section 6.2 presents the implementation of T-KiBaM in a WSN simulator, including an application example. Finally, Section 6.3 presents the main considerations of the chapter.

6.1 EXPERIMENTAL ASSESSMENTS

This section presents the experimental validation of the T-KiBaM model for environments with temperature variations over time. The objective is to emulate the operation of sensor nodes in different ambient conditions. Particularly, the interest is in the observation of the effects caused by the temperature variations during the day in the behaviour of the batteries, mainly their lifetime. Thus, this section is divided into three parts: (i) description of the experimental assessments; (ii) implementation of the T-KiBaM algorithm for environments with temperature variations; and (iii) T-KiBaM validation.

6.1.1 Description of the Experimental Assessments

The discharge currents (I) used in the experimental assessments are as follows: 20 and 30 mA. These values represent discharges in the order of 0.026C and 0.04C (refer to Section 2.1.3 for details regarding the C-Rate), respectively, since the nominal capacity of the battery is 750 mAh. This produces tests lasting approximately 25 hours (for $I =$ 30 mA) and 37.5 hours (for $I = 20$ mA). The temperature profiles used in the experimental assessments consider these times for discharging the batteries. The temperature ranges from 15 °C to 40 °C in all experimental assessments. Thus, the implemented temperature profiles are as follows: two constant ramps, (i) ascending and (ii) descending; and two customized sinusoidal curves with different frequencies, (iii) F1 and (iv) F2, created to mimic temperature variation in one day. Figures 26 and 27 depicts the implemented temperature profiles.

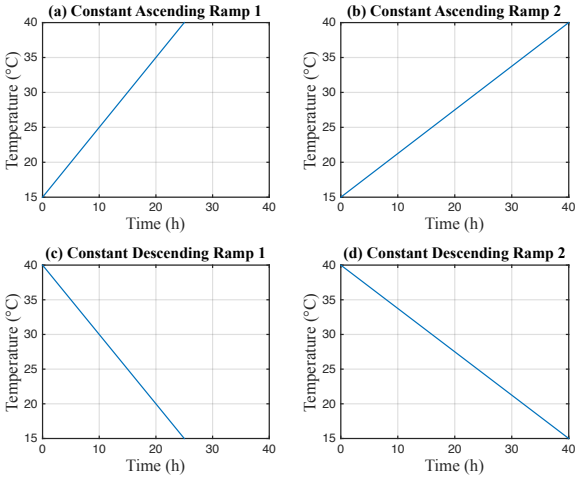

Figure 26 – Temperature profiles with constant ramp behaviour.

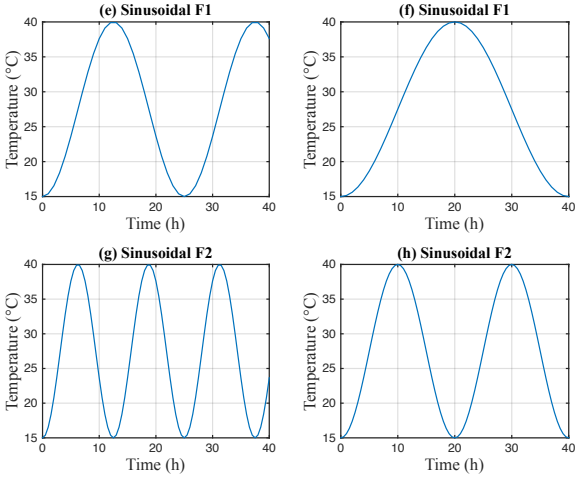

Figure 27 – Temperature profiles with sinusoidal behaviour.

In Figures 26 and 27, note that the graphs to the left refer to experiments for discharge currents equal to 30 mA. The graphs on the right refer to the experiments for discharge currents equal to 20 mA. For easy viewing, the scale of the graphics is the same in all cases.

6.1.2 T-KiBaM for Variable Temperatures

In order to become possible to estimate the lifetime of sensor nodes in typical WSN scenarios, this section presents the implementation of a function to describe the operation of the T-KiBaM model in environments with temperature variations. The implemented function receives as input parameters the variables/constants corresponding to the T-KiBaM and TVM models, as well as the discharge and temperature profiles. Algorithm 3 presents the implementation of this function.

Algorithm 3: T-KiBaM_call

Input: $\{E_a, A, R, q_0, c\}$, $\{E_0, R_b, K_b, \tau_b, B, prExp\}$, $\{DP_{set}, TP_{set}\}$
Output: q_1, q_2, t_0, V_b

$It = 0$;
$t_0 = 0$;
$q_x = q_0$;
$q_0 = q_0 \cdot CF(TP_{set}(T_1))$;
$task_{avg} = \text{sum}(DP_{set}(I_x) \cdot DP_{set}(t_x))/\text{sum}(DP_{set}(t_x))$;
foreach $T_x \in TP_{set}$ **do**
    $lifetime = (q_x \cdot CF(TP_{set}(T_x)))/(task_{avg} \cdot 1000)$;
    $q_x = q_x + (q_x \cdot (CF(TP_{set}(T_x)) - 1.0)/lifetime)$;
    $q_1 = (c) \cdot q_x$;
    $q_2 = (1 - c) \cdot q_x$;
    $k = A \cdot e^{-Ea/(R \cdot T_x)}$;
    update_TVM_Parameters $(E_0, R_b, K_b, \tau_b, B, T_x)$;
    foreach $[I_x, t_x] \in DP_{set}$ **do**
        if $q_1 > 0$ **then**
            $[q_1, q_2, t_0]$ = T-KiBaM_function $(c, k, q_1, q_2, t_0, I_x, t_x)$;
            $It = It + (I_x \cdot t_x)$;
            $Exp = (1/(1 + (B \cdot I_x \cdot t_x \cdot \tau_b))) \cdot prExp$;
            V_b = TVM_function $(E_0, R_b, K_b, \tau_b, B, q_0, I_x, It, Exp)$;
            $prExp = Exp$;
        end
    end
end
return (q_1, q_2, t_0, V_b);

The first group of parameters are related to the T-KiBaM model, where: E_a, A and R are the Arrhenius constants that define the new rate constant k of the KiBaM model; q_0 and c are the constants that

represent the initial battery charge and the fraction of charge stored in the Available Charge tank, respectively; the second group of parameters (E_0, R_b, K_b, τ_b, B, $prExp$) are related to the TVM model; the sets DP_{set} and TP_{set} refer to the discharge and temperature profiles, respectively. These latter parameters are described in more detail below.

As presented in Section 4.3.1, the discharge profile of a sensor node can be written as $DP_{set} = [(I_1,t_1);(I_2,t_2);\ldots;(I_n,t_n)]$, where $n \in \mathbb{N}$. Note that the discharge profile must contain the tasks performed by each sensor node. Therefore, a task is defined by the pair $task_x = (I_x,t_x)$, for $x = 1,2,3,\ldots,n$, where I_x and t_x represent, respectively, the discharge current and the execution time of $task_x$.

The temperature profile of a sensor node can be written as $TP_{set} = \{T_1,T_2,T_3,\ldots,T_n\}$. Each input of TP_{set} refers to the average temperature in an hour interval. Note that the temperature profiles should represent the simulated environment, such as those shown in Figures 26 and 27. This choice is arbitrary and can be modified according to the requirements of each WSN application.

After some initial definitions in Algorithm 3, Line 4 performs the correction of the initial battery charge through the CF function, already described in Section 4.2.4. The average discharge current of DP_{set} is calculated in the Line 5. For each temperature input (Line 6), the following steps are performed: (i) compute the estimated battery lifetime according to the average discharge current (Line 7); (ii) compute the amount of charge to be added to/removed from the battery (q_x) according to the instantaneous temperature (Line 8); (iii) update the rate constant value according to the temperature, in Kelvin scale (Line 11); (iv) update the parameters of the TVM model according to the temperature, also in Kelvin scale (Line 12); and (v) update q_1, q_2, t_0, and V_b considering $task_x$ (Lines 15 and 18), according to Equations (2.7) and (4.7), respectively. Finally, Algorithm 3 returns the contents in the available and bound charge tanks, as well as the elapsed time and the voltage of the battery (Line 23).

6.1.3 T-KiBaM Validation

This section presents the validation of the T-KiBaM model by comparing experimental and analytical results. Matlab was used to generate analytical results. This assessment relates to the battery lifetime for different temperature profiles, as mentioned in Section 6.1.1. In this case, two battery models are used for comparison purposes: KiBaM and Peukert's Law. Some considerations are presented below.

The KiBaM model does not take into account the temperature. Therefore, its parameters must be adjusted according to an arbitrary temperature. In this case, the room temperature (i.e., 25 °C) is used in the analytical assessments. This means that $c = 0.56486$ and $k = 0.59526\ s^{-1}$. In addition, the nominal capacity of the Panasonic HHR-4MRT battery is used as the initial value for the battery capacity of the KiBaM model, i.e., $q_0 = 2700$ As (750 mAh). These parameters may be easily adjusted, in case of using another battery technology.

Peukert's law is also used in these comparisons and, since this battery model does not consider temperature effects, its constants are adjusted according to experimental results at 25 °C using $I = 30$ mA. Thus, $a = 0.75$ A and $b = 1.0067$. Table 20 presents a comparison of the experimental and analytical results for the mentioned battery models.

In Table 20, the T-KiBaM model presents a large Relative Error (ERR) in only one case, i.e., in the test with $I = 20$ mA and temperature profile in the form of a constant descending ramp, where ERR = 2.21%. This is due to the fact that the T-KiBaM model increases the initial amount of battery charge through the function CF. Given the discharge current and the experiment time, the T-KiBaM model can not properly consume the battery charge as the temperature decreases. One possible solution concerns a change in the algorithm to satisfy such a condition. This situation can be an interesting concern in future work, including the evaluation of the algorithm for smaller currents, e.g., 10 mA. The last column of Table 20 shows the average ERR (AVG) of each model in all temperature profiles. Note that the T-KiBaM model provides the lowest average ERRs regarding the battery lifetime.

Table 20 – T-KiBaM validation.

Battery Model	I (mA)	Ascending Ramp EXP (h)	Ascending Ramp SIM (h)	Ascending Ramp ERR (%)	Descending Ramp EXP (h)	Descending Ramp SIM (h)	Descending Ramp ERR (%)	Sinusoidal F1 EXP (h)	Sinusoidal F1 SIM (h)	Sinusoidal F1 ERR (%)	Sinusoidal F2 EXP (h)	Sinusoidal F2 SIM (h)	Sinusoidal F2 ERR (%)	AVG (%)
T-KiBaM	20	38.171	37.8203	0.92	36.975	37.7936	2.21	37.426	37.7253	0.80	38.135	37.7658	0.97	1.22
	30	25.680	25.3878	1.14	25.168	25.3706	0.81	25.629	25.3419	1.12	25.510	25.2914	0.86	0.98
KiBaM	20	38.171	36.9397	3.22	36.975	36.9397	0.24	37.426	36.9397	1.30	38.135	36.9397	3.13	1.97
	30	25.680	24.7994	3.43	25.168	24.7994	1.46	25.629	24.7994	3.24	25.510	24.7994	2.79	2.73
Peukert's Law	20	38.171	36.2059	5.15	36.975	36.2059	2.08	37.426	36.2059	3.26	38.135	36.2059	5.06	3.88
	30	25.680	24.2424	5.60	25.168	24.2424	3.68	25.629	24.2424	5.41	25.510	24.2424	4.97	4.91

EXP: Experimental time; SIM: Analytical time; ERR: Relative Error; AVG: Average ERR.

6.2 SIMULATION ASSESSMENTS

This section presents the implementation of the T-KiBaM model in a WSN simulator that is widely used by the scientific community. The objective is to evaluate the possibility of implementing a more accurate battery model in a simulator for low-power WSNs and also verify the impact of this new model in the performed simulations. Thus, this section is divided into three parts: (i) a brief introduction to the used WSN simulator; (ii) the simulation set-up, which includes details about the implementation and its validation for continuous discharge currents; and (iii) an application example with simulation results.

6.2.1 The Castalia WSN Simulator

There are many alternatives to perform WSN simulations, e.g., Cooja (Cooja, 2017), TOSSIM (TOSSIM, 2017), and NS-2 (NS-2, 2017). Several factors must be taken into account to choose a simulator. WSNs with low-power devices is the main interest of this thesis. In this scenario, communications between nodes require low-power consumption and typically occur at predetermined time periods by using a duty cycle scheme. Thus, the simulator must be able of dealing with such network characteristics. As presented in Section 3.3, the Castalia simulator is one of the candidates capable of meeting such requirements.

The Castalia simulator (Castalia Team, 2017) is able to perform simulations involving WSNs, Body Area Networks (BANs) and general purpose networks with low-power devices. Its main advantage is the realistic radio and wireless channel models, which makes simulations more reliable. Besides not being constrained to a specific sensor platform, this simulator allows to create distributed algorithms and protocols, as well as to evaluate the WSN behaviour in several scenarios by enabling a wide combination of parameters during the simulation set-up. On the other hand, the energy consumption model in Castalia is inaccurate since it does not consider the thermal effect and its influence in the batteries. Thus, it becomes necessary to use a more appropriate battery model for realistic simulations.

6.2.1.1 Castalia Architecture and Node Structure

The architecture of the Castalia simulator comprises three modules. The *node* module is responsible for interactions on the network. The *wireless channel* module forwards the messages to the correct recipients when a node sends packets. The *physical process* links the nodes according to what they monitor. Figure 28 depicts both the Castalia architecture and node structure.

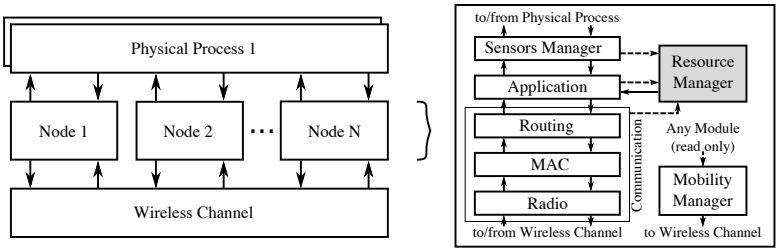

Figure 28 – Castalia architecture and node structure.

Five sub-modules compose the node structure. The *application module* coordinates the main task of the node. The *communication module* (Routing, MAC and Radio) processes the packages to/from the node. The *mobility manager module* provides the ability to move the node, periodically reporting its position to the wireless channel. The *sensor manager module* allows the creation of different types of sensors, including some of their operating characteristics (e.g., sensitivity and resolution). The *resource manager module* performs the energy consumption and sets up some hardware features. The focus of this thesis is on resource manager module, as highlighted in the Figure 28.

The resource manager receives messages from other modules. Such messages notify how much power each module consumes. Thus, the resource manager can register the consumed energy, either periodically or whenever there is a change in the power consumption. This module contains an important variable called `initialEnergy`, which stores the initial battery energy (in Joules). Its default value is 18720 J, corresponding to the energy of two hypothetical AA alkaline batteries.

Castalia subtracts that energy linearly over time. However, this approach is not adequate for many simulations, since batteries suffer influences both from the network configuration (e.g., duty cycle, radio power, and sleep mode consumption) and from their chemical characteristics. Such influences can modify the battery behaviour over time.

6.2.2 Simulation Set-up

This section presents the details about the simulation set-up. In this sense, this section is divided into two topics: (i) T-KiBaM implementation into Castalia simulator; and (ii) the validation of the implementation, which includes adjustments in the simulator to reflect the characteristics of experiments using constant discharge currents.

6.2.2.1 Implementing T-KiBaM Methods in Castalia

The resource manager module has three source codes files: ResourceManager.ned, ResourceManager.h and ResourceManager.cc. All mentioned files undergo changes as described below.

`ResourceManager.ned` includes T-KiBaM parameters that receive default values in their initialization. However, users can change the default values in the `.ini` file of any simulation. For example, initial values are given for the constants used in the Arrhenius equation, i.e., A, E_a, R, and T. Similarly, the T-KiBaM variables/constants, c, k, q_0, and nV, also receive initial values. Initially, q_0 has the same value of the `initialEnergy` variable. Then, such a variable undergoes adjustments according to the simulated temperature by using the CF function. The variable nV represents the nominal battery voltage.

`ResourceManager.h` defines two new methods:

- `void startKibam()`: a protected method that initializes the model parameters and check their values before the simulation starts.
- `double kibam(double t, double I)`: a public method that updates the content within both Available and Bound Charge tanks, according to Equation (2.7).

`ResourceManager.cc` implements the methods above. The `kibam (double t, double I)` method sets the value of the `amount` parameter in the `consumeEnergy (double amount)` method (already present in Castalia), as the following: `consumeEnergy (kibam(t,I))`, where t is the operational time of the discharge current I.

The `amount` parameter indicates the quantity of energy removed from the battery. When a node performs a task[1] for a specific period of time, its battery loses an amount of energy proportional to the task requirements. In this case, this parameter reflects the behaviour of the Available Charge tank in the T-KiBaM model.

Figure 29 depicts a class diagram of the Castalia simulator. Note that modules inherit the "CastaliaModule" class characteristics, as in the case of the "ResourceManager" module. This module includes the public method which implements the T-KiBaM, as described above.

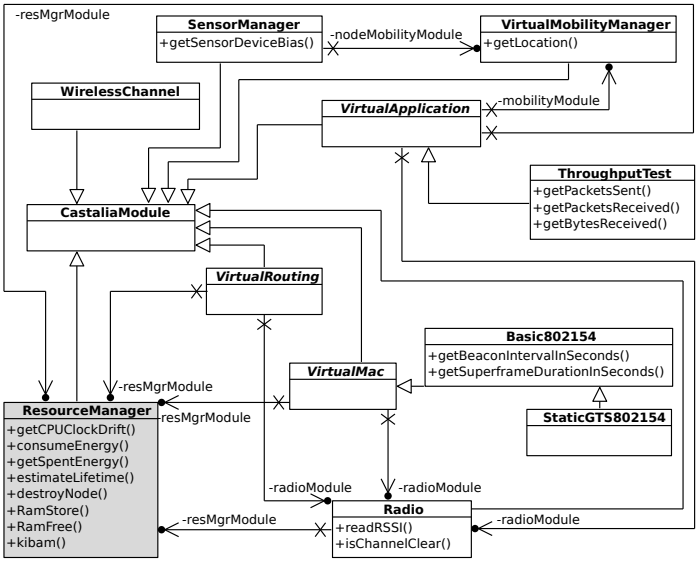

Figure 29 – A class diagram of the Castalia simulator.

[1] A task is any activity that consumes energy, including idle periods.

6.2.2.2 Validating the Implementation

This section sets Castalia parameters so that the simulations reflect the settings used in the experiments with continuous discharge currents. In addition, a simulation is performed to validate the implementation of the T-KiBaM model in the Castalia Simulator.

First, it is necessary to change some parameters from the IEEE 802.15.4[2] standard to implement different DCs in Castalia. In this case, by setting `beaconOrder` = 10 and `frameOrder` = {5, 6, 7, 8, 9, 10}, simulations can use the following duty cycles, respectively: 3.125, 6.25, 12.5, 25, 50 and 100%. Next, it is also important to eliminate both the energy consumption in the 'power transition matrix' and the switching delay between radio states in 'delay transition matrix'. In this case, all matrix values are set to zero. Finally, beacon losses may occur during network operation, which can affect the energy consumption throughout the simulation. To avoid this situation, it is necessary to disable the path loss mapping in the simulator. By using these modifications, the node behaviour becomes similar to the experiments. Both the simulation scenario and evaluated metrics are presented below.

Simulations follow an example from Castalia, named BANtest[3]. An application called "ThroughputTest" comes with BANtest. In such application, all network nodes send packets to the sink (node 0) at a constant rate. BANtest uses the standard IEEE 802.15.4 MAC implementation, `StaticGTS802154`, which inherits the parameters of the `Basic802154` class. Table 21 presents the settings used in BANTest simulation. The values of the parameters of the T-KiBaM model are the same as those presented in Chapter 4.

The scenario has two nodes in an area of 52 × 32 m. Nodes have no mobility. The simulation runs until the battery energy ends, i.e., SoC decreases to 0%. Simulations with 500 seconds are also performed for the battery estimated lifetime assessment.

The sensor node remains in the Rx state for the entire simulation

[2] <http://standards.ieee.org/getieee802/download/802.15.4-2015.pdf>
[3] See Section 3.6.1 of the Castalia User Manual (Castalia Team, 2017) for details.

Table 21 – Simulation characteristics.

Environment	Parameter	Specification
Castalia	Nodes	2 (0 is the sink)
	Terrain	52 x 32 meters
	Mobility	None
	Simulation Time	Until SoC = 0%
	Radio (Standard values in BANtest Simulation)	Tx = 2.93 mW @ -15 dBm Rx = 3.10 mW @ -87 dBm Sleep = 0.05 mW
	Battery	2.4 V (750 mAh)
	Initial Energy	6480 Joules
	Data Rate	1024 Kbps
	Baseline	0

time. Thus, the radio power in the Rx state needs to be changed to three new values. By considering the battery nominal voltage (nV) and $P = V \cdot I$, the new Rx values are as follows:

$$25.0176 \text{ mW} \approx 10.424 \text{ mA@2.4 V},$$
$$48.7272 \text{ mW} \approx 20.303 \text{ mA@2.4 V},$$
$$72.5808 \text{ mW} \approx 30.242 \text{ mA@2.4 V}.$$

Sensor nodes are configured to have the same energy of the HHR-4MRT batteries from Panasonic, i.e., $\approx$ 6480 J. Since this thesis does not address the sink behaviour, this particular node has an initial energy of 100 KJ to ensure that its lifetime is greater than the sensor nodes. Baseline parameter (minimum energy consumption) is set to 0.

The simulations are performed at the following temperatures: – 5, 10, 25, 32.5, and 40 °C. WSNs face similar conditions when used, particularly, in places with the incidence of snow (low temperatures) or in an industrial environment (room or high temperatures). In the first case, the battery usually provides a smaller effective charge capacity and consequently a shorter lifetime; in the second case, the battery

can provide charge beyond its nominal capacity and therefore a longer lifetime, as shown in the experiments performed for this thesis.

There are two criteria (metrics) to assess the network operating time: the total lifetime and the estimated lifetime. In (DIETRICH; DRESSLER, 2009), authors cite several definitions regarding network lifetime. In Castalia, by default, the network lifetime refers to the time that the first node fails due to lack of energy. Therefore:

- **Total Network Lifetime (TNL)**: refers to the total time that the network lasts when performing a complete simulation, i.e., until the first node's battery runs out of energy. This is the main metric evaluated in this thesis.

- **Estimated Network Lifetime (ENL)**: refers to the estimated network lifetime when the user performs a partial simulation. Usually, the battery does not deplete its entire energy. However, the Castalia simulator provides an estimated network lifetime based on the energy consumption of the sensor nodes.

Table 22 shows the simulation results comparing the T-KiBaM and the original battery model of Castalia regarding the experimental data at different temperatures. In this case, the TEMP column indicates the temperature of the simulation and the EXP column represents the average battery lifetime of three experimental assessments. The T-KiBaM ERR and Original ERR columns represent the relative error between the TNL and EXP columns.

Note that the average ERR (AVG) obtained by simulating the T-KiBaM in Castalia is less than 0.3%, with a standard deviation (STDEV) of 0.30%. On the other hand, the original battery simulator model in Castalia has an average relative error of 1.39%, with a standard deviation of 0.92%. The ENL shows little or no variation at all with respect to the TNL in each model, indicating that the estimates concerning the network lifetime are consistent in both models.

Table 22 – Simulation results comparison.

TEMP (°C)	Discharge Current (mA)	EXP (h)	T-KiBaM TNL (h)	T-KiBaM ENL (h)	T-KiBaM ERR (%)	Original TNL (h)	Original ENL (h)	Original ERR (%)
-5	10.424	72.306	71.806	71.805	0.69	71.951	71.950	0.49
	20.303	36.714	36.866	36.866	0.42	36.941	36.941	0.62
	30.242	24.749	24.750	24.750	0.00	24.800	24.800	0.21
10	10.424	72.728	72.770	72.769	0.06	71.951	71.950	1.07
	20.303	37.402	37.361	37.361	0.11	36.941	36.941	1.23
	30.242	25.087	25.082	25.082	0.02	24.800	24.800	1.14
25	10.424	73.557	73.653	73.652	0.13	71.951	71.950	2.18
	20.303	37.984	37.814	37.815	0.45	36.941	36.941	2.75
	30.242	25.385	25.387	25.387	0.01	24.800	24.800	2.30
32.5	10.424	73.201	73.968	73.967	1.05	71.951	71.950	1.71
	20.303	37.835	37.976	37.976	0.37	36.941	36.941	2.36
	30.242	25.560	25.495	25.496	0.25	24.800	24.800	2.97
40	10.424	72.263	72.595	72.594	0.46	71.951	71.950	0.43
	20.303	37.133	37.271	37.271	0.37	36.941	36.941	0.52
	30.242	25.022	25.022	25.022	0.00	24.800	24.800	0.89
AVG					0.29			1.39
STDEV					0.30			0.92

6.2.3 Application Example with Simulation Results

This section presents an application example of the T-KiBaM model running in the Castalia simulator. The objective is to analyse the behaviour of WSN nodes in an environment with variable temperature over time. In this sense, this section is divided into two topics: (i) scenario description; and (ii) simulation results.

6.2.3.1 Scenario Description

In the scenario presented in this section, the application example employs 10 sensor nodes plus 1 coordinator, which are distributed over an area of 30 × 30 m. The network uses a star topology, i.e., the sensor nodes communicate only with the coordinator of the network. All parameters removed or modified in Section 6.2.2.2 have been re-established in this simulation. Figure 30 depicts the described scenario.

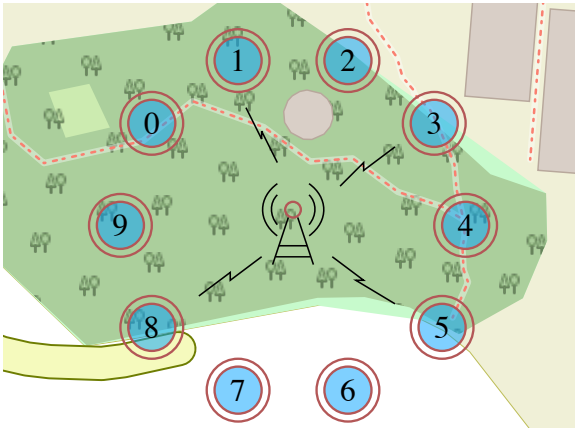

Figure 30 – Scenario overview.

In this scenario, the network coordinator accepts the connection of only four sensor nodes at a time. The other sensor nodes, which initially were unable to connect to the network coordinator, enter into a deep duty cycle, waking up sporadically (every 16.6 minutes) to check the possibility of connecting to the network coordinator. When one of

the active sensor nodes loses connection for some reason (e.g., lack of battery power, communication interference or other hardware failures), the network coordinator allows a new connection. This is done until all the sensor nodes in the network have their batteries depleted, which determines the WSN lifetime. The temperature varies from hourly in the same way for all sensor nodes, according to the temperature profile used in the simulation. For these simulations, the temperature profiles are the same as shown in Figure 26 (a) and (c), and in Figure 27 (e) and (g). Such behaviours are cyclically repeated every 24 hours until the end of the simulation.

The value of other simulation parameters is presented below. All sensor nodes use a 350 mAh battery. Such a value was chosen according to the Panasonic HHR-35AA/FT battery (PANASONIC, 2016) in order to reduce the time of the simulations since such capacity is considered small compared to traditional batteries offered in the consumer market. Thus, the initial energy of the sensor nodes is $\approx$ 3024 J @ 2.4 V. As in Section 6.2.2.2, the network coordinator has an "infinite" energy, i.e., 100 KJ. The radio transceiver used in the simulation is the C2420, which has the following power consumption per state: Rx = 62 mW, Tx = 55.18 mW @ –1 dBm and Sleep = 1.4 mW. The delay and power transition matrices are also considered in the simulations.

6.2.3.2 Simulation Results

This section presents a comparison of the simulation results using Castalia's original energy model and T-KiBaM. The objective is to emphasize that the temperature interferes with the behaviour of the batteries in sensor nodes deployed in environments with temperature variations. Table 23 shows the results of the simulations using different temperature profiles[4]. Figure 31 depicts the results of Node ID = 0.

[4] The simulation time in each of the described scenarios was approximately 10 minutes.

Table 23 – Simulation results.

TP	Constant Ascending Ramp		Constant Descending Ramp		Sinusoidal F1		Sinusoidal F2		Sinusoidal LT	
Node ID	Original Time (h)	T-KiBaM Time (h)	Original Time (h)	T-KiBaM Time (h)	Original Time (h)	T-KiBaM Time (h)	Original Time (h)	T-KiBaM Time (h)	Original Time (h)	T-KiBaM Time (h)
0	93.269	96.835	93.269	96.890	93.269	96.615	93.269	96.509	93.269	93.034
1	171.596	178.111	171.596	246.418	171.596	177.694	171.596	177.592	171.596	236.619
2	171.598	178.113	171.598	178.260	171.598	177.685	171.598	177.595	171.598	171.139
3	171.584	178.099	171.584	178.251	171.584	177.682	171.584	177.580	171.584	171.130
4	93.275	96.842	93.275	96.897	93.275	96.622	93.275	96.516	93.275	93.041
5	93.281	96.848	93.281	96.903	93.281	96.628	93.281	96.522	93.281	93.047
6	237.079	246.160	237.079	178.248	237.079	245.665	237.079	245.358	237.079	171.126
7	171.598	178.113	171.598	178.260	171.598	177.694	171.598	177.594	171.598	171.138
8	93.269	96.835	93.269	96.890	93.269	96.615	93.269	96.509	93.269	93.034
9	237.082	246.166	237.082	246.422	237.082	245.669	237.082	245.361	237.082	236.621

TP: Temperature Profile; LT: Low Temperature.

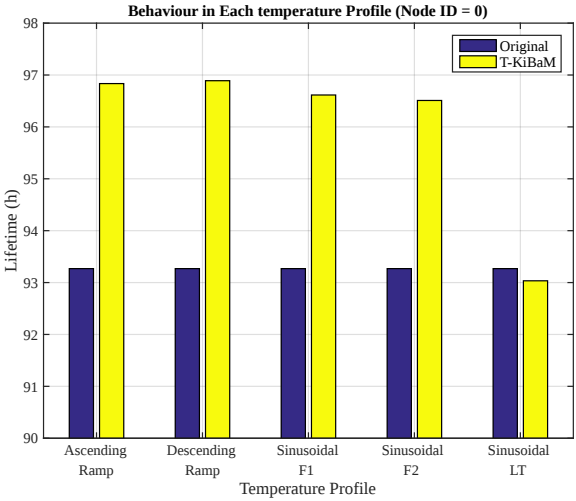

Figure 31 – Results of Table 23 for Node ID = 0.

Table 23 shows that in all simulations using Castalia's original energy model, the sensor nodes have the same battery lifetime, regardless of the ambient temperature. However, by using the T-KiBaM model, the sensor nodes present different battery lifetimes according to the temperature profile. For example, by comparing the battery lifetime of node 9 in the second and fourth scenarios (when using the T-KiBaM model), there is a difference of 63.66 minutes in its lifetime.

These results showed that there is a significant difference between the two battery models. For example, when comparing the results in the constant descending ramp scenario, node 0 has a 3.88% increase in its lifetime, which represents a difference of more than 14 days in a sensor node operating for one year. However, there will not always be an increase in lifetime. When simulating a sinusoidal profile with low temperatures (Sinusoidal LT, which considers a behaviour similar to the F1 curve, but with temperatures between –5 and –4 °C), the lifetime of the sensor nodes is lower than that found using the original model. Thus, T-KiBaM allows analysing the behaviour of the network in specific scenarios (e.g., environments with extreme temperatures), which optimizes the management/maintenance of the WSN.

6.3 CHAPTER REMARKS

This chapter explored the use of an accurate battery model for WSN simulations in environments with constant and variable temperatures. This is the case of the T-KiBaM, a battery model that takes into account the influence of temperature on the performance of electrochemical cells, particularly their lifetimes. Thus, the T-KiBaM was implemented in Castalia simulator in order to compare the results of simulations in environments with different temperature conditions.

This assessment found an average difference of 1.39% between experimental data and the Castalia's original energy model when analysing constant discharge currents. Conversely, T-KiBaM showed better results, with an average relative error of 0.30% in the same conditions, as this model considers the thermal effect on battery performance.

In environments with variable temperatures, the T-KiBaM model was able to perform adequately, since it presented different results in each of the analysed scenarios. In one of them, the difference between the battery models reached 3.88%, which may represent several days for a node operating for long periods of time (e.g., months or years).

Through these results, this chapter have shown that T-KiBaM is an appropriate model to estimate the battery lifetime of WSN nodes deployed in harsh environments, i.e., where the temperature plays an important role in the battery behaviour. If the simulation purpose is to evaluate the battery lifetime, the correct choice of the battery model may influence the results. The T-KiBaM approach can help WSN designers regarding the battery behaviour over time in both complete and short simulations. Moreover, T-KiBaM allows the use of different battery technologies, e.g., Ni-MH or Li-ion. For this, one need to apply the method to obtain the new model parameters according to experimental data. Hence, simulations may model different behaviours, particularly with respect to thermal effect. Although T-KiBaM provides realistic results, it is important to note that it may take more time than Castalia's original model to complete a simulation. The comparison of these simulation times can be an interesting concern for future work.

7 CONCLUSIONS AND FUTURE WORK

WSNs are very important in the modern world as they allow the interconnection of computing devices without the need for a cable to mediate communication. In spite of this, WSNs present a great energy restriction, since batteries power the sensor nodes. Such electrochemical devices have limited operating time and need to be used efficiently to avoid unnecessary power consumption.

The focus of this thesis was to evaluate the behaviour of the batteries in the context of WSNs. In this regard, Chapter 2 presented some relevant information on batteries, ranging from basic concepts to a study on battery models. Concerning this last aspect, it was verified that there are several battery models, being each one indicated for a particular kind of application. For example, electrochemical models are highly accurate. However, they require the use of high-performance hardware for the execution of estimates on battery behaviour. On the other hand, analytical battery models appear as a good alternative for use in the context of WSNs, since they present an adequate trade-off between the level of computational effort and accuracy on estimates regarding the behaviour of batteries in different discharge conditions. Such kind of performance is ideal for use in low-power sensor nodes.

Chapter 3 presented a review about state of the art in the context of battery models. It was possible to notice that several works are dealing with this subject. Particularly, the use of battery models in the context of Electric Vehicles (EVs) and Hybrid Electric Vehicles (HEVs) is in a moment of ascension, and several battery models have been proposed to deal with this type of application. However, such models usually require an extensive number of parameters for their use, which increases their computational complexity and hinders their application in WSN sensor nodes. This chapter showed that some studies use battery models to evaluate the behaviour of batteries in sensor nodes, either via hardware or software. On the other hand, it was possible to observe that the study of these approaches is still quite superficial. Important phenomena, such as the thermal effect, are often neglected in

practical implementations, which can lead to simulation or estimation errors on the behaviour of the batteries over time in sensor nodes.

From the gap presented in Chapter 3, it was verified the need to implement a battery model that is appropriate to the characteristics and constraints found in WSNs. Thus, a new analytical battery model capable of dealing with thermal effects was proposed in Chapter 4. Such a battery model, called Temperature-Dependent Kinetic Battery Model (T-KiBaM), is based on the concepts of chemical kinetics for modelling the behaviour of batteries typically used in WSNs. The key features of the proposed battery model are (i) the use of the Arrhenius equation to model the transfer of charge between the tanks of the "battery" (cf. Figure 6) and (ii) the implementation of a function capable of determining the charge capacity of the battery according to the ambient temperature. A significant number of experimental assessments with Ni-MH batteries at different temperatures were required for the validation of the analytical results obtained with the T-KiBaM model.

In order to demonstrate the utility of the proposed battery model, it was decided to perform its evaluation under two aspects: (i) its computational cost in low-power hardware; and (ii) its use in a WSN simulator. The first item was discussed in Chapter 5, which presented a complete study regarding the execution time of the algorithm in several micro-controllers typically used in WSN nodes. The memory usage ratio and the estimated power consumption were also evaluated in this chapter. In addition, Chapter 5 presented an application example of the proposed battery model. The results of the chapter indicate the feasibility of implementing the T-KiBaM model in hardware with low computational capacity since the presented values are compatible with the results of other well-known algorithms applied in the same context (e.g., cryptographic algorithms). The second item was discussed in Chapter 6, which also presented the results on the possibility of using the proposed battery model in environments with variable temperatures. The obtained analytical values indicated a high accuracy in relation to the results of the experiments (both were compared under the same conditions). Regarding the implementation of the T-KiBaM

model in a WSN simulator (Castalia), it was possible to observe that the use of a more accurate lifetime estimation method is essential. In particular, the simulations showed that the thermal effect can significantly influence the behaviour of the batteries in sensor nodes, which in turn are exposed to environmental conditions (e.g., pressure, temperature and humidity). Such conditions may modify the behaviour of the hardware, which includes the batteries of the sensor nodes.

7.1 LIST OF PUBLICATIONS

This research resulted in the following publications:

1. Rodrigues, L.M.; Montez, C.; Vasques, F.; Portugal, P. Recovery Effect in Low-Power Nodes of Wireless Sensor Networks. In: Branco, K.; Pinto, A.; Pigatto, D. (eds) Communication in Critical Embedded Systems. WoCCES 2013, WoCCES 2014, WoCCES 2015, WoCCES 2016. Communications in Computer and Information Science, vol. 702, 2017. Springer, Cham. <https://doi.org/10.1007/978-3-319-61403-8_3>

2. Rodrigues, L.M.; Montez, C.; Budke, G.; Vasques, F.; Portugal, P. Estimating the Lifetime of Wireless Sensor Network Nodes through the Use of Embedded Analytical Battery Models. Journal of Sensor and Actuator Networks, 2017, 6, 8. <http://dx.doi.org/10.3390/jsan6020008>

3. Rodrigues, L.M.; Montez, C.; Moraes, R.; Portugal, P.; Vasques, F. A Temperature-Dependent Battery Model for Wireless Sensor Networks. Sensors, 2017, 17, 422. <http://dx.doi.org/10.3390/s17020422>

4. Rodrigues, L.M.; Montez, C.; Vasques, F.; Portugal, P. Experimental Validation of a Battery Model for Low-Power Nodes in Wireless Sensor Networks. IEEE World Conference on Factory Communication Systems (WFCS). 3-6 May, 2016. Aveiro, Portugal. <https://doi.org/10.1109/WFCS.2016.7496519>

7.2 FUTURE WORK

The energy problem is, in fact, highly relevant in the context of WSNs. Particularly, predicting the behaviour of the sensor nodes' batteries according to the activities performed and environmental conditions is a complex task. This work presented a possible solution to the problem through the use of a temperature-dependent analytical battery model and its validation through comparison with experimental data. At the same time, some lines of research were identified during this thesis. These topics are discussed below.

On the proposed model, it was identified the need to perform a complete set of experiments, which includes tests with different temperatures, to validate the accuracy of the T-KiBaM model when using it to predict the behaviour of the battery in a duty cycle scheme. This type of operation is most common in WSNs nodes. As mentioned in this thesis, this project created a test-bed platform for battery discharge experiments. Such hardware can be used in future experimental analyses, which facilitates the investigation of energy-aware approaches and their comparison with experimental data in the context of WSNs. However, the time for these experiments is quite large, which should be taken into account before deciding to carry them out.

Another aspect that can be considered in future research is the extraction of parameters and validation of the T-KiBaM model for different types of batteries, particularly, Li-ion. This battery technology is one of the most used in the market and can be used in the context of WSNs. However, one must take into account the cost of acquiring the material needed to carry out the experiments, e.g., batteries and chargers. According to this thesis, Li-ion batteries usually present a higher price compared to Ni-MH batteries. In addition, Li-ion technology requires the use of specific and generally more expensive chargers.

The present work also identified the possibility of using the T-KiBaM model in a closed-loop way. For this, it is important to determine a form of feedback of the model, which includes a set of parameters from the battery, e.g., voltage level, temperature, and in-

stantaneous discharge current. The rationale points out that such an approach would allow the use of T-KiBaM embedded in an Integrated Circuit (IC). However, this is just a "guess". It is important to check the requirements for the implementation of this approach, identifying its feasibility before starting the project itself.

Another relevant aspect in the use of batteries relates to their State of Health (SoH), a percentage value similar to the SoC. However, the SoH parameter considers the reduction of battery capacity over time (GUASCH; SILVESTRE, 2003). That is, the modelling of this parameter allows to establish the loss of capacity of the battery according to its use. This is a factor that can be included in the proposed battery model, T-KiBaM. The rationale points to two ways of accomplishing this task: (i) by performing experiments under the same conditions with real batteries and to measure the provided charge capacity, which makes it possible to estimate the behaviour of the battery over time; and (ii) by using models available in the literature to estimate the SoH. The first case requires many experiments and, therefore, a long time to complete. The second case eliminates the need for experiments, however, the model chosen to estimate the SoH should consider the desired type of application.

In the context of simulations, there are still many scenarios that can be analysed using the T-KiBaM model. For example, the entire set of experiments performed in this thesis can be implemented in simulators for the verification of battery behaviour in environments with varying temperatures. In addition, the T-KiBaM model allows the analysis of other algorithms/protocols concerning energy consumption in certain types of applications, e.g., industrial WSNs or environments with extreme temperature profiles (e.g., snow and desert scenarios).

BIBLIOGRAPHY

AGARWAL, V. et al. Development and Validation of a Battery Model Useful for Discharging and Charging Power Control and Lifetime Estimation. *IEEE Transactions on Energy Conversion*, v. 25, n. 3, p. 821–835, 2010. 72, 73

AKYILDIZ, I. F. et al. Wireless Sensor Networks: A Survey. *Computer Networks*, v. 38, n. 4, p. 393–422, 2002. 11, 33

ALIPPI, C. et al. Adaptive Sampling for Energy Conservation in Wireless Sensor Networks for Snow Monitoring Applications. *IEEE International Conference on Mobile Adhoc and Sensor Systems (MASS)*, 2007. 86

ANALOG DIGITAL INC. *4-/6-Channel Digital Potentiometer AD5204/AD5206*. 2016. Available at: <http://www.analog.com/media/en/technical-documentation/data-sheets/AD5204_5206.pdf>. Accessed on December 12, 2016. 82

ANASTASI, G. et al. Energy Conservation in Wireless Sensor Networks: A Survey. *Ad Hoc Networks*, Elsevier B.V., v. 7, n. 3, p. 537–568, 2009. 12, 34

ANTOLÍN, D.; MEDRANO, N.; CALVO, B. Reliable Lifespan Evaluation of a Remote Environment Monitoring System Based on Wireless Sensor Networks and Global System for Mobile Communications. *Journal of Sensors*, v. 2016, 2016. 75

ANYAEGBUNAM, I. The Development of a Battery Management System with Special Focus on Capacity Estimation and Thermal Management. 2016. University of Texas. PhD Thesis. 73

ARDUINO. *Arduino UNO*. 2016. Available at: <https://www.arduino.cc/en/Main/ArduinoBoardUno>. Accessed on December 12, 2016. 81

ARON, A.; GIRBAN, G.; KILYENI, S. A Geometric Approach of a Battery Mathematical Model for On-line Energy Monitoring. *IEEE International Conference on Computer as a Tool (EUROCON)*, p. 1–4, 2011. 73

ARON, A.; GÎRBAN, G.; POP, C. About the Solution of a Battery Mathematical Model. *Proceedings of the International Conference of Differential Geometry and Dynamical Systems (DGDS)*, n. January 2015, p. 1–10, 2011. 74

ASHWIN, T. R.; CHUNG, Y. M.; WANG, J. Capacity Fade Modelling of Lithium-ion Battery Under Cyclic Loading Conditions. *Journal of Power Sources*, Elsevier B.V, v. 328, p. 586–598, 2016. 73

ATMEL. *Home Page*. 2016. Available at: <http://www.atmel.com>. Accessed on June 2, 2016. 106

ATMEL. *8-Bit AVR Microcontroller with 4/8/16/32K Bytes In-System Programmable Flash*. 2017. Available at: <http://www.atmel.com/pt/br/devices/ATMEGA328P.aspx>. Accessed on February 9, 2017. 110

ATMEL. *8-Bit AVR Microcontroller with Low Power 2.4 GHz Transceiver for ZigBee and IEEE 802.15.4 (ATmega128RFA1)*. 2017. Available at: <http://www.atmel.com/pt/br/Images/Atmel-8266-MCU_Wireless-ATmega128RFA1_Summary_Datasheet.pdf>. Accessed on February 9, 2017. 110

ATMEL. *8/16-bit Atmel XMEGA A3U Microcontroller*. 2017. Available at: <http://www.microchip.com/wwwproducts/en/ATxmega256A3U>. Accessed on March 6, 2017. 110

ATMEL. *ATSAMG55*. 2017. Available at: <http://ww1.microchip.com/downloads/en/DeviceDoc/Atmel-11289-32-bit-Cortex-M4-Microcontroller-SAM-G55_Datasheet.pdf>. Accessed on March 9, 2017. 110

ATMEL. *ATSAMV*. 2017. Available at: <http://www.atmel.com/products/microcontrollers/arm/sam-v-mcus.aspx>. Accessed on June 3, 2017. 110

ATMEL. *SMART ARM-Based Wireless Microcontroller*. 2017. Available at: <http://www.atmel.com/Images/Atmel-42223\T1\textendashSAM-R21_Datasheet.pdf>. Accessed on March 6, 2017. 110

BANNISTER, K.; GIORGETTI, G.; GUPTA, S. K. Wireless Sensor Networking for Hot Applications: Effects of Temperature on Signal Strength, Data Collection and Localization. *Proceedings of the 5th Workshop on Embedded Networked Sensors (HotEmNets)*, p. 1–5, 2008. 12, 34, 127

BARCELLONA, S.; GRILLO, S.; PIEGARI, L. A Simple Battery Model for EV Range Prediction: Theory and Experimental Validation. *International Conference on Electrical Systems for Aircraft, Railway, Ship Propulsion and Road Vehicles and International Transportation Electrification Conference (ESARS-ITEC)*, 2017. 73

BEHRENS, C. et al. Energy-Efficient Topology Control for Wireless Sensor Networks Using Online Battery Monitoring. *Advances in Radio Science*, v. 5, p. 205–208, 2007. 76

BEHRENS, C. et al. An Effective Method for State-of-Charge Estimation in Wireless Sensor Networks. *Proceedings of the International Conference on Embedded Networked Sensor Systems (SenSys)*, p. 427, 2007. 76

BENABDELAZIZ, K.; MAAROUFI, M. Battery Dynamic Energy Model for Use in Electric Vehicle Simulation. *International Journal of Hydrogen Energy*, Elsevier, p. 1–8, 2017. Available at: <http://linkinghub.elsevier.com/retrieve/pii/S0360319917321067>. 72, 73

BENEDETTI, D.; PETRIOLI, C.; SPENZA, D. GreenCastalia: An Energy-Harvesting-Enabled Framework for the Castalia Simulator. *Proceeding of the International Workshop on Energy Neutral Sensing Systems (ENSSys)*, 2013. 77

BOANO, C. A. et al. The Impact Of Temperature On Outdoor Industrial Sensornet Applications. *IEEE Transactions on Industrial Informatics*, v. 6, n. 3, p. 451–459, 2010. 12, 34, 90, 127

BRAMAS, Q. et al. WiSeBat: Accurate Energy Benchmarking of Wireless Sensor Networks. *Forum on Specification and Design Languages (FDL)*, 2015. 77

BUCHLI, B.; ASCHWANDEN, D.; BEUTEL, J. Battery State-of-Charge Approximation for Energy Harvesting Embedded Systems. *European Wireless Sensor Networks*, p. 179–196, 2013. 76, 105

CADEX ELECTRONICS INC. *Smart Battery Technology*. 2017. Available at: <http://www.cadex.com/en/batteries/smart-battery-technology>. Accessed on March 31, 2017. 105

Castalia Team. *Castalia – Wireless Sensor Network Simulator*. 2017. Available at: <https://castalia.forge.nicta.com.au/index.php/en/>. Accessed on August 1, 2017. 134, 138

CHAN, H.; SUTANTO, D. A New Battery Model for Use with Battery Energy Storage Systems and Electric Vehicles Power Systems. *Proceedings of the IEEE Power Engineering Society Winter Meeting*, v. 1, n. c, p. 470–475, 2000. 72

CHAU, C.-k. et al. Harnessing Battery Recovery Effect in Sensor Networks. *IEEE Journal on Selected Areas in Communications*, v. 28, n. 7, p. 1222–1232, 2010. 74

CHEN, D. et al. Modeling of a Pouch Lithium Ion Battery Using a Distributed Parameter Equivalent Circuit for Internal Non-Uniformity Analysis. *Energies*, v. 9, n. 11, 2016. 73

CHEN, M.; RINCÓN-MORA, G. a. Accurate Electrical Battery Model Capable of Predicting Runtime and I-V Performance. *IEEE Transactions on Energy Conversion*, v. 21, n. 2, p. 504–511, 2006. 75, 88

CHIASSERINI, C.; RAO, R. A Model for Battery Pulsed Discharge with Recovery Effect. *1999 IEEE Wireless Communications and Networking Conference (WCNC)*, 1999. 65

CHIASSERINI, C.; RAO, R. Energy Efficient Battery Management. *Proceedings of the 9th Annual Joint Conference of the IEEE Computer and Communications Societies (INFOCOM)*, p. 396–403, 2000. 65

CHIASSERINI, C. F.; RAO, R. R. Pulsed Battery Discharge in Communication Devices. *MobiCom*, p. 88–95, 1999. 19, 64, 66

CHIASSERINI, C.-f.; RAO, R. R.; MEMBER, S. Improving Battery Performance by Using Traffic Shaping Techniques. v. 19, n. 7, p. 1385–1394, 2001. 65

CICCONI, P.; LANDI, D.; GERMANI, M. Thermal Analysis and Simulation of a Li-ion Battery Pack for a Lightweight Commercial EV. *Applied Energy*, Elsevier, v. 192, p. 159–177, 2017. 73

Cooja. *The Contiki Network Simulator*. 2017. Available at: <http://www.contiki-os.org/start.html>. Accessed on August 1, 2017. 134

CROSSBOW. *MICAz: Wireless Measurement System*. 2016. Available at: <http://www.openautomation.net/uploadsproductos/micaz_datasheet.pdf>. Accessed on December 12, 2016. 82

CUNHA, A. B. da; ALMEIDA, B. R. de; SILVA, D. C. da. Remaining Capacity Measurement and Analysis of Alkaline Batteries for Wireless Sensor Nodes. *IEEE Transactions on Instrumentation and Measurement*, v. 58, n. 6, p. 1816–1822, 2009. 74

DANIIL, N.; DRURY, D.; MELLOR, P. H. Performance Comparison of Diffusion , Circuit-based and Kinetic Battery Models. *IEEE Energy Conversion Congress and Exposition (ECCE)*, p. 1382–1389, 2015. 35

DIDIOUI, A. et al. HarvWSNet: A Co-Simulation Framework for Energy Harvesting Wireless Sensor Networks. *International Conference on Computing, Networking and Communications (ICNC)*, p. 808–812, 2013. 76

DIETRICH, I.; DRESSLER, F. On the Lifetime of Wireless Sensor Networks. *ACM Transactions on Sensor Networks*, v. 5, n. 1, p. 1–39, 2009. ISSN 15504859. 140

DOERFFEL, D.; SHARKH, S. A. A Critical Review of Using the Peukert Equation for Determining the Remaining Capacity of Lead-Acid and Lithium-Ion Batteries. *Journal of Power Sources*, v. 155, n. 2, p. 395–400, 2006. 54, 100

DRON, W. et al. An Emulation-Based Method for Lifetime Estimation of Wireless Sensor Networks. *Proceedings of the IEEE International Conference on Distributed Computing in Sensor Systems*, n. 3, p. 241–248, 2014. 74

DRON, W.; HACHICHA, K.; GARDA, P. A Fixed Frequency Sampling Method for Wireless Sensors Power Consumption Estimation. *IEEE International New Circuits and Systems Conference (NEWCAS)*, 2013. 74

EGEA-LOPEZ, E. et al. Simulation Scalability Issues in Wireless Sensor Networks. *IEEE Communications Magazine*, v. 44, n. 7, p. 64–73, 2006. 76

ERDINC, O.; VURAL, B.; UZUNOGLU, M. A Dynamic Lithium-ion Battery Model Considering the Effects of Temperature and Capacity Fading. *International Conference on Clean Electrical Power (ICCEP)*, p. 383–386, 2009. 76

FEENEY, L. M. et al. A Testbed for Measuring Battery Discharge Behavior. *Proceedings of the 7th ACM International Workshop on Wireless Network Testbeds, Experimental Evaluation and Characterization (WiNTECH)*, p. 91–92, 2012. 12, 34, 38

FEENEY, L. M.; ROHNER, C. Demo: Making Batteries a First Class Element in the Design and Evaluation of Embedded Wireless Systems. *International Conference on Embedded Wireless Systems and Networks (EWSN)*, p. 242–243, 2017. 77

FEENEY, L. M.; ROHNER, C.; LINDGREN, A. How Do the Dynamics of Battery Discharge Affect Sensor Lifetime? *11th Annual Conference on Wireless On-demand Network Systems and Services (WONS)*, p. 49–56, 2014. 12, 34, 38, 41

FERRY, N. et al. Fast Electrical Battery Model Builder for Embedded Systems. *Faible Tension Faible Consommation (FTFC)*, p. 47–50, 2011. 76

FERRY, N. et al. Power/Energy Estimator for Designing WSN Nodes with Ambient Energy Harvesting Feature. *Eurasip Journal on Embedded Systems*, v. 2011, 2011. 76

FÖRSTER, A.; MURPHY, A. L. FROMS: A Failure Tolerant and Mobility Enabled Multicast Routing Paradigm with Reinforcement Learning for WSNs. *Ad Hoc Networks*, v. 9, n. 5, p. 940–965, 2010. 73

GANDOLFO, D. et al. Dynamic Model of Lithium Polymer Battery – Load Resistor Method for Electric Parameters Identification. *Journal of the Energy Institute*, v. 88, n. 4, p. 470–479, nov. 2015. Available at: <http://linkinghub.elsevier.com/retrieve/pii/S1743967114202492>. 61, 105

GAO, L.; LIU, S.; DOUGAL, R. A. Dynamic Lithium-ion Battery Model for System Simulation. *IEEE Transactions on Components and Packaging Technologies*, v. 25, n. 3, p. 495–505, 2002. 75

GAO, Z. et al. Integrated Equivalent Circuit and Thermal Model for Simulation of Temperature-Dependent $LiFePO_4$ Battery in Actual Embedded Application. *Energies*, v. 10, n. 1, 2017. 73

GARG, K. et al. Towards Realistic and Credible Wireless Sensor Network Evaluation. In: SIMPLOT-RYL, D. et al. (Ed.). *ADHOCNETS*. Lecture notes of the institute for computer sciences, social informatics and telecommunications engineering. Berlin, Heidelberg: Springer, 2012. v. 89, cap. Ad Hoc Net, p. 49–64. ISBN 9783642290954. 76

GAUDETTE, B. et al. Optimal Range Assignment in Solar Powered Active Wireless Sensor Networks. *Proceedings of the Annual IEEE International Conference on Computer Communications (INFOCOM)*, p. 2354–2362, 2012. 74

GÎRBAN, G.; POPA, M. A Glance on WSN Lifetime and Relevant Factors for Energy Consumption. *Proceedings of the IEEE International Joint Conferences on Computational Cybernetics and Technical Informatics (ICCC-CONTI)*, p. 523–528, 2010. 76

GREENLEAF, M. et al. A Temperature-Dependent Study of Sealed Lead-Acid Batteries Using Physical Equivalent Circuit Modeling with Impedance Spectra Derived High Current/Power Correction. *IEEE Transactions on Sustainable Energy*, v. 6, n. 2, p. 380–387, 2015. 73

GUASCH, D.; SILVESTRE, S. Dynamic Battery Model for Photovoltaic Applications. *Progress in Photovoltaics: Research and Applications*, v. 11, n. 3, p. 193–206, 2003. 72, 151

GUO, W.; HEALY, W. M. Power Supply Issues in Battery Reliant Wireless Sensor Networks: A Review. *International Journal of Intelligent Control and Systems*, v. 19, n. 1, p. 15–23, 2014. 75

HAASE, J.; MOLINA, J.; DIETRICH, D. Power-Aware System Design of Wireless Sensor Networks: Power Estimation and Power Profiling Strategies. *IEEE Transactions on Industrial Informatics*, v. 7, n. 4, p. 601–613, 2011. 76, 127

HÖRMANN, L. B. et al. State-of-Charge Measurement Error Simulation for Power-Aware Wireless Sensor Networks. *IEEE Wireless Communications and Networking Conference: Mobile and Wireless Networks (WCNC)*, p. 2209–2214, 2012. 74, 127

HSIEH, Y.-c.; CHIU, Y.-c.; WU, W.-t. A Third-order Reaction Li-ion Battery Model. *International Symposium on Fundamentals of Electrical Engineering (ISFEE)*, jul. 2016. 72

HU, Y. et al. A Technique for Dynamic Battery Model Identification in Automotive Applications Using Linear Parameter Varying Structures. *Control Engineering Practice*, Elsevier, v. 17, n. 10, p. 1190–1201, 2009. Available at: <http://dx.doi.org/10.1016/j.conengprac.2009.05.002>. 72

HU, Y. et al. Electro-Thermal Battery Model Identification for Automotive Applications. *Journal of Power Sources*, v. 196, n. 1, p. 449–457, 2011. 72, 73

HUSSEIN, A.; SAMARA, G. Mathematical Modeling and Analysis of ZigBee Node Battery Characteristics and Operation. *MAGNT Research Report*, v. 3, n. 6, p. 99–106, 2015. 74

IEC. *Internet of Things: Wireless Sensor Networks*. Geneva, Switzerland: [s.n.], 2014. Available at: <http://www.iec.ch/whitepaper/pdf/iecWP-internetofthings-LR-en.pdf>. Accessed on April 13, 2017. 11, 33

JABBAR, S. et al. Energy Efficient Strategy for Throughput Improvement in Wireless Sensor Networks. *Sensors (Basel, Switzerland)*, v. 15, n. 2, p. 2473–95, 2015. 106

JAGUEMONT, J. et al. Lithium-Ion Battery Aging Experiments at Subzero Temperatures and Model Development for Capacity Fade Estimation. *IEEE Transactions on Vehicular Technology*, v. 65, n. 6, p. 4328–4343, 2016. 12, 35, 88

JIANI, D. et al. A Fuzzy Logic-Based Model for Li-ion Battery with SOC and Temperature Effect. *IEEE International Conference on Control and Automation (ICCA)*, p. 1333–1338, 2014. 73

JIN, R. et al. Battery Optimal Scheduling Based on Energy Balance in Wireless Sensor Networks. *IET Wireless Sensor Systems*, v. 5, n. 6, p. 277–282, 2015. 74, 76, 105

JONGERDEN, M.; HAVERKORT, B. Battery Modeling. *Thecnical Report in Faculty Electrical Engineering, Mathematics and Computer Science*, p. 18, 2008. 19, 35, 48, 55, 57, 58, 65, 67, 68, 69, 106, 173

JONGERDEN, M.; HAVERKORT, B. Which Battery Model to Use? *IET Software*, v. 3, n. 6, p. 445, 2009. Available at: <http://digital-library.theiet.org/content/journals/10.1049/iet-sen.2009.0001>. 61, 69

JONGERDEN, M. R. Model-Based Energy Analysis of Battery Powered Systems. p. 215, 2010. University of Twente. PhD Thesis. 19, 56, 57, 61

KERASIOTIS, F. et al. Battery Lifetime Prediction Model for a WSN Platform. *Proceedings of the International Conference on Sensor Technologies and Applications (SENSORCOMM)*, p. 525–530, 2010. 74

KERKEZ, B. et al. Design and Performance of a Wireless Sensor Network for Catchment-Scale Snow and Soil Moisture Measurements. *Water Resources Research*, v. 48, n. 9, p. 1–18, 2012. 90

KHAN, M. Z. et al. Limitations of Simulation Tools for Large-Scale Wireless Sensor Networks. *Proceedings of the IEEE International Conference on Advanced Information Networking and Applications Workshops (WAINA)*, p. 820–825, 2011. 127

KIM, J. U. et al. A Simple But Accurate Estimation of Residual Energy for Reliable WSN Applications. *International Journal of Distributed Sensor Networks*, v. 2015, 2015. 76

KIM, T.; QIAO, W. A Hybrid Battery Model Capable of Capturing Dynamic Circuit Characteristics and Nonlinear Capacity Effects. *IEEE Transactions on Energy Conversion*, v. 26, n. 4, p. 1172–1180, 2011. 19, 67, 74, 105

KROEZE, R. C.; KREIN, P. T. Electrical Battery Model for Use in Dynamic Electric Vehicle Simulations. *IEEE Power Electronics Specialists Conference*, p. 1336–1342, 2008. Available at: <http://ieeexplore.ieee.org/lpdocs/epic03/wrapper.htm?arnumber=4592119>. 72, 73

LAJARA, R. J.; PEREZ-SOLANO, J. J.; PELEGRÍ-SEBASTIA, J. A Method for Modeling the Battery State of Charge in Wireless Sensor Networks. *IEEE Sensors Journal*, v. 15, n. 2, p. 1186–1197, 2015. 55, 105

LATTANZI, E. et al. A Fast and Accurate Energy Source Emulator for Wireless Sensor Networks. *EURASIP Journal on Embedded Systems*, v. 2016, n. 1, 2017. 77

LAUNCHPAD.NET. *Poorly Optimised Code Generation for Cortex M0/M0+/M1 vs M3/M4*. 2017. Available at: <https://bugs.launchpad.net/gcc-arm-embedded/+bug/1502611>. Accessed on June 2, 2017. 113

LAZARESCU, M. T. Design and Field Test of a WSN Platform Prototype for Long-Term Environmental Monitoring. *Sensors (Switzerland)*, v. 15, n. 4, p. 9481–9518, 2015. 100

LEVEQUE, A. et al. SystemC-AMS Models for Low-Power Heterogeneous Designs: Application to a WSN for the Detection of Seismic Perturbations. *International Conference on Architecture of Computing Systems (ARCS)*, 2010. 77

LI, H.; YI, C.; LI, Y. Battery-Friendly Packet Transmission Algorithms for Wireless Sensor Networks. *IEEE Sensors Journal*, v. 13, n. 10, p. 3548–3557, 2013. 74

LI, K.; SOONG, B. H.; TSENG, K. J. A High-Fidelity Hybrid Lithium-Ion Battery Model for SOE and Runtime Prediction. *IEEE Applied Power Electronics Conference and Exposition (APEC)*, p. 2374–2381, 2017. 73

LINDEN, D.; REDDY, T. B. *Handbook of Batteries*. 3rd. ed. [S.l.]: McGraw-Hill Handbooks, 2001. 41, 50

LIU, X. et al. A New State-of-Charge Estimation Method for Electric Vehicle Lithium-ion Batteries Based on Multiple Input Parameter Fitting Model. *International Journal of Energy Research*, n. January, p. 1265–1276, 2017. 73

LIU, X. et al. MIROS: A Hybrid Real-Time Energy-Efficient Operating System for the Resource-Constrained Wireless Sensor Nodes. *Sensors*, v. 14, p. 17621–17654, 2014. 114

MA, C.; YANG, Y.; ZHANG, Z. Constructing Battery-Aware Virtual Backbones in Sensor Networks. *Proceedings of the International Conference on Parallel Processing (ICPP)*, v. 2005, p. 203–210, 2005. 74

MADUREIRA, H. M. G. et al. System-Level Power Consumption Modeling of a SoC for WSN Applications. *Proceedings of the IEEE International Conference on Networked Embedded Systems for Enterprise Applications (NESEA)*, p. 4–9, 2011. 74

MAJDABADI, M. M. et al. Simplified Electrochemical Multi-Particle Model for $LiFePO_4$ Cathodes in Lithium-ion Batteries. *Journal of Power Sources*, v. 275, p. 633–643, 2015. 73

MAMMU, A. S. i. K. et al. Cross-Layer Cluster-Based Energy-Efficient Protocol for Wireless Sensor Networks. *Sensors (Basel, Switzerland)*, v. 15, n. 4, p. 8314–8336, 2015. 106

MANWELL, J. F.; MCGOWAN, J. G. Lead Acid Battery Storage Model for Hybrid Energy Systems. *Solar Energy*, v. 50, n. 5, p. 399–405, maio 1993. Available at: <http://linkinghub.elsevier.com/retrieve/pii/0038092X93900602>. 19, 60, 61, 62, 72, 83, 184

MANWELL, J. F.; MCGOWAN, J. G. Extension of the Kinetic Battery Model for Wind/Hybrid Power Systems. In: *Proceedings of the European Wind Energy Association Conference (EWEC)*. [S.l.: s.n.], 1994. p. 284–289. 60, 86

MANWELL, J. F. et al. Evaluation of Battery Models for Wind/Hybrid Power Systems Simulation. In: *Proceedings of the European Wind Energy Association Conference*. Thessaloniki, Greece.: [s.n.], 1994. p. 1182–1187. 60

MATHWORKS INC. *Smoothing Splines*. 2016. Available at: <https://www.mathworks.com/help/curvefit/smoothing-splines.html>. Accessed on December 12, 2016. 89

MAXIM. *DS2780 Standalone Fuel Gauge IC*. 2007. Available at: <https://datasheets.maximintegrated.com/en/ds/DS2780.pdf>. Accessed on April 18, 2017. 105

MAXIM. *DS18B20 Programmable Resolution 1-Wire Digital Thermometer*. 2016. Available at: <https://datasheets.maximintegrated.com/en/ds/DS18B20.pdf>. Accessed on December 12, 2016. 82

MEHNE, J.; NOWAK, W. Improving Temperature Predictions for Li-ion Batteries: Data Assimilation with a Stochastic Extension of a Physically-Based, Thermo-Electrochemical Model. *Journal of Energy Storage*, Elsevier, v. 12, p. 288–296, 2017. 73

MEIER, R. *CoolTerm: A Simple Serial Port Terminal Application*. 2016. Available at: <http://freeware.the-meiers.org>. Accessed on December 12, 2016. 82

MENZEL, T.; WOLISZ, A. *Overpotential-Based Battery End-of-Life Indication in WSN Nodes*. Lecture notes of the institute for computer sciences, social informatics and telecommunications engineering. [S.l.]: Springer, Cham, 2013. v. 122. 34–46 p. 76

MERRETT, G. V. et al. Energy-Aware Simulation for Wireless Sensor Networks. *Proceedings of the IEEE Communications Society Conference on Sensor, Mesh and Ad Hoc Communications and Networks (SECON)*, 2009. 77

MIKHAYLOV, K.; TERVONEN, J. Novel Energy Consumption Model for Simulating Wireless Sensor Networks. *International Congress on Ultra Modern Telecommunications and Control Systems (ICUMT)*, p. 15–21, 2012. 21, 77, 118, 172

MINAKOV, I.; PASSERONE, R. PASES: An Energy-Aware Design Space Exploration Framework for Wireless Sensor Networks. *Journal of Systems Architecture*, Elsevier B.V., v. 59, n. 8, p. 626–642, 2013. 77

MINAKOV, I. et al. A Comparative Study of Recent Wireless Sensor Network Simulators. *ACM Transactions on Sensor Networks*, v. 12, n. 3, p. 20:20–20:39, 2016. 76

MIT ELECTRIC VEHICLE TEAM. A Guide to Understanding Battery Specifications. n. December, p. 1–3, 2008. Available at: <http://web.mit.edu/evt/summary_battery_specifications.pdf>. Accessed on May 8, 2017. 41

MORA-MERCHAN, J. M. et al. MTOSSIM: A Simulator that Estimates Battery Lifetime in Wireless Sensor Networks. *Simulation Modelling Practice and Theory*, Elsevier B.V, v. 31, p. 39–51, 2013. 77

MORAVEK, P.; KOMOSNY, D.; SIMEK, M. Specifics of WSN Simulations. *Electrotechnics Magazine – Communication Technology*, v. 2, n. 3, 2011. 127

MOTAPON, S. N. et al. A Generic Electro-Thermal Li-Ion Battery Model for Rapid Evaluation of Cell Temperature Temporal Evolution. *IEEE Transactions on Industrial Electronics*, v. 0046, n. c, p. 1–1, 2016. Available at: <http://ieeexplore.ieee.org/document/7592876/>. 73

MUSZNICKI, B.; ZWIERZYKOWSKI, P. Survey of Simulators for Wireless Sensor Networks. *International Journal of Grid and Distributed Computing*, v. 5, n. 3, p. 23–50, 2012. 35, 127

NATAF, E.; FESTOR, O. Online Estimation of Battery Lifetime for Wireless Sensor Network. n. September, p. 28, 2012. 77

NAVARRO, M. et al. A Study of Long-Term WSN Deployment for Environmental Monitoring. *IEEE International Symposium on Personal, Indoor and Mobile Radio Communications (PIMRC)*, p. 2093–2097, 2013. 100

NEWMAN, J. FORTRAN Programs for the Simulation of Electrochemical Systems. 1998. Available at: <http://www.cchem.berkeley.edu/jsngrp/fortran.html>. Accessed on May 29, 2017. 55

NIGHOT, V. P.; LAMBOR, S. M.; JOSHI, S. M. Efficient Battery Management in Wireless Sensor Node: Review Paper. *International Conference on Wireless and Optical Communications Networks (WOCN)*, 2014. 74

NS-2. *The Network Simulator*. 2017. Available at: <http://nsnam.sourceforge.net/wiki/index.php/Main_Page>. Accessed on August 1, 2017. 134

OTHMAN, S. B.; TRAD, A.; YOUSSEF, H. Performance Evaluation of Encryption Algorithm for Wireless Sensor Networks. *International Conference on Information Technology and e-Services (ICITeS)*, p. 1–8, 2012. 113, 115

PADMANABH, K.; ROY, R. Maximum Lifetime Routing in Wireless Sensor Network by Minimizing Rate Capacity Effect. *Proceedings of the International Conference on Parallel Processing Workshops (ICPPW)*, p. 155–160, 2006. 74

PANASONIC. Ni-MH Handbook. 2015. Available at: <https://eu.industrial.panasonic.com/sites/default/pidseu/files/downloads/files/ni-mh-handbook-2014_interactive.pdf>. Accessed on May 8, 2017. 41

PANASONIC. *Ni-MH Handbook*. 2016. Available at: <http://www.mouser.com/pdfdocs/PanasonicBatteries_NI-MH_Handbook.pdf>. Accessed on December 12, 2016. 82, 87, 143

PANCHAL, S. Experimental Investigation and Modeling of Lithium-ion Battery Cells and Packs for Electric Vehicles. 2016. Faculty of Engineering and Applied Science, University of Ontario Institute of Technology. PhD Thesis. 73

PARK, C. P. C.; LAHIRI, K.; RAGHUNATHAN, a. Battery Discharge Characteristics of Wireless Sensor Nodes: an Experimental Analysis. *2005 Second Annual IEEE Communications Society Conference on Sensor and Ad Hoc Communications and Networks, 2005. IEEE SECON 2005.*, 2005. 55, 75, 107

PENELLA-LÓPEZ, M. T.; GASULLA-FORNER, M. *Powering Autonomous Sensors*. [S.l.]: Springer Science+Business Media B.V., 2011. v. 1. 41–80 p. ISBN 978-94-007-1572-1. 76

PEREIRA, R. M.; RUIZ, L. B.; GHIZONI, M. L. A. MannaSim: A NS-2 Extension to Simulate Wireless Sensor Network. *International Conference on Networks (ICN)*, p. 95–101, 2015. 127

PERLA, E. et al. PowerTOSSIM z: Realistic Energy Modelling for Wireless Sensor Network Environments. *PM2HW2N*, p. 35–42, 2008. 77

PESARAN, A. A. Battery Thermal Models for Hybrid Vehicle Simulations. *Journal of Power Sources*, v. 110, n. 2, p. 377–382, 2002. 73

PFLUG, H. W. et al. Zinc-Air Battery Modeling for Small Form Factor IR-UWB Wireless Sensor Network Radios. *IEEE International Symposium on Personal, Indoor and Mobile Radio Communications (PIMRC): Fundamentals and PHY Track*, p. 223–227, 2013. 76

POURAZARM, S. Control and Optimization Approaches for Energy-Limited Systems: Applications to Wireless Sensor Networks and Battery-Powered Vehicles. 2017. 74

RAHIMI-EICHI, H. et al. Battery Management System: An Overview of Its Application in the Smart Grid and Electric Vehicles. *IEEE Industrial Electronics Magazine*, n. June, p. 4–16, 2013. 105

RAKHMATOV, D.; VRUDHULA, S. An Analytical High-Level Battery Model for Use in Energy Management of Portable Electronic Systems. *IEEE-ACM International Conference on Computer Aided Design (ICCAD)*, p. 488–493, 2001. 57, 59

RAKHMATOV, D.; VRUDHULA, S.; WALLACH, D. Battery lifetime prediction for energy-aware computing. *Proceedings of the International Symposium on Low Power Electronics and Design*, 2002. 55

RAKHMATOV, D.; VRUDHULA, S.; WALLACH, D. a. A Model for Battery Lifetime Analysis for Organizing Applications on a Pocket Computer. *IEEE Transactions on Very Large Scale Integration (VLSI) Systems*, v. 11, n. 6, p. 1019–1030, 2003. 100

RAMOTAR, L. et al. Experimental Verification of a Thermal Equivalent Circuit Dynamic Model on an Extended Range Electric Vehicle Battery Pack. *Journal of Power Sources*, Elsevier B.V, v. 343, p. 383–394, 2017. 73

RAO, J.; FAPOJUWO, A. O. A Battery Aware Distributed Clustering and Routing Protocol for Wireless Sensor Networks. *IEEE Wireless Communications and Networking Conference (WCNC)*, p. 1538–1543, 2012. 74

RAO, R.; VRUDHULA, S.; RAKHMATOV, D. N. Battery Modeling for Energy-Aware System Design. *Computer*, v. 36, n. 12, 2003. 68

RAO, V. et al. Battery Model for Embedded Systems. *18th International Conference on VLSI Design held jointly with 4th International Conference on Embedded Systems Designs (VLSID)*, p. 105–110, 2005. 65

RAZAQUE, A.; ELLEITHY, K. Energy-Efficient Boarder Node Medium Access Control Protocol for Wireless Sensor Networks. *Sensors*, v. 14, n. 3, p. 5074–5117, 2014. 106

ROHNER, C.; FEENEY, L. M.; GUNNINGBERG, P. Evaluating Battery Models in Wireless Sensor Networks. *Lecture Notes in Computer Science (including subseries Lecture Notes in Artificial Intelligence and Lecture Notes in Bioinformatics)*, v. 7889 LNCS, p. 29–42, 2013. 56, 68, 69, 74

RONG, P.; PEDRAM, M. An Analytical Model for Predicting the Remaining Battery Capacity of Lithium-Ion Batteries. *Proceedings of the Design, Automation and Test in Europe*, v. 14, n. 5, p. 1148–1149, 2006. 55, 75

RUIZ-GARCIA, L. et al. A Review of Wireless Sensor Technologies and Applications in Agriculture and Food Industry: State of the Art and Current Trends. *Sensors (Basel, Switzerland)*, v. 6, n. 9, p. 4728–4750, 2009. 86

RUKPAKAVONG, W.; GUAN, L.; PHILLIPS, I. Dynamic node lifetime estimation for wireless sensor Networks. *IEEE Sensors Journal*, v. 14, n. 5, p. 1370–1379, 2014. 38, 39, 100

SANGWAN, V. et al. Equivalent Circuit Model Parameters Estimation of Li-ion Battery: C-Rate, SoC and Temperature Effects. *IEEE International Conference on Power Electronics, Drives and Energy Systems (PEDES)*, 2016. 73

SBS IMPLEMENTERS FORUM. *Smart Battery Data Specification–Addendum for Fuel Cell Systems*. 2007. Available at: <http://sbs-forum.org/specs/sbdata_addendum_fuel_cells_20070411.pdf>. Accessed on March 31, 2017. 105

SCHNEIDER, K. K.; SAUSEN, P. S.; SAUSEN, A. Análise Comparativa do Tempo de Vida de Baterias em Dispositivos Móveis a Partir da Utilização de Modelos Analíticos. *Tendências em Matemática Aplicada e Computacional*, v. 12, n. 1, p. 43–54, 2001. 57

SILICON LABS INC. *The Evolution of Wireless Sensor Networks*. Austin, TX, USA, 2013. Available at: <http://www.silabs.com/documents/public/white-papers/evolution-of-wireless-sensor-networks.pdf>. Accessed on April 12, 2017. 33

SOMMER, P.; KUSY, B.; JURDAK, R. Power Management for Long-Term Sensing Applications with Energy Harvesting. *Proceedings of the International Workshop on Energy Neutral Sensing Systems*, p. 3:1–3:6, 2013. Available at: <http://doi.acm.org/10.1145/2534208.2534213>. 76

SOMOV, A. et al. A Methodology for Power Consumption Evaluation of Wireless Sensor Networks. *IEEE Conference on Emerging Technologies & Factory Automation*, 2009. 74

STANKOVIC, J. A. How Things Work: Wireless sensor networks. *IEEE Computer (Invited Paper)*, 2008. 11, 33

STETSKO, A.; STEHLÍK, M.; MATYAS, V. Calibrating and Comparing Simulators for Wireless Sensor Networks. *Proceedings of the IEEE International Conference on Mobile Adhoc and Sensor Systems (MASS)*, p. 733–738, 2011. 35, 127

THANGARAJ, M.; ANURADHA, S. A Study on Energy Model Prototyping in Various Simulators of WSN. *IOSR Journal of Computer Engineering (IOSR-JCE)*, v. 16, n. 2, p. 48–57, 2014. 76

TOSSIM. *A Simulator for TinyOS Networks*. 2017. Available at: <http://tinyos.stanford.edu/tinyos-wiki/index.php/TOSSIM>. Accessed on August 1, 2017. 134

TREMBLAY, O.; DESSAINT, L.-A. Experimental Validation of a Battery Dynamic Model for EV Applications. *World Electric Vehicle Journal V*, v. 3, n. October, p. 289–298, 2009. 63, 64, 90

TREMBLAY, O.; DESSAINT, L.-A.; DEKKICHE, A.-I. A Generic Battery Model for the Dynamic Simulation of Hybrid Electric Vehicles. *IEEE Vehicle Power and Propulsion Conference*, n. V, p. 284–289, 2007. 63, 72

VALLE, O. T. et al. Polynomial Approximation of the Battery Discharge Function in IEEE 802.15.4 Nodes: Case Study of MicaZ. *Advances in Intelligent Systems and Computing*, v. 206 AISC, p. 901–910, 2013. 74

VASILEVSKI, M. et al. SystemC AMS Modeling of a Sensor Node Energy Consumption and Battery State-of-Charge for WSN. *International Conference on New Circuits and Systems Conference (NEWCAS)*, p. 2–6, 2015. 74

VERMA, V. K.; SINGH, S.; PATHAK, N. P. Optimized Battery Models Observations for Static, Distance Vector and On-Demand Based Routing Protocols Over 802.11 Enabled Wireless Sensor Networks. *Wireless Personal Communications*, v. 81, n. 2, p. 503–517, 2015. 74

WANG, Y. et al. Probability Based Remaining Capacity Estimation Using Data-Driven and Neural Network Model. *Journal of Power Sources*, Elsevier B.V, v. 315, p. 199–208, 2016. 105

WANG, Y.; ZHANG, C.; CHEN, Z. A Method for State-of-Charge Estimation of $LiFePO_4$ Batteries at Dynamic Currents and Temperatures using Particle Filter. *Journal of Power Sources*, Elsevier B.V, v. 279, p. 306–311, 2015. 105

WATFA, M.; YAGHI, L. An Efficient Online-Battery Aware Geographic Routing Algorithm for Wireless Sensor Networks. *International Journal of Communication Systems*, v. 23, n. 5, p. 633–652, 2010. 74

YANG, Y.; FAN, Z.; GAO, R. X. Optimal Battery Control Strategy for Wireless Sensor Networks with Solar Energy Supply. *American Control Conference (ACC)*, p. 3559–3564, 2014. 75

ZHANG, Y. et al. Investigation of Current Sharing and Heat Dissipation in Parallel-Connected Lithium-ion Battery Packs. *Proceedings of the IEEE Energy Conversion Congress and Exposition (ECCE)*, 2016. 73

ZYTOUNE, O.; ABOUTAJDINE, D. Energy Usage Analysis of Digital Modulations in Wireless Sensor Networks with Realistic Battery Model. *Wireless Networks*, Springer US, v. 22, n. 8, p. 2713–2725, 2016. 74

Appendix

APPENDIX A – RECOVERY EFFECT IN LOW-POWER NODES OF WIRELESS SENSOR NETWORKS

This chapter describes the set-up used in the analysed scenarios. The simulations are performed in the Matlab[1], a scientific software for numerical computations. This choice is justified mainly by the following reasons: (i) easy implementation of mathematical models; (ii) ability to conduct simulations quickly using a multi-core computer; and (iii) ability to represent the results through custom graphics. Thus, the KiBaM functions are implemented to perform the simulations in Section A.1. This chapter also presents the set of tasks used in the simulations, as well as a study on the impact of different values for the KiBaM constants. Finally, Section A.4 focuses on the analysis of the recovery effect on batteries of WSN nodes.

A.1 KIBAM IMPLEMENTATION

This section presents the KiBaM implementation in the function format, which is used in the assessments regarding the battery lifetime estimation on Matlab.

The KiBaM implementation can be summarized as a loop that performs function calls that drain the battery capacity, accounting for the time required to exhaust all its charge. Thus, it becomes possible to obtain the battery estimated lifetime according to the applied discharge current and its execution time. Algorithm 4 shows how to implement the KiBaM function.

Algorithm 4: KiBaM function.

Data: c, k, $q_{1,0}$, $q_{2,0}$, t_0, I, t_I

1 $q_0 = q_{1,0} + q_{2,0}$;
2 $t_0 = t_0 + t_I$;
3 $q_{1,0}$ = compute-q1 $(c, k, q_0, q_{1,0}, q_{2,0}, I, t_I)$;
4 $q_{2,0}$ = compute-q2 $(c, k, q_0, q_{1,0}, q_{2,0}, I, t_I)$;
5 **return** $(q_{1,0}, q_{2,0}, t_0)$;

[1] http://www.mathworks.com/products/matlab/

Lines 3 and 4 update the amount of charge in the Available and Bound Charge tanks, respectively, according to Equation (2.7). An example of the KiBaM function call is presented in Algorithm 5.

Algorithm 5: KiBaM function call.

```
   Data: c, k, q_0, I, t_I
1  q_{1,0} = (c) · q_0;
2  q_{2,0} = (1 − c) · q_0;
3  t_0 = 0;
4  while q_{1,0} > 0 do
5  |  [q_{1,0}, q_{2,0}, t_0] = KiBaM (c, k, q_{1,0}, q_{2,0}, t_0, I, t_I);
6  end
7  print (q_{1,0}, q_{2,0}, t_0);
```

The parameters that need an initial value are c, k and q_0 (the initial battery capacity), I (the discharge current) and t_I (the execution time of I). However, it becomes necessary to observe the amount of charge in the Available Charge tank, which can not be less than or equal to zero. Line 4 of the Algorithm 5 performs this verification.

A.2 TASK SET

This section presents the tasks used in the assessment. In this case, a task consists of a node state and its execution time. Here, the tasks have the same power consumption of the Mica2 node, as described by Mikhaylov and Tervonen (MIKHAYLOV; TERVONEN, 2012). Table 24 shows the discharge currents in each of the node states as well as its execution times, according to the simulated application.

Table 24 – Mica2 node states (MIKHAYLOV; TERVONEN, 2012).

Short Name	State	Discharge Current (mA)	Execution Time (min)
Tx	MCU+Tx	25.400	4
Rx	MCU+Rx	15.100	10
Ac	MCU-Active	8.000	6
NS	Node-Standby	0.019	0-20

For easy understanding, the tasks are named as follows: Tx (MCU+Tx), Rx (MCU+Rx), Ac (MCU-Active), and NS (Node-Standby). The first task, Tx, consumes 25.4 mA with an execution time of 4 minutes, representing the microcontroller (MCU) activity and the use of the transceiver to transmit data (Tx). The Rx task consumes 15.1 mA with an execution time equal to 10 minutes, representing the MCU activity and the use of the transceiver to receive data (Rx). The Ac task consumes 8 mA and has 6 minutes of execution time, representing only the MCU activity (transceiver off). Lastly, the NS task consumes 19 μA with execution times ranging between 0-20 minutes, according to the simulated scenario. This task represents the period in low-power mode (or sleep mode). Such task set is equivalent to an environmental monitoring application.

A.3 COMPARISON BETWEEN DIFFERENT VALUES OF k

This section presents a study regarding the use of various battery technologies (e.g., Lead-Acid, Ni-MH, Li-ion), which implies in different values for the KiBaM constants since the electrochemical characteristics of these technologies are distinct. This may change the recovery effect behaviour so that the battery technology can be chosen according to the application requirements (e.g., current discharge, duty cycle and battery capacity).

The constant k is a time-dependent value. Thus, its value becomes critical to determine the time needed to transpose the charge from the Bound Charge tank to Available Charge tank, until they reach the equilibrium point. From this moment, it becomes unnecessary to maintain a low-power state, since there is no significant charge recovery. The time to reach the equilibrium point (stability) is called threshold.

In this study, the values of c and q_0 are set in 0.625 and 2700 As, respectively (JONGERDEN; HAVERKORT, 2008). The values for the constant k are as follows: 0.05, 0.01, 0.005, 0.001, 0.0005 and 0.0001 s^{-1}. Besides, the following task sequence is performed: an MCU+Tx state followed by a Node-Standby state (with an 8-minute execution time).

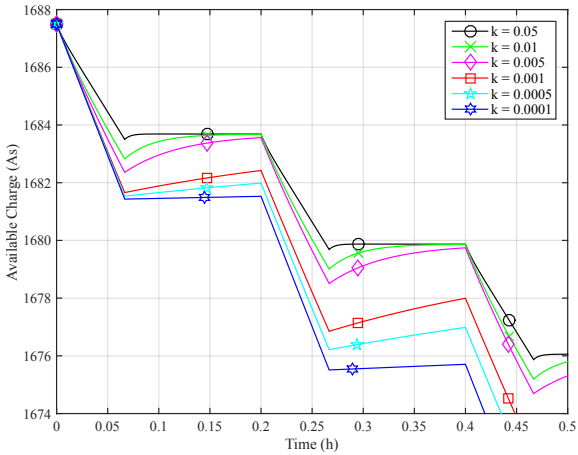

Figure 32 – Simulation with different k values.

This means a 33.33% duty cycle, i.e., the period in sleep mode is twice the period in active mode. Figure 32 depicts the simulation results with different values for the k constant.

Table 25 – Difference in battery lifetime according to the k value.

k (s^{-1})	Battery Lifetime (s)	Battery Lifetime (h)
0.0500	318289	88.4136
0.0100	318280	88.4111
0.0050	317738	88.2606
0.0010	317622	88.2283
0.0005	316933	88.0369
0.0001	311951	86.6531

Note that the behaviour of the discharge curves is different depending on the value of the k constant. In this case, the larger the value of k, the faster the charge transposition between the tanks and, thus, the shorter the time to reach the threshold. On the other hand, the lower the k value, the slower the charge transposition between the tanks. Consequently, the greater the time required to reach the threshold. Besides the difference in the recovery effect, there is a noticeable difference in battery lifetime. Table 25 shows the battery lifetime ac-

cording to the value of the k.

For this application, the most appropriate k value is 0.01 s^{-1} since it represents the best fit for a full charge recovery, i.e., without wasting time. This example highlights the importance of choosing the battery parameters that have characteristics similar to those used in batteries of real-world WSN nodes.

A.4 ASSESSMENT RESULTS

This section aims to present the assessment results from different scenarios, focusing on the analysis of the charge recovery effect on batteries. Briefly, the recovery speed is analysed for the simulated application, as well as the influence of changing the sleep period order among the performed tasks. The execution order between tasks is also analysed in this section. Finally, this section presents a case study regarding the frequency of switching between tasks. The settings shown in Section A.1 are used in these simulations, including the values of the KiBaM constants.

A.4.1 Recovery Effect: Speed Evaluation

This section shows how to choose the sleep period correctly, according to the application characteristics. In this sense, a comparison between different recovery times is performed. The objective is to select an optimised sleep period for the set of tasks used so that recovery effect occurs without wasting time after reaching the threshold. Other details are presented below.

In this experiment, the task execution order is as follows: Tx, Rx, Ac, and NS. The execution times are the same as shown in Table 24. In this case, the adopted periods for the Node-Standby task are 5, 10, 15 and 20 minutes. Such periods represent duty cycles of 20%, 33.33%, 42.85% and 50%, respectively. All simulated experiments are performed cyclically until the content in the Available Charge tank reaches the minimum level. Figure 33 (a) depicts the behaviour of the simulations when these tasks are used.

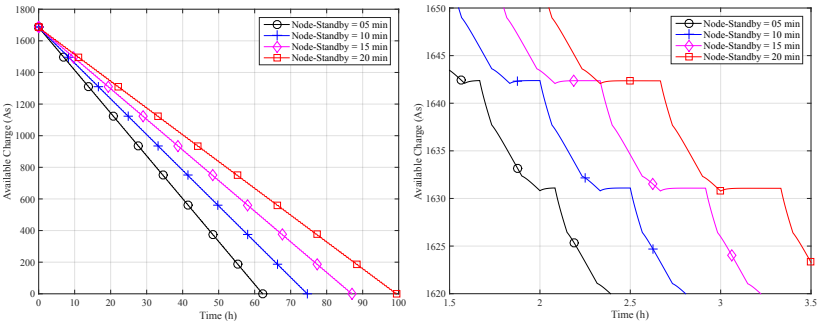

(a) Full simulation. (b) Zoomed interval.

Figure 33 – Simulations using different sleep periods.

The battery lifetimes in each situation are: 62.2375 hours (NS = 5 min), 74.6383 hours (NS = 10 min), 87.0389 hours (NS = 15 min), and 99.4389 hours (NS = 20 min). Figure 33 (b) depicts the behaviour of the simulations with zoom. Note the behaviour of the recovery effect in each situation. In this case, it is possible to note that a sleep period equal to 5 minutes is not enough since the threshold was not reached. The situations with greater sleep times (15 and 20 minutes) offer a longer battery lifetime. However, the charge recovery is insignificant as from 10 minutes. Thus, if the interest lies only in the recovery effect without wasting time, the most suitable task combination is the one that provides a sleep time of 10 minutes.

A.4.2 Recovery Effect: Changing the Sleep Period Order

This section performs a variation of the previous simulation. In this case, the sleep period is placed at different moments to evaluate the impact on battery lifetime. The tasks are ordered as follows: NS-Tx-Rx-Ac, Tx-NS-Rx-Ac, Tx-Rx-NS-Ac, and Tx-Rx-Ac-NS. The experiments are performed cyclically until the content in the Available Charge tank reaches the minimum level. Table 26 shows the results, including the charge recovered after a sleep period, at $t \approx 36$ h.

Note that there is a little difference between the times obtained

Table 26 – Results when the sleep period is at different moments.

Simulation	Order	Battery Lifetime (s)	Battery Lifetime (h)	Charge Recovered (%)
1	NS-Tx-Rx-Ac	269297	74.8047	0.034
2	Tx-NS-Rx-Ac	269304	74.8067	0.102
3	Tx-Rx-NS-Ac	268698	74.6383	0.065
4	Tx-Rx-Ac-NS	268698	74.6383	0.035

in the simulations. Simulation 2, which has a sleep period after a Tx task, achieved longer battery lifetime and a higher percentage of charge recovered. This can be explained by the simple fact that there is a greater benefit with the recovery effect after performing a higher consumption task, as depicted in Figure 34, which presents a zoom of the final simulation period (74 h $\leq t \leq$ 74.9 h). Simulations 3 and 4 reached the same time, although they presented different values of charge recovered. It may indicate a model inconsistency regarding this situation. The relative difference between the Simulations 2 and 3 is 0.22%, which represents 606 seconds (10.1 min) in the battery lifetime.

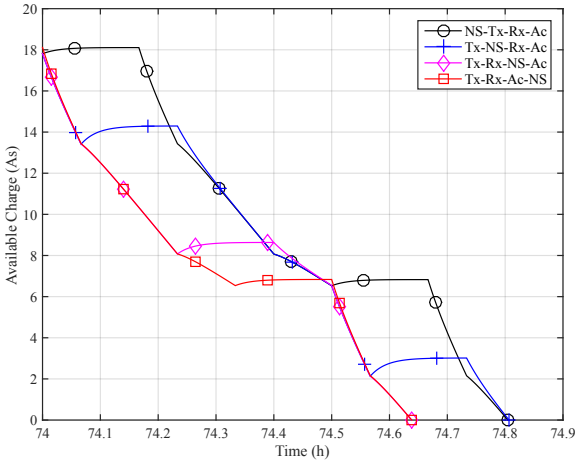

Figure 34 – Simulated experiments with different sleep period order.

A.4.3 Assessing Changes in Task Execution Order

This section presents a comparison between simulations with different task execution order. The objective is to evaluate the difference in battery lifetime in each situation. In this scenario, the sleep period is not included in the task set. Although there is not a period in sleep mode itself, note that the recovery effect also has its share in this scenario since the tasks present different discharge currents. The tasks are divided as shown in Table 27.

Table 27 – Results with different task order.

Simulation	Order	Battery Lifetime (s)	Battery Lifetime (h)
1	Tx-Rx-Ac	179412	49.8367
2	Tx-Ac-Rx	179586	49.8850
3	Rx-Tx-Ac	179490	49.8583
4	Rx-Ac-Tx	179765	49.9347
5	Ac-Tx-Rx	179576	49.8822
6	Ac-Rx-Tx	179746	49.9294

Note that all simulations have different battery lifetimes, even if the tasks are the same, although in a different execution order. In this case, Simulation 4 showed longer battery lifetime, 179765 seconds (49.9347 hours). The task with the highest discharge current (Tx) is performed lastly in this simulation. On the other hand, Simulation 1 had the shortest battery lifetime, 179412 seconds (49.8367 hours). In this case, the task with the highest discharge current (Tx) is performed first. The relative difference in these two cases (Simulations 1 and 4) is 0.19%, which represents 353 seconds (5.88 min) in the battery lifetime. Figure 35 depicts a zoom with the last moments of the performed simulations.

A.4.4 Evaluating Task Switching Frequency

This section evaluates the KiBaM behaviour on the influence of the task switching frequency in battery lifetime. The purpose is to establish a frequency range in which the execution time is feasible.

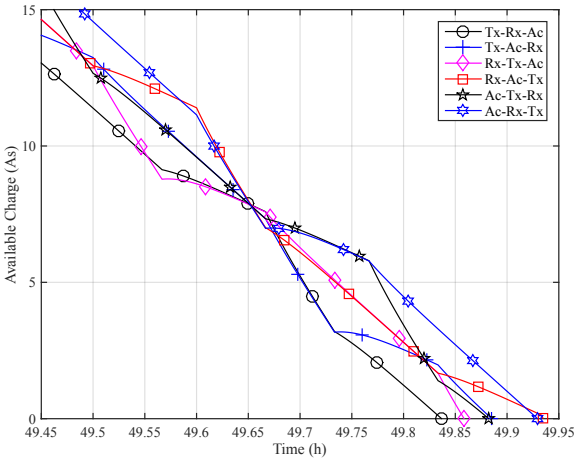

Figure 35 – Simulations with different task order.

Table 28 – Results with different frequencies.

Frequency (Hz)	Period (s)	Tasks	Battery Lifetime (s)	Battery Lifetime (h)	Execution Time (s)
0.015625	64.0	Tx-NS	212352.00	58.9867	0.004814
0.03125	32.0	Tx-NS	212352.00	58.9867	0.008408
0.0625	16.0	Tx-NS	212368.00	58.9911	0.016665
0.125	8.0	Tx-NS	212376.00	58.9933	0.029949
0.25	4.0	Tx-NS	212376.00	58.9933	0.054279
0.5	2.0	Tx-NS	212378.00	58.9939	0.108964
1	1.0	Tx-NS	212379.00	58.9942	0.223868
2	0.5	Tx-NS	212379.00	58.9942	0.406734
4	0.25	Tx-NS	212379.25	58.9942	0.812888
8	0.125	Tx-NS	212379.38	58.9943	1.657588
16	0.0625	Tx-NS	212379.50	58.9943	3.262296
32	0.03125	Tx-NS	212379.50	58.9943	6.655759
64	0.015625	Tx-NS	212379.50	58.9943	12.757468

In this scenario, only two tasks are used: Tx and NS. The execution times are defined according to the duty cycle, which in this case is 50%. For example, if the duty cycle period is 16 seconds, each task runs for 8 seconds. The simulated frequencies are as follows: 0.015625, 0.03125, 0.0625, 0.125, 0.25, 0.5, 1, 2, 4, 8, 16, 32, and 64 Hz. Table 28

shows the results in each situation.

Note that the battery lifetime is virtually the same within the simulated frequencies range. The differences in battery lifetimes arise due to the simulation step, which is different in each simulated frequency. However, the simulation execution time increases considerably as the rate of task switching increases. It was found a linear growth in the performed simulations. This is due to the increase in the number of iterations required to run the model. That is, the higher the frequency, the lower the amount of charge drained from the battery at each iteration of the algorithm, and therefore the greater the number of iterations required. This makes the simulation execution time impractical from a particular frequency value since the period of the tasks is too small.

A.5 FINAL REMARKS

The energy constraint is a primary challenge within WSN context since it forces network designers to use energy-aware algorithms and protocols to avoid extra costs by replacing batteries. Also, batteries have intrinsic effects due to electrochemical reactions, which provide energy to the connected device. Two widely studied effects are the rate capacity and charge recovery. Since batteries are complex devices, the use of battery models assists WSN designers to predict the network behaviour since such models are capable of providing an estimate of the battery lifetime according to the used load profile.

An analytical battery model, known as KiBaM, was evaluated in this chapter to assess the impact of the recovery effect on the batteries of low-power WSN nodes. It was possible to verify that the way the recovery effect is used can influence the battery lifetime. Our results presented a difference up to 10.1 minutes in battery lifetime just by changing the sleep period order. Besides, a minimum standby time (sleep period) is required to achieve a satisfactory charge recovery, i.e., a threshold. For the parameters used in this simulation (discharge currents, execution times, KiBaM constants), a time between 5 and 10 minutes is enough to recover the battery charge. Finally, the frequency

of task switching and its impact on the KiBaM execution time was evaluated. The results showed that higher switching frequencies increase the simulation execution times.

APPENDIX B – EXPERIMENTAL VALIDATION OF A BATTERY MODEL FOR LOW-POWER NODES IN WSNS

This chapter presents the methodology used to validate the KiBaM model experimentally, which involves the use of a test-bed prototype for discharging Ni-MH batteries. KiBaM parameters are obtained from experimental data. A set of experiments in a duty cycle scheme was performed to assess the behaviour of KiBaM in these conditions.

B.1 EXPERIMENTAL SET-UP

The battery used in the experiments is from Panasonic, model HHR-4MVE (2xAAA, rechargeable Ni-MH, 2.4 V, 750 mAh). The battery starts at full charge in all experiments, being discharged until it reaches the cut-off value of 2.0 V, which is the safest value for this type of battery. Recharge time is around 7 hours by using a common Ni-MH battery charger. The battery rests for 20 minutes before the start of each experiment. All experiments were performed at room temperature, varying between 25 °C and 30 °C.

A test-bed prototype, which includes a discharge-controlled circuit and an Arduino UNO, has been developed to assess the behaviour of Ni-MH batteries through experiments. The test-bed allows the application of controlled discharge currents to the battery. It can also collect the experimental data and store it for future analysis.

The test-bed has a discharge-controlled circuit to discharge the battery, which is capable of applying discharge currents in the range from 0.03 to 30.847 mA. A digital potentiometer (AD5206) allows selecting 256 values in that range. The test-bed guarantees a constant discharge current, independently of the battery voltage level. This circuit also includes a temperature sensor (Maxim 18B20).

An Arduino UNO controls all circuit components and collects the experimental data over time: battery voltage and temperature. The data log interval is 10 s. A computer receives the data from the UNO board through a USB connection using an application called CoolTerm.

B.2 EXPERIMENTAL RESULTS

Three experimental assessments were performed to estimate the KiBaM parameters. Such experiments used the following discharge currents (I): 5.498, 19.852 and 30.237 mA. The battery lifetimes (t) were, respectively: 138.5, 35.7 and 23.1 hours. The battery provided the following capacities ($I \times t$), respectively: 761.725, 709.488 and 698.180 mAh. Figure 36 depicts the battery discharge curves over time, including the experiment average temperature. Using the methodology proposed Manwell and McGowan (MANWELL; MCGOWAN, 1993), the KiBaM parameters are: $c = 0.828164$ and $k = 0.021139\ s^{-1}$.

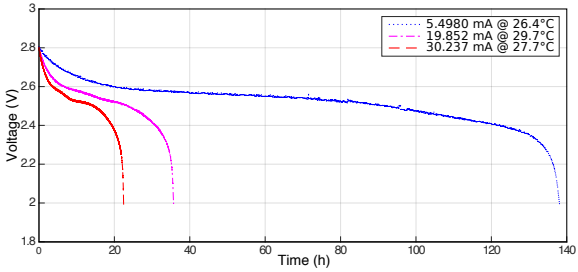

Figure 36 – Results with continuous discharge currents.

We also carried out experiments using a set of discharge currents according to the following DC schemes: 6.25%, 12.5%, 25% and 50%. The purpose of these experiments is to evaluate the battery behaviour regarding the recovery effect. Figure 37 depicts the DCs used in the experiments, where 1.92 s is the DC period.

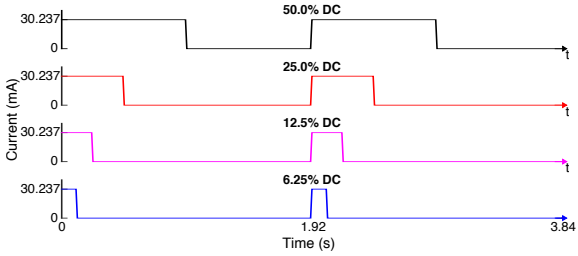

Figure 37 – Duty cycle settings.

The experimental values for the battery lifetime using the above referred duty cycle schemes (t_{DC}) are: 377.8 h (6.25%), 182.2 h (12.5%), 92.2 h (25%) and 49.5 h (50%). Thus, the capacities provided by the battery (30.237 mA $\times$ t_{DC} $\times$ DC) were, respectively: 713.9947, 688.9205, 697.4035 and 748.7437 mAh.

B.3 SIMULATION RESULTS

By using the experimentally estimated c and k parameters, it is possible to simulate KiBaM. The objective is to validate the simulation results through the performed experiments. Matlab was used to implement, simulate and evaluate the model.

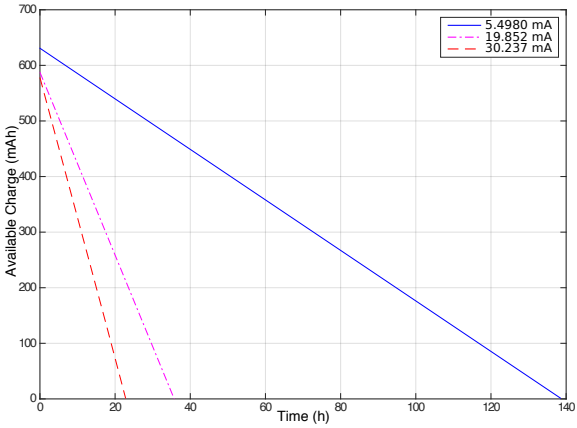

Figure 38 – KiBaM simulation using continuous discharge currents.

The input values are the KiBaM parameters (c and k) and the battery capacity, which can be obtained from each test. Table 29 presents a comparison of all experiments and simulations. KiBaM was also simulated with the nominal battery capacity, 750 mAh, indicated in Table 29 as KiBaM*. Figures 38 and 39 depict the simulation results using KiBaM, respectively, with continuous and intermittent discharge currents. Note the recovery effect in the enlarged part of Figure 39. Only the Available Charge tank behaviour is represented in this figure.

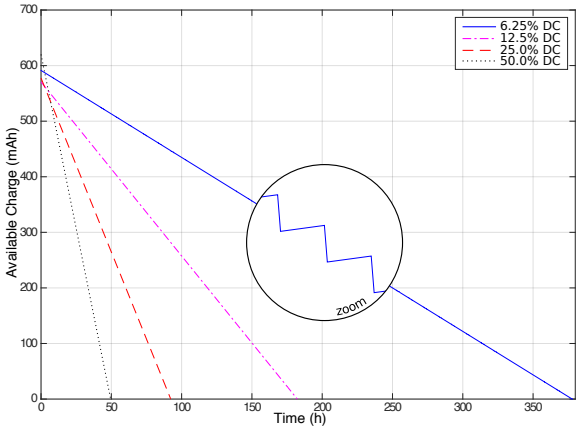

Figure 39 – KiBaM simulation using duty cycle scheme.

Table 29 – Estimating battery lifetime with KiBaM.

Current (mA)	DC (%)	EXPT (h)	KiBaM (h)	RE (%)	KiBaM* (h)	RE (%)
5.4980	100	138.5458	138.5428	0.0022	136.4103	1.54
19.852	100	35.7389	35.7358	0.0086	37.7767	5.70
30.237	100	23.0903	23.0872	0.0133	24.8011	7.40
[30.237, 0]	50.0	49.5250	49.5221	0.0059	49.6048	0.16
[30.237, 0]	25.0	92.2583	92.2549	0.0037	99.2128	7.53
[30.237, 0]	12.5	182.2722	182.2693	0.0016	198.4293	8.86
[30.237, 0]	6.25	377.8125	377.8096	0.0008	396.8619	5.04

The results using KiBaM are very close to those obtained with experiments (EXPT column in Table 29) for both continuous and intermittent discharge currents (in duty cycle scheme). The average relative error is 0.0052%, with a standard deviation of 0.0041%. The average relative error is 5.17% when considering the results with the nominal battery capacity (KiBaM*), with a standard deviation of 2.99%. Since KiBaM is not ready to model the voltage behaviour of Ni-MH batteries, the results apply only if the cut-off value is 2.0 V.

At the beginning of each experiment, despite the knowledge about the voltage level (V), it is not possible to accurately determine

the amount of charge (mAh) existing in the batteries. In other words, each experiment starts with a different amount of charge due to chemical reactions within the battery, which justifies the average and standard deviation values reached in the KiBaM* simulations.

B.4 FINAL REMARKS

This chapter presented the experimental validation of an analytical battery model when used within a WSN context. A set of experiments was performed using different discharge currents that allowed the estimation of the KiBaM parameters. The model was implemented to perform simulations with the same experimental characteristics and to assess its accuracy regarding the battery lifetime. The obtained results indicate that, if the model selected parameters are correct, KiBaM is suitable for estimating the battery lifetime within the WSN context.